(12)

Final Report
for the period
1 June 1984 to
31 August 1985

Orbital-Maneuver-Sequence Optimization

December 1985

Authors:
H. J. Kelley
E. M. Cliff
F. H. Lutze

Optimization, Incorporated
29 High Meadow Drive
Blacksburg, VA 24060

K 505-1
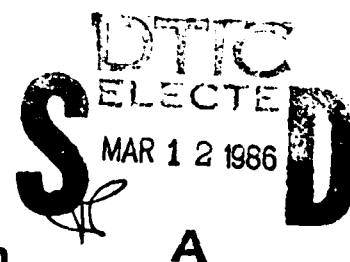F04611-84-C-0014

AD-A165 138

Approved for Public Release

DTIC
ELECTE
MAR 12 1986
S   A   D

DTIC FILE COPY

prepared for the: **Air Force**
Rocket Propulsion
Laboratory

Air Force Space Technology Center
Space Division, Air Force Systems Command
Edwards Air Force Base,
California 93523-5000

86   3   12   005

NOTICE

When U.S. Government drawings, specifications, or other data are used for any purpose other than a definitely related government procurement operation, the government thereby incurs no responsibility nor any obligation whatsoever, and the fact that the government may have formulated, furnished, or in any way supplied the said drawings, specifications, or other data, is not to be regarded by implication or otherwise, or conveying any rights or permission to manufacture, use, or sell any patented invention that may in any way be related thereto.

FOREWORD

This final report was submitted by Optimization, Incorporated, in fulfillment of contract F04611-83-C-0014. Work described herein was performed during the period 1 June 1984 to 31 August 1985. Project manager for the Air Force Rocket Propulsion Laboratory (AFRPL) was Dr Alan R. Weston.

Helpful discussions with the following USAF personnel are gratefully acknowledged: Dr Alan Weston, and Mssrs Michael Powell, Kevin Slimak, Richard Matlock and John Clark of the AFRPL; and Dr William Matoush, Maj. Richard Seid, Lt Col Dennis Eagan, and Mr Jerry Brown of Space Command.

This technical report has been reviewed and is approved for publication and distribution in accordance with the distribution statement on the cover and on the DD Form 1473.
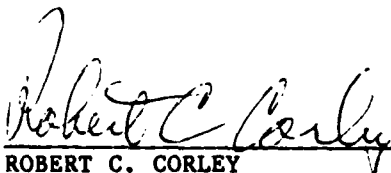
ALAN R. WESTON
Project Manager

RICHARD S. MATLOCK
Chief, Application Analysis
Branch

FOR THE DIRECTOR

ROBERT C. CORLEY
Deputy Chief, Propulsion Analysis Division

AD-A165138

REPORT DOCUMENTATION PAGE

1a. REPORT SECURITY CLASSIFICATION UNCLASSIFIED		1b. RESTRICTIVE MARKINGS		
2a. SECURITY CLASSIFICATION AUTHORITY		3. DISTRIBUTION/AVAILABILITY OF REPORT APPROVED FOR PUBLIC RELEASE. DISTRIBUTION IS UNLIMITED.		
2b. DECLASSIFICATION/DOWNGRADING SCHEDULE				
4. PERFORMING ORGANIZATION REPORT NUMBER(S) K 505-1		5. MONITORING ORGANIZATION REPORT NUMBER(S) AFRPL-TR-85-090		
6a. NAME OF PERFORMING ORGANIZATION Optimization, Incorporated	6b. OFFICE SYMBOL (If applicable)	7a. NAME OF MONITORING ORGANIZATION Air Force Rocket Propulsion Laboratory		
6c. ADDRESS (City, State and ZIP Code) 29 High Meadow Drive Blacksburg, VA 24060		7b. ADDRESS (City, State and ZIP Code) AFRPL/DYA, Stop 24 Edwards Air Force Base, CA 93523-5000		
8a. NAME OF FUNDING/SPONSORING ORGANIZATION	8b. OFFICE SYMBOL (If applicable)	9. PROCUREMENT INSTRUMENT IDENTIFICATION NUMBER F04611-84-C-0014		
8c. ADDRESS (City, State and ZIP Code)		10. SOURCE OF FUNDING NOS.		

	PROGRAM ELEMENT NO.	PROJECT NO.	TASK NO.	WORK UNIT NO.
11. TITLE (Include Security Classification) ORBITAL-MANEUVER-SEQUENCE OPTIMIZATION (U)	62302F	2864	00	EL

12. PERSONAL AUTHOR(S) Kelley, H. J., Cliff, E. M., and Lutze, F. H.				
13a. TYPE OF REPORT Final	13b. TIME COVERED FROM 84/6/1 TO 85/8/31	14. DATE OF REPORT (Yr., Mo., Day) 85/12		15. PAGE COUNT 145

16. SUPPLEMENTARY NOTATION

17. COSATI CODES			18. SUBJECT TERMS (Continue on reverse if necessary and identify by block number)
FIELD	GROUP	SUB. GR.	Orbital Maneuvering, Space Defense.

19. ABSTRACT (Continue on reverse if necessary and identify by block number)

This 15-month effort developed an orbital maneuver-sequence optimization computer program and applied it to the generation of optimal co-orbital attack-maneuver sequences and to the generation of optimal evasion-and-return maneuver sequences. Rocket burns were modeled as impulse and coasts as conic arcs, or as near-circular-orbit approximations thereto. Parameters consisting of impulse components and coast lengths are adjusted iteratively by a variable-metric (BFGS) gradient process with projection treatment of constraints. A minimum-radius constraint, not ordinarily included in orbit-transfer optimization studies, proved to be important for co-orbital attack maneuver sequences. Families of such sequences are explored and the effects of various operational constraints investigated. Optimal in-plane evasive maneuvering is studied subject to return-to-orbit and return-to-position-in-orbit constraints. keywords

20. DISTRIBUTION/AVAILABILITY OF ABSTRACT UNCLASSIFIED/UNLIMITED ☒ SAME AS RPT. ☐ DTIC USERS ☐	21. ABSTRACT SECURITY CLASSIFICATION UNCLASSIFIED	
22a. NAME OF RESPONSIBLE INDIVIDUAL Dr Alan R. Weston	22b. TELEPHONE NUMBER (Include Area Code) (805) 277-5552	22c. OFFICE SYMBOL DYAA

DD FORM 1473, 83 APR EDITION OF 1 JAN 73 IS OBSOLETE.

LIST OF FIGURES

LIST OF TABLES

TABLE OF CONTENTS

1. INTRODUCTION

This reports the results of an AFRPL-sponsored effort spanning the period 1 June 1984 - 31 August 1985 which developed computer programs for optimization of orbital maneuvering and applied them to the study of attack and evasion sequences.

Rocket burns are modelled impulsively, the fuel consumed in such a maneuver being related directly to the magnitude of the velocity-vector increment, ΔV, in the usual way. Coasting arcs are conics, corresponding to an inverse-square-law gravity model, in one version of the computer program developed, this choice facilitating future development of a general-purpose program. In another version, near-circular-orbit coast modelling is adopted, which offers simplifications attractive for evasion-and-return sequences and their real-time calculation (Refs. 1, 2 and 3). A variety of operational constraints on maneuver sequences is provided including minimum-radius constraints, which turn out to be important in the generation of optimal co-orbital attack-maneuver sequences. Performance indices employed are minimum fuel, with or without time constraints, and minimum time with limited fuel.

The optimization is cast in the form of a nonlinear-programming problem: a n-vector, x, is to be found so as to minimize a performance index $f(x)$ subject to some equality constraints of the form $g_i(x) = 0$, i = 1, ---, m, and some inequality constraints of the form $g_{m+j}(x) \geq 0$, j = 1, ---, p. Here the x components include the ΔV components of each burn and the times (or positions) at which they occur. The g functions describe constraints such as the intercept condition (position vectors

equal at final time) and the rendezvous condition (velocity vectors equal at final time) as well as various other constraints. The non-linear-programming algorithm presently employed is basically that of Refs. 4 and 5. Updating includes the use of the BFGS variable metric in place of the older DFP and the addition of advanced active-constraint logic (Ref. 6) in connection with projection treatment of constraints. The algorithm is described in Appendix A.

The computer software developed (some of it adapted from earlier efforts) is herein applied to the study of co-orbital attack-maneuver sequences against a nonmaneuvering target. Initially minimum-ΔV sequences are explored with intercept time open and a bare minimum of operational constraints. As will be seen, it turns out to be important to include minimum-radius constraints for realistic results; this feature has rarely previously been included in orbit-transfer studies. (The state of the art in the context of analytical methods is described in Ref. 7 while Ref. 8 is representative of current computational approaches.) The effects of various operational constraints are explored and qualitative comparisons drawn with observed Soviet ASAT-system maneuver sequence (Ref. 9).

Optimal in-plane evasive maneuvering is investigated analytically and computationally herein with the use of the Clohessy-Wiltshire near-circular-orbit model (Refs. 1, 2 and 3) which is adequate for low altitude maneuvering studies and attractive for its analytical simplicity. The evasive maneuver optimization of Ref. 3 is extended to include return-to-orbit and return-to-position-in-orbit constraints.

Some suggestions are offered for future extension and applications in a closing section.

2. IMPULSE-COAST MANEUVER-SEQUENCE MODELLIŃG

This section details the mathematical models used for the intercept-maneuver sequences and the evasive-maneuver sequences. The former uses the complete inverse-square-law gravitational model while the latter uses a linearized version of the inverse-square-law suggested by Clohessy and Wiltshire for near-circular orbits (Ref. 1).

Intercept-Maneuver Modelling

The intercept-maneuver sequences studied subsequently model the motion of the vehicle as a sequence of unpowered coasting arcs with velocity impulses of their junctions. The coasting arcs are Keplerian orbits (conics) with the exception of the first arc which consists of circular motion due to a fixed point on the surface of a rotating earth. The computer code developed for the intercept portion of the mission models the coasting arcs as either an earth-bound arc or a Keplerian arc. The structure of the code, however, allows for other models to be incorporated such as, for example, oblateness corrections for the Kepler orbits.

Keplerian Orbits

Under the assumption of a spherical earth with no atmosphere, the solution for the coasting arcs of the vehicle becomes simply the solution to the classical two-body problem. The governing equation of motion is given by [22]

$$\ddot{\bar{r}} + \frac{\mu}{r^3} \bar{r} = 0 \qquad (2.1)$$

where $\bar{r}$ = the position vector from the center of the earth to the vehicle and $\mu = GM_e$, the mass constant associated with the earth. Unfortunately, there is no closed-form solution to eq. (2.1) which yields $\bar{r}(t)$. However, by transforming both the independent and dependent variables a solution of a sort is possible. Typically the independent variable is transformed from time to an angle variable. The nature of the problem at hand leads one to consider the central angle or change in true anomaly as a candidate for the independent variable. The true anomaly itself is not a particularly good candidate because for circular orbits it is undefined. However, we resort to the true anomaly to recover an expression for time.

Trajectory Equations

By taking the cross product of $\bar{r}$ with eq. (2.1) we can extract a constant of the motion

$$\bar{r} \times \dot{\bar{r}} = \bar{h} = \overline{\text{const}} \qquad (2.2)$$

where $\bar{h}$ = angular momentum of the system. Equation (2.2) indicates that the unforced motion of the satellite remains in a plane determined by $\bar{r}$ and $\dot{\bar{r}}$ which passes through the center of the earth. If we view the orbit in that plane, the position vector moves from one position through an angle to another position. This angle is designated as the change in the true anomaly, that is

$$\eta = \nu - \nu_o \qquad (2.3)$$

where η = change in true anomaly

ν_0 = true anomaly of epoch

ν = current true anomaly

As indicated previously, since the true anomaly is measured from the position in the orbit closest to the earth's center (perigee) it is not well-defined for circular orbits. As a result, it is useful to use the change in true anomaly as the independent variable. The angular momentum constant can then be used to eliminate time from the problem in favor of the change in true anomaly. The magnitude of $\bar{h}$ is easily determined using plane polar coordinates to be

$$|\bar{h}| = h = r^2 \frac{d\eta}{dt} \tag{2.4}$$

Equation (2.4) can be used to eliminate time by noting that

$$\frac{d(\cdot)}{dt} = \frac{h}{r^2} \frac{d(\cdot)}{d\eta} \tag{2.5}$$

Substituting eq. (2.5) into the radial component of eq. (2.1) and in addition making the dependent variable transformation

$$u = \frac{1}{r} \tag{2.6}$$

leads directly to the differential equation

$$u'' + u = \frac{\mu}{h^2} \tag{2.7}$$

where ( )' means differentiation with respect to η. The solution to eq. (2.7) is given by

$$u(\eta) = \frac{\mu}{h^2} + \left[u(o) - \frac{\mu}{h^2} \right] \cos\eta + u'(o) \sin\eta \tag{2.8}$$

Alternatively eq. (2.8) can be written as

$$u(\eta) = \frac{\mu}{h^2} [1 + e \cos (\eta + \nu_0)] \qquad (2.9)$$

By comparing eqs. (2.8) and (2.9) we can obtain the constants which appear in eq. (2.8) in terms of the initial true anomaly. (Note that this step is not necessary but only identifies the constants in eq. (2.8) with those associated with the classical results.) The initial conditions relate to the true anomaly as follows:

$$u(o) - \frac{\mu}{h^2} = \frac{\mu}{h^2} e \cos \nu_0 \qquad (2.10)$$

$$u'(o) = - \frac{\mu}{h^2} e \sin \nu_0 \qquad (2.11)$$

Furthermore, the true anomaly could be determined from

$$\text{Tan } \nu_0 = \frac{- u'(o)}{u(o) - \mu/h^2} \qquad (2.12)$$

and the eccentricity, e, from

$$e^2 = \frac{[u(o) - \frac{\mu}{h^2}]^2 + u'(o)^2}{(\mu/h^2)^2} \qquad (2.13)$$

If the initial position and velocity are known, the constants required for eq. (2.8) can be determined with the help of eq. (2.5) to be

$$u(o) = \frac{1}{r_0}$$

$$u'(o) = \frac{r^2}{h} \dot{u} = \frac{r^2}{h} \frac{d}{dt} (\frac{1}{r}) = - \frac{1}{hr_0} (\bar{r}_0 \cdot \bar{V}_0) \qquad (2.14)$$

The problem is still not complete since eq. (2.8) establishes only the magnitude of $\bar{r}$ and not its direction in space. To address the problem of determining the direction of the position vector we can track the behavior of a unit vector along the position vector. Such a vector designated as $\hat{r}$ is defined by

$$\hat{r} = \frac{\bar{r}}{r} \tag{2.15}$$

It is easily shown that

$$\hat{r}' = \hat{h} \times \hat{r} \tag{2.16}$$

where

$$\hat{h} = \bar{h}/h.$$

It follows that

$$\hat{r}'' + \hat{r} = 0 \tag{2.17}$$

The solution to eq. (2.17) is

$$\hat{r}(\eta) = \hat{r}_0 \cos\eta + \hat{r}_0' \sin\eta \tag{2.18}$$

where

$$\hat{r}_0 = \bar{r}_0/r_0$$
$$\tag{2.19}$$
$$\hat{r}_0' = \bar{h}/h \times \hat{r}_0$$

If the initial position, $\bar{r}_0$ and velocity $\bar{V}_0$ are given, along with the change in true anomaly, the new position and velocity can be determined as follows:

Given: $\bar{r}_0$, $\bar{V}_0$, η

Find:
1. $\bar{h} = \bar{r}_0 \times \bar{V}_0$

2. $u(o) = 1/r_0$

3. $u'(o) = \dfrac{-1}{hr_0} (\bar{r}_0 \cdot \bar{V}_0)$

4. $\hat{r}_0 = \dfrac{\bar{r}_0}{r_0}$

5. $\hat{r}'_0 = \bar{h}/h \times \hat{r}_0$

6. $u(n) = \dfrac{\mu}{h^2} + [u(o) - \dfrac{\mu}{h^2}]\cos n + u'(o) \sin n$ (2.20)

7. $u'(n) = -[u(o) - \dfrac{\mu}{h^2}]\sin n + u'(o) \cos n$

8. $\hat{r}(n) = \hat{r}_0 \cos n + \hat{r}'_0 \sin n$

9. $\hat{r}'(n) = - \hat{r}_0 \sin n + \hat{r}'_0 \cos n$

10. $\bar{r} = \dfrac{1}{u} \hat{r}$

11. $\dot{\bar{r}} = \bar{V} = h(u\hat{r}' - u'\hat{r})$

A short discussion of eq. (2.20) is in order. By using the change in true anomaly as the independent variable, straightforward solutions are available for finding the final position and velocity given the initial position and velocity. More important, however, is the fact that the solutions do not use the classical orbital elements in any manner and hence are not subject to any singularities which can occur when these elements are used. In addition the results are independent of the type of orbit encountered and are valid for

elliptic, parabolic, and hyperbolic orbits and hence the equations can be considered universal equations.

Time Equations

Unfortunately reintroducing time into the problem is not quite as straightforward and leads to some complications. Although there is a universal formulation for determining time in terms of the change in true anomaly [20], there are still some unanswered questions which make it unreliable for coupling with an optimization code. Consequently for now we must resort to classical time calculations in terms of the true anomaly. Further it should be noted that there is a different calculation for each type of orbit. To separate these out it is necessary to determine the two orbital elements a, semi-major axis and e, the eccentricity. In addition, one needs to know the initial true anomaly and the change in true anomaly. Once this information is established, the time calculations are as follows:

Elliptic Orbits [22,23,24]

1. Examine the change in true anomaly to determine the number of orbits required and subtract those out.

2. Determine the final true anomaly.

3. Determine the eccentric anomaly at the initial and final point from

$$\text{Tan } E_i = \frac{\sqrt{1 - e^2} \sin \nu_i}{e + \cos \nu_i} \qquad i = 1,2 \qquad (2.21)$$

4. Determine the time of flight from perigee to initial and final true anomaly from

$$t_i - t_p = (E_i - e \sin E_i)/n \qquad i = 1,2 \qquad (2.22)$$

where

$$n = \frac{\mu}{a^3}$$

a = semi-major axis

5. Take the o fference in the times determined in (4) and add on an orbit period for each additional orbit established in (1).

$$TOF = (t_2 - t_p) - (t_1 - t_p) + N \cdot P \qquad (2.23)$$

where N = number of orbits

$$P = 2\pi \sqrt{\frac{a^3}{\mu}} = \text{period of orbit.}$$

Parabolic Orbits [22,23,24]

1. Compute time from perigee to beginning and final location directly from

$$t_i - t_p = (\text{Tan} \frac{\nu_i}{2} + \frac{1}{3} \text{Tan}^3 \frac{\nu_i}{2})/2\bar{n} \qquad i = 1,2 \qquad (2.24)$$

where $\bar{n} = \sqrt{\dfrac{\mu}{p^3}}$

and $p = h^2/\mu$ = orbit parameter

2. $TOF = (t_2 - t_p) - (t_1 - t_p)$ (2.25)

Hyperbolic Orbits

1. Compute time perigee to beginning and final location directly from

$$t_i - t_p = \frac{e\sqrt{e^2 - 1}\, \sin \nu_i}{1 + e \cos \nu_i} - \ln \left[\frac{1 + \sqrt{\frac{e-1}{e+1}}\, \tan \frac{\nu_i}{2}}{1 - \sqrt{\frac{e-1}{e+1}}\, \tan \frac{\nu_i}{2}} \right]$$

$$i = 1,2 \qquad (2.26)$$

2. $TOF = (t_2 - t_p) - (t_1 - t_p)$ \qquad (2.27)

Conventions and Non-Dimensionalization

The time-of-flight relations above require the two orbital elements (a,e) and the initial and final true anomaly. In most cases these calculations are straightforward and no problems are encountered. However, one should note that for circular orbits the true anomaly is not defined. A standard default for definition of the true anomaly for a position on a circular orbit has been defined as the angle from the ascending node line to the position vector. If the inclination of the orbit is zero, the true anomaly is measured from the inertial x axis to the position vector in the plane of the equator. It should be pointed out that to date no problems have been encountered with this convention and none are anticipated. However, it is a weakness in the formulation and should be noted.

All calculations for the position, velocity, and time are performed using non-dimensional units. These are obtained by defining a reference circular orbit and dividing lengths by the reference orbit radius and velocities by the reference orbit velocity. A unit of time, therefore, becomes the time it takes to travel through one radian in the reference orbit. This procedure for non-dimensionalization causes all the equations to appear as if they were the dimensional

equations with the gravitational constant $\mu = 1$. Typically the reference orbit is at the radius of the earth's surface.

Rotating Earth

While waiting on the launch pad the interceptor performs an inertial motion due to Earth rotation. This is calculated by first converting the initial inertial position from Cartesian to polar representation (declination and right ascension). The right ascension is altered by adding to it the (prescribed) angular change; the result is then transformed back to Cartesian co-ordinates. To preserve similarity with the treatment of Keplerian arcs the change in right ascension is prescribed and the time is calculated by dividing by the (fixed) Earth angular rate.

Velocity Impulse

The code keeps track of the inertial position and velocity, represented in Cartesian coordinates, at both ends of each coasting arc. At the junctions of these arcs, impulsive burns are modelled as discontinuities in these quantities. In the current version only the velocity vector suffers a discontinuity; the position is the same before and after an impulse. Note that other approximations which account for some effects of finite burn-time (e.g., Robbins' generalized impulses) could be handled in the present structure of the code.

The simplest impulse is described by three parameters which represent the velocity impulse in Cartesian co-ordinates. Early in the present research it was thought that certain special maneuvers

might also be of interest so that two additional impulse-types are possible. One is a two-parameter impulse to allow a change in velocity, <u>in the current orbit plane</u>. The third impulse is a one-parameter affair where a component of velocity is added to cause a <u>pure plane change</u>. These additional impulse-types were not used extensively in the research.

The Clohessy-Wiltshire (CW) Equations

The CW equations describe the motion of a particle (satellite) in space relative to a coordinate system which moves as if it were fixed to a particle moving in a circular orbit. Consequently if the original orbit of the target were circular, the target position would always be at the origin of the CW coordinate system. If the coordinate system is oriented as shown in Figure 2.1, the relative motion of a particle moving in the same force field as the reference circular orbit is described by the CW equations given by

$$\ddot{x} - 2\omega\dot{y} = 0$$
$$\ddot{y} + 2\omega\dot{x} - 3\omega^2 y = 0 \qquad\qquad (2.28)$$
$$\ddot{z} + \omega^2 z = 0$$

where ω = angular rate of axes system which moves in the reference
circular orbit

By a suitable selection of a time scale, the above set of equations can be simplified and non-dimensionalized. In particular define a non-dimensionalized time (really an angle) as $\tau = \omega t$. Then the above equations reduce to

$$x'' - 2y' = 0$$

$$y'' + 2x' - 3y = 0 \tag{2.29}$$

$$z'' + z = 0$$

where $( )' = \dfrac{d( )}{d\tau}$

and x, y and z can be scaled by any arbitrary length. Typically the reference orbit radius is used although any convenient length is appropriate. It is this property that allows results obtained from the CW equations to be scaled up or down directly [25].

A solution to the above equations is given by

$$\begin{Bmatrix} x \\ y \\ x' \\ y' \end{Bmatrix} = \begin{bmatrix} 1 & 6(\tau - \sin\tau) & 4\sin\tau - 3\tau & 2(1 - \cos\tau) \\ 0 & (4 - 3\cos\tau) & -2(1 - \cos\tau) & \sin\tau \\ 0 & 6(1 - \cos\tau) & (4\cos\tau - 3) & 2\sin\tau \\ 0 & 3\sin\tau & -2\sin\tau & \cos\tau \end{bmatrix} \begin{Bmatrix} x_0 \\ y_0 \\ x_0' \\ y_0' \end{Bmatrix}$$

$$\tag{2.30}$$

and

$$\begin{Bmatrix} z \\ z' \end{Bmatrix} = \begin{bmatrix} \cos\tau & \sin\tau \\ -\sin\tau & \cos\tau \end{bmatrix} \begin{Bmatrix} z_0 \\ z_0' \end{Bmatrix} \tag{2.31}$$

where $x_0 = x(o)$, $x_0' = x'(o)$, etc.

The solution exhibited by eq. (2.30) can be utilized in several ways. Of particular interest are the solutions to initial-condition problems, and to boundary-value problems. For the initial-condition problem, eq. (2.30) can be used in its present form to determine the position and velocity at any non-dimensional time, τ, given the initial position and velocity, the so-called Kepler problem. On the other

hand if one is given two positions and the time-of-flight between
them, it would be useful to be able to determine the initial velocity
required to carry out this intercept maneuver, the so-called Lambert
(or Gauss) problem. For this boundary value problem it is necessary
to partially invert eq. (2.30) in order to obtain the following
result:

$$
\begin{Bmatrix} x'_0 \\ y'_0 \end{Bmatrix} = \frac{1}{\Delta} \begin{bmatrix} \sin\tau & 2(1-\cos\tau) & -\sin\tau & 14(1-\cos\tau)-6\tau\sin\tau \\ 2(1-\cos\tau) & 4\sin\tau-3\tau & -2(1-\cos\tau) & 3\tau\cos\tau-4\sin\tau \end{bmatrix} \begin{Bmatrix} x \\ y \\ x_0 \\ y_0 \end{Bmatrix}
$$

$$(2.32)$$

where

$$\Delta = 8(1 - \cos\tau) - 3\tau\sin\tau$$

The computer code for the evasive-maneuvering sequences uses
the CW equations to generate the coasting arcs. As in the interceptor
model, these arcs are joined by velocity impulses which allow dis-
continuities in velocity only. Since the CW equations can be solved
analytically in terms of time, time rather than true anomaly is used
as the independent variable for the evasive-maneuver calculations.
Consequently the awkward time equations are unnecessary.
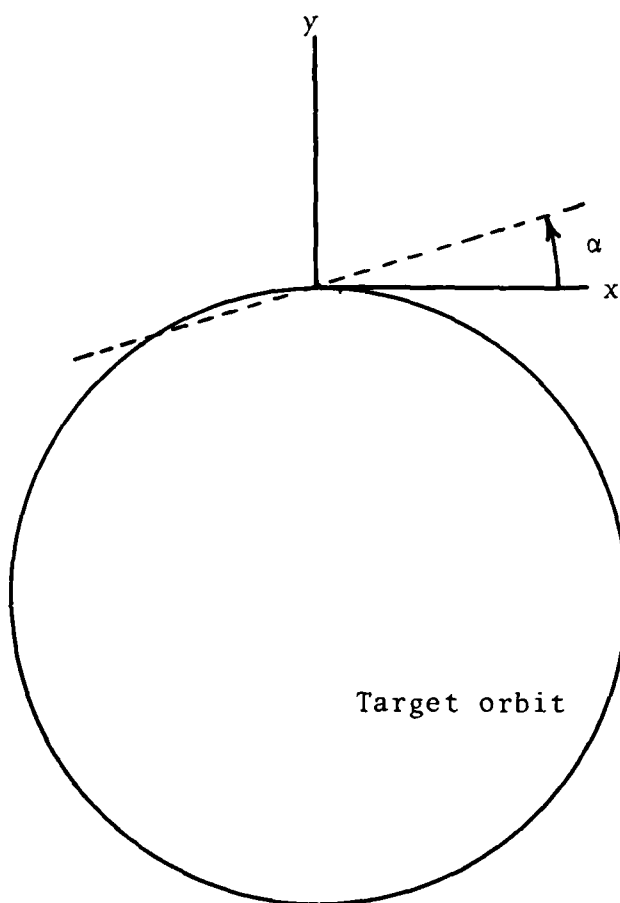
FIGURE 2.1   Clohessy - Wiltshire Axes

3. INTERCEPT-MANEUVER-SEQUENCE STUDY

The class of problems studied here involve efficient maneuver sequences to intercept a non-maneuvering target in low-Earth orbit. In all of the present studies the target is in a circular orbit at ᵫ00 km, inclined at 65°. This is typical of targets used in Soviet ASAT-system trials. The period of the target's orbit is about 97 minutes (see Figure 3.1).

The interceptor is to be launched from a location at 45° 38' N. latitude (Tyuratəm). It is clear that the intercept problem depends on many parameters including the target's orbital elements and the interceptor's launch latitude. Somewhat more subtly the problem also depends on the relative 'phasing' between the target's orbital motion and the interceptor's (inertial) motion while on the launch pad. We next present a way to quantify this phasing. It should be noted, however, that since the periods of the two motions need not be commensurate the 'phase' will change from day to day.

We define epoch to be the time when the launch point is one orbital period (of the target) west of the target's orbital plane. Thus, one period after epoch the launch point will be in the plane of the target's orbit (specifically where the target would be ascending or moving North). For convenience we measure the target's true anomaly from this point of intersection between the orbit plane and the launch latitude. In these terms we define phase angle to be the target's true anomaly at epoch. Note that one orbital period after epoch the target will return to the same true anomaly and the launch

point will be at the location of zero true anomaly (see Figure 3.1).

As noted above the phase angle may be different at subsequent orbit crossings by the launch point. In an operational setting it is expected that the exigency would rule out the possibility of waiting for a subsequent orbit crossing.

General Formulation

The scenario assumed is as follows: Starting from epoch the interceptor may wait on the launch pad for some time. Following the initial impulse the interceptor coasts along an ascent ellipse. At some point a second impulse is applied and this is followed by another coast. A third impulse is possible and the subsequent coast must lead to intercept. At this point a fourth burn may be needed to produce velocity match, possibly within a given tolerance.

Such a maneuver sequence is specified by thirteen parameters as enumerated in Table 3.1. Since the target does not maneuver, its location at intercept depends on a single parameter, namely, the coast angle, which is a fourteenth parameter. The components of the fourth burn can be computed from the condition of the required velocity match between the two vehicles. Each impulse adds a total of four parameters, so that a three-burn intercept sequence requires ten parameters and a two-burn sequence requires six.

It is clear that an 'arbitrary' choice of these fourteen parameters would not produce a final position of the interceptor that matched the target. Indeed, the times at which the endpoints were reached would likely not match either. Thus, we must add four

important constraints, the first four in Table 3.2. If these constraints
are satisfied then the target is indeed intercepted. The additional
nine constraints are generally inequalities and will be discussed
later.

Nonlinear Programming

Thus far we have described many of the ingredients of an optimal-
intercept problem. The parameters needed to specify the maneuver
have been listed and the constraints have been enumerated. As an
index of performance the sum of the impulse magnitudes is a
measure of fuel-required. Thus, for minimum-fuel intercept we take

$$f(x) = \sum_{i=1}^{4} \| \Delta \bar{V}_i \|$$

and consider the nonlinear-programming problem: find x to minimize
f subject to the constraint

$g \geq 0$.

The first four constraints are equalities while the last nine
are inequalities. Of these, certain constraints (g_8, g_9, g_{11} and g_{13})
are needed to insure that the interceptor's path does not strike the
Earth. Other constraints (g_6, g_7, g_{10} and g_{12}) are needed to prevent
the solution algorithm from choosing a negative coast angle (and
hence a negative time-of-flight).

The algorithm used to solve this problem is a modern quasi-
Newton scheme with important features for adapting to difficult
problems. It is described in Appendix A.

Minimum-Propellant Intercept-Maneuver Sequences

The first problem studied is that of minimum-propellant, time-open intercept. For each phase angle one seeks an intercept-maneuver sequence which uses the least propellant. The total time-of-flight inequality constraint g_5 (see Table 3.2) was specified as 500 minutes, which is sufficiently large that time is effectively not constrained. Fig. 3.2 displays the total-fuel cost as a function of phase angle. In these calculations it was required that the two vehicles rendezvous, that is the last burn had to produce a velocity for the interceptor equal to that of the target.

Some of the salient features of these optimal-maneuver sequences are shown in Figs. 3.2-3.5. From Fig. 3.3 it is seen that for phase-angles in the range $[-170°, -20°]$ the launch is timed to occur with the target about 2° past overhead. To accomplish this with large negative phase angle the launch must be delayed well beyond the point where the launch site passes through the target's orbital plane. For example, with a phase-angle at -150° the launch occurs with the launch-site about 10° East (past the orbital plane of the target). The impulse trade-off is such that it's preferable to 'pay' for the out-of-plane condition at launch in order to obtain favorable target geometry. For phases in this range (i.e. $[-170°, -20°]$) the inter-cepts are nominally three-burn affairs; however, the third burn (at rendezvous) is very small ($|\Delta \bar{V}_3| \approx .5$ ft/sec). After the second burn the interceptor is in nearly the same orbit as the target. The optimization algorithm chooses to have the interceptor fly in a nearly station-keeping mode with the very small third-burn timed to occur

when the vehicle velocities match most closely. In effect, then, the
fuel-optimal maneuver sequence is a direct-ascent intercept. For the
phase-angle at -150° the intercept is accomplished about 20 minutes
after launch.

For phase angles in the range [60°, 190°] the launch occurs
with the target about 70° past overhead. To achieve this target
geometry the launch is 'early'; that is, it occurs before the launch
site reaches the target's orbital plane [West]. For example, with a
phase-angle of 90° the launch occurs with the site about 1° West of
the orbital plane and the target 69° past overhead. This first burn
is at nearly zero path-angle and results in a near-circular orbit at
the Earth's surface. The second burn ($|\Delta \bar{V}_2| \approx 600$ ft/sec) puts the
interceptor in an orbit that is (nearly) co-planar with the target and
with apogee altitude at 600 km. The minimum-radius constraint is
active on the "ascent" ellipse and on the orbit segment leading to
intercept. The third-burn is a substantial ($|\Delta \bar{V}_3| \approx 570$ ft/sec)
speed-up to match velocity of the target which is 'overtaking' the
interceptor. In this family the intercepts are rather long affairs;
e.g., the 90° phase case takes about 198 minutes from launch, and about
289 minutes from epoch.

For some intermediate range of phase-angles one finds two
distinct (local) minimum-fuel intercept sequences. These sequences
differ principally in the second and third burns. For example, at
15° phase-angle both sequences initiate launch when the site is at
the target's orbit plane (and hence the target is 15° past overhead).
In both cases the ascent ellipse is co-planar with the target and has

an apogee near 600 km. In one sequence the second burn ($|\Delta \bar{V}_2| \approx 475$ ft/sec) occurs near apogee on the ascent ellipse and it effectively adjusts the interceptor's period so that intercept will occur one orbit later. The third burn at about 85 ft/sec is a speed-up maneuver to match velocity with the overtaking target.

The second sequence also applies the second burn ($|\Delta \bar{V}_2| \approx 525$ ft/sec) at apogee of the ascent ellipse. Since the second burn is larger than before, the interceptor's period is now closer to the target's so that the intercept takes three orbits, instead of one. The final catch-up burn is now reduced to 37 ft/sec. Note that the sum of the two final burns is nearly the same in both sequences. The time to intercept is, however, quite different (140 min. vs. 330 min.). One expects that there is another sequence 'between' these in which the second burn is sufficient to achieve intercept in two revolutions. Indeed, there are likely to be other local minima with four-, five-, etc. revolution intermediate arcs.

At a phase of 45° another maneuver-sequence family appears with the same character as the 90° phase case (i.e., "ascent" to a circular orbit at one Earth-radius, a second burn to achieve intercept at apogee and a third burn to rendezvous). The launch timing is different from the [60°, 190°] phase family in that the launch site is nearly in the orbit plane.

The launch doctrine that emerges from this study can be described with the help of Fig. 3.5. The heavy curve is a cross-plot of launch longitude (from the target's orbit plane) and target true-anomaly (from overhead) at launch. Also shown are lines of constant phase.

Since the target's orbital period is about 97 min. while the Earth's
rotational period is 24 hrs these lines have a slope of about 14.8.
Given any initial launch-site longitude and target true-anomaly one
moves along the constant-phase line through the point until it inter-
sects the cross-plot.

The last part of this initial study is a first look at the
effects of a time-constraint. Operationally one expects that early
intercept may be of value. Indeed, with a given booster configuration
there is little virtue in saving fuel at all. Thus, one is led to
consider how 'quickly' intercept can be accomplished for a given
total-impulse budget. This may be done by introducing a time
constraint (i.e. reduce the total time specification in constraint
g_5). Note that only total time is considered (i.e. 'wait' time on
Earth is included in the time calculation). It would also be worth-
while to consider constraining the time from launch to intercept.
This, in effect, amounts to the warning time and makes evasion, if
any, more difficult. This version is considered in a later section.

The phase-angle parameter, defined and used above, is very valuable in understanding the structure of minimum-propellant inter-cept maneuver sequences, when the final time is free. Perhaps of equal importance, at least in an operational setting, is a time constraint.

Since there is a genuinely two-parameter family of problems (phase-angle and elapsed-time) it will only be possible to present representative results. To this end consider the 90° phase-angle case. The minimum-propellant time-open maneuver sequence was described above. It consists of a launch-burn into a circular orbit at the Earth's surface; a second-burn to a Hohmann-like intercept ellipse with apogee at the target's altitude and, a rendezvous burn after one and one-half revolutions in the intercept ellipse. Intercept occurs about 290 minutes after epoch and requires a total delta-vee of 26,500 ft/sec. If one now restricts the allotted time the propellant-cost will, as expected, increase. With a maximum time of 275 min. an additional 155 ft/sec delta-vee is required, while a 265 min. intercept requires 625 ft/sec more than the time-open case.

Further restricting the time produces a result that, at first, seems somewhat surprising. With a time allotment of about 250 min. one finds a maneuver-sequence which requires only an additional 145 ft/sec. While this seems puzzling, if one examines the maneuver sequence, it is seen to be quite different from that of the time-open case. The initial orbit has an eccentricity of .06 and a semi-major axis of .96 Re; it is not a surface circular orbit. At a point past apogee on the ascent ellipse a second burn is imparted. This results

in an orbit with perigee at zero altitude and apogee at the target's altitude. After about one and one-half revolutions, at apogee in this intercept-orbit, a third (rendezvous) burn is imposed.

If one continues to restrict the time allotted below 250 min. the minimum-propellant intercept sequences remain of the type just described until the time reaches about 200 min. At this point a third family emerges which is similar to that of the time-open case, except that the intercept ellipse is followed for only one-half an orbit, not one and one-half orbits. This is reasonable since these intercepts occur in the (target's) orbit prior to those of the original family.

When the time allotment is restricted to 150 min. a fourth family is found. These orbits are similar to those in the second family except that the intercept ellipse is traversed for only one-half an orbit, in contrast to the second family of orbits which employed about one and one-half revolutions.

Finally, when time-to-intercept is restricted to 90 min. the intercept sequence becomes a two-burn affair. Initially the first burn results in an ascent ellipse with apogee at the target's altitude. The second burn produces the required velocity match.

The results of this fuel-time trade-off are shown in Fig. 3.6. The solid curves depict performance along each of the five sub-families described in the preceding. Perhaps the most significant result is that a small increase in propellant allocation can greatly reduce the time-to-intercept. Specifically, an additional 675 ft/sec of delta-vee reduces the time from about 290 min. to 90 min. Thus, it would seem that the Soviet ASAT is fundamentally capable of much more rapid engagements than the observed tests would indicate.

Mimicking Soviet ASATs

The intercept maneuver sequences that emerged from the above formulation are quite different from the procedures employed by the Soviets [9]. The observed pattern of the test shots suggests that they were constrained, for various reasons including tracking and kill-assessment considerations. Thus, we are led to introduce additional "operational" constraints into our problem.

It has been observed that Soviet ASAT intercepts occur while the target is passing near Moscow. To implement such a constraint one looks for a time (from epoch) when the target is closest to Moscow. In general one expects two close approaches; one with the target passing East of Moscow and a second, approximately one period later, with the target West of Moscow.

In order to investigate these close approaches a small FORTRAN code was written. The launch-site is located at epoch one period West of the orbit plane and a phase of the target thus is specified. True anomaly change of the target is varied on $[0,2\pi]$ and the minimum is sought for the Moscow-target separation distance. The interval $[2\pi,4\pi]$ is then searched and so on. One of these produces a close approach just East of Moscow and the next produces one to the West. Since the target's orbit is circular, the time-of-flight is simply related to the target's true anomaly change. The results are shown in Fig. 3.7 as a function of phase angle. Note that for each phase there are two solutions: East and West.

One might select from the two possible intercept points the one that is closer to Moscow for test purposes. Miss distances are shown as a function of phase in Fig. 3.8. The discontinuities are a

consequence of the fact that, depending on the phase, the closest
approach may occur on the 2nd, 3rd or 4th pass near Moscow. In an
operational setting the earlier of the two close approaches might be
favored.

The candidate family is described by the lower bound from
Fig. 3.8. Note that for phases in the range $135° \leq \phi \leq 300°$ the
intercept point is East of Moscow, while other phases produce inter-
cept to the West. The "fold" at 360° is smooth, but there is a switch
between the East-West families at 300° phase. The switch at 135°
phase angle is more a matter of semantics. At this phase the inter-
cept occurs directly North of Moscow; slight perturbations of phase
produce intercepts to the East or West.

This family has several deficiencies. Most significantly, inter-
cepts West of Moscow take place about one orbital period ($\sim$ 100 min)
after the previous Easterly intercept would have. Secondly, since
Moscow is about 26° West and 10° North of Tyuratam, it arrives at the
target's orbit plane about 140 minutes after Tyuratam. This time
must be made up by a costly trade-off between a delayed launch
(Tyuratam East of the orbit plane) and a longer-duration intercept
orbit (higher energy). For these reasons it was decided for purposes
of the present calculations to intercept the target on its Easterly
pass closest to Moscow (i.e., on the next pass the target would be
West of Moscow). Note that this will not necessarily provide the
(global) minimum-fuel intercept. Indeed, results show that for
certain phases intercept on a prior pass (i.e., well East of Moscow)
require less fuel.

In addition to the intercept point specification several new constraints are added exploratively to force the maneuver-sequence to be similar to that of observed Soviet ASAT shots. It has been observed that the Soviet sequences produce final intercept orbits that are nearly co-planar with the target's orbit. To enforce this it is required that the second burn occur at the intersection of the ascent ellipse with target's orbit plane and that the 2nd burn be such as to produce a new velocity vector that lies in that plane. Since both the position vector and the velocity vector (after the 2nd burn) lie in this plane it will also be the interceptor's orbital plane. Note that the second burn is not required to be a _pure_ plane change; some energy change is permitted. The two new constraints are

$$g_p = \langle \bar{h}_T, \bar{r}_I(t_3^-) \rangle = 0$$

and

$$g_q = \langle \bar{h}_T, \bar{V}_I(t_3^+) \rangle = 0$$

In these equations, as in Chapter 2, $\bar{h}_T$ is the angular momentum of the target's orbit, $\bar{r}_I(t_3^-)$ is interceptor's position at t_3, the end of the ascent orbit, and $\bar{V}_I(t_3^+)$ is the interceptor's velocity after the second impulse has been applied. Constraint g_p requires that the second burn occur in the target's orbit, plane while g_q requires that the subsequent orbit be co-planar with the target.

A family of minimum-propellant maneuver-sequences with phase-angle as a parameter was studied numerically. Some significant features of the family are presented in Table 3-3. For this study

the final burn (rendezvous) was required to match the relative velocity within a specified tolerance. In each case the velocity match was sufficiently close that the fourth burn was omitted. Indeed, for most phase-angles (30° exception) the third burn (catch-up) was virtually absent. Thus, the second burn, which was required to make the interceptor's orbit co-planar with that of the target, generally included the necessary in-plane speed change to effect intercept.

In all cases the flight-time (from launch to intercept) is about 90 min. The interceptor remains on the Earth's surface until the target is about 25° past the intersection of its orbit plane with the parallel of latitude through the launch site. The interceptor goes about one-fourth of a revolution (to near apogee) in an ascent ellipse. The second burn provides the required plane-change and puts the interceptor in an orbit with perigee at one Earth radius and apogee beyond the target's altitude. The interceptor travels about 300° in this orbit. A third burn occurs on this segment but is of such small magnitude that the orbit is virtually unchanged. Intercept occurs near (but not quite at) apogee on this orbit with the target overtaking the interceptor. The speed difference is typically 500 ft/sec, well within the allowed value.

The relatively long (300°) coast on the intercept ellipse warrants further testing to validate the optimality of these maneuver-sequences. A test based on primer-vector theory (see, for example [8]) would be an attractive addition to the current analysis.

In addition to the basic family, several problems were investigated to gain an indication of the effects of certain specific

features. For example, the minimum-radius constraint was specified
as one Earth-radius in all cases discussed above. The phase-angle-
equals-330° case of Table 3.3 was re-run with the minimum radius value
of 1.02 Earth radii. The results are displayed in the next-to-last
line of Table 3.3. It can be seen that the maneuver-sequence is nearly
the same as before, except that the higher minimum radius results in
an increase of 9U ft/sec in the total propellant requirement.

A second special problem was formulated to assess the impact of
the plane-change requirement. Specifically, the phase-angle-equals-
120° problem was re-run with the constraints g_p and g_q (defined above)
omitted. These results are shown in the last line of Table 3.3. The
maneuver-sequence is again quite similar to the constrained 120°
phase-angle case (5th line in Table 3.3). The less constrained
maneuver is slightly more fuel-efficient; it requires about 160 ft/sec
less total impulse. The third impulse, which is not shown in the
table, is 530 ft/sec. This is much larger than the constrained cases
which typically have third impulses of several ft/sec.

Two more attack families were generated in further attempts to
approach realism. For one of these the minimum-fuel index was retained
but the first-burn magnitude was specified. The rationale for this is
that an existing space booster (SL-11) is employed for launch without
provisions for shut-down and re-light. A first-burn delta-vee of 1.03
was assumed as well as a velocity-match tolerance of 1000 ft/sec. at
intercept. Coplanar flight following the second burn was required.
The results are shown in Table 3.4. The maneuver sequences are
typically three-burn; for a range of phase angles the intercept burn

fades to zero also, resulting in two-burn sequences.

Fragmentary results for a minimum-time-of-flight family are given in Table 3.5. Alterations were 1.03 delta-vee first burn and 1.15 delta-vee total. Three of the four maneuver sequences calculated exhibit four burns; in one the intercept-burn is missing. These generally resemble the observed Soviet ASAT system shots. It should be borne in mind that there is considerable arbitrariness in the allocations assumed. A more thorough study and comparison with flight data is of future interest.

Summary

Perhaps the most significant insight that can be gained from the intercept-maneuver-sequence study is that the current Soviet ASAT approach has the potential to be considerably more effective than the tests to date would indicate. That is, the documented Soviet tests have employed maneuver sequences that use more propellant and allow more warning time than the "optimal" sequences (in the sense and with the constraints employed here).

While we have provided no explanation for the observed Soviet intercept strategy one may hypothesize that the current Soviet ASAT could be made considerably more effective by:

1) better communication for transmittal of commands

2) more flexible software and hardware to generate and implement burn commands

3) improved tracking and kill-assessment capabilities

These are mostly external to the fundamental interceptor design and likely represent planned improvements in the normal course of development. In systems-optimization terms they represent relaxation of constraints. Other obvious opportunities for improvement are the use of higher-performance boosters and improved on-board sensors for target acquisition which would permit higher closing rates.

Table 3.1

Optimization Parameters

Number	Description
1	Wait-angle on Earth's surface
2,3,4	Components of first velocity impulse
5	Coast-angle along ascent orbit
6,7,8	Components at second velocity impulse
9	Coast angle along Kepler orbit
10,11,12	Components at third velocity impulse
13	Coast angle along Kepler orbit
14	Target's coast angle along its Kepler orbit

Table 3.2

Optimization Constraints

Number	Description
1-3	Difference of position components of target and interceptor
4	Difference in total time-of-flight of target and interceptor
5	Difference between input time-of-flight and target's tof
6	Interceptor's wait time on Earth
7	Difference between coast angle on ascent ellipse and input minimum coast angle
8	Difference between coast angle where ascent ellipse reencounters the Earth and the actual coast angle
9	Difference between path angle at launch and input minimum path-angle
10	Difference between coast angle on third orbit and minimum coast
11	Difference between least radius on third orbit and input minimum radius
12	Difference between coast angle on fourth orbit and minimum coast
13	Difference between least radius on fourth orbit and input minimum radius

Table 3.3
Mimicked Maneuver - Sequence Study

Phase-Angle (deg)	Launch Impulse	Launch Site wrt Tgt's Orbit Plane (deg)	Target True-Anomaly at Launch (deg)	Eccentricity of Ascent Ellipse	Second Impulse	Plane Change (deg)	Coast Angle on Ascent Ellipse (deg)	Time-of-Flight (min)	Total Impulse
0.	.9582	1.8E	27.	.090	.0437	0.9	273.	91.9	1.0002
30.	.9747	0.1E	31.	.022	.0190	0.9	210.	90.2	0.9980
60.	.9588	2.5W	24.	.095	.0475	1.3	278.	91.2	1.0066
90.	.9447	4.7W	21.	.136	.0733	2.8	295.	92.5	1.0181
120.	.9353	6.8N	19.	.161	.0972	4.2	300.	93.1	1.0327
150.	.9061	15.8E	25.	.211	.1753	8.7	300.	93.3	1.0814
180.	.9084	14.2E	25.	.205	.1603	7.8	300.	93.3	1.0687
210.	.9043	11.8E	25.	.211	.1504	7.3	304.	93.3	1.0557
240.	.9160	9.6E	23.	.186	.1271	5.6	302.	93.3	1.0431
270.	.9220	7.6E	23.	.173	.1087	4.5	301.	93.0	1.0308
300.	.9311	5.6E	23.	.154	.0884	3.2	299.	92.8	1.0194
330.	.9428	3.6E	24.	.127	.0666	2.0	290.	92.5	1.0094
330.	.9503	3.3E	20.	.117	.0625	1.8	290.	93.6	1.0128
120.	.9251	6.9W	19.	.157	.0707	2.9	302.	91.6	1.0264

Table 3.4

Mimicked Maneuver-Sequence Study with First Burn Constrained to 1.03 (26,714 ft/sec)

Phase-Angle (deg)	Eccentricity of Ascent Ellipse	Launch Site wrt Target's Orbit Plane (deg)	Target True-Anomaly at Launch (deg)	Second Impulse	Plane Change (deg)	Third Impulse	Fourth Impulse	Time-of-Flight (min)	Total Impulse
0	.114	2.1 W	-31.5	.0336	+ 0.7	–	–	195.2	1.0638
30	.116	4.1 W	-30.9	.0496	+ 2.6	–	–	187.2	1.0797
60	.115	6.0 W	-28.9	.0652	+ 3.6	–	–	179.0	1.0953
90	.114	7.8 W	-26.6	.0817	+ 4.6	–	–	170.7	1.1118
150	.133	10.7 E	-51.6	.0934	- 5.4	–	.0079	253.2	1.1314
180	.130	8.7 E	-50.3	.0798	- 4.7	.0002	.0064	244.9	1.1163
210	.127	6.8 E	-48.3	.0663	- 3.8	–	.0047	236.6	1.1010
240	.124	5.0 E	-45.8	.0533	- 2.9	–	.0026	228.4	1.0859
270	.121	3.2 E	-42.5	.0407	- 2.0	.0002	.0004	220.1	1.0715
300	.121	1.3 E	-40.0	.0288	- 0.9	–	–	211.9	1.0590
330	.114	0.0	-29.9	–	0.0	.0207	–	203.6	1.0508

Table 3.5
Mimicked Maneuver-Sequence Study with First Burn Constrained to 1.03 (26,714 ft/sec), the Total Delta-V to 1.15 (29,827 ft/sec), and Flight Time Minimized.

Phase Angle (deg)	Eccentricity of Ascent Ellipse	Launch Site wrt Target's Orbit Plane (deg)	Target-True Anomaly at Launch (deg)	Second Impulse	Plane Change (deg)	Third Impulse	Fourth Impulse	Time of Flight (min)
0	.111	2.8 E	41.7	.0924	3.3	.0265	.0010	195.4
30	.110	0.9 E	43.2	.0682	1.7	.0341	.0177	187.2
60	.113	1.2 W	41.9	.0742	- 2.1	.0325	.0132	179.0
90	.112	3.5 W	37.8	.0989	- 3.4	.0213	-	170.7
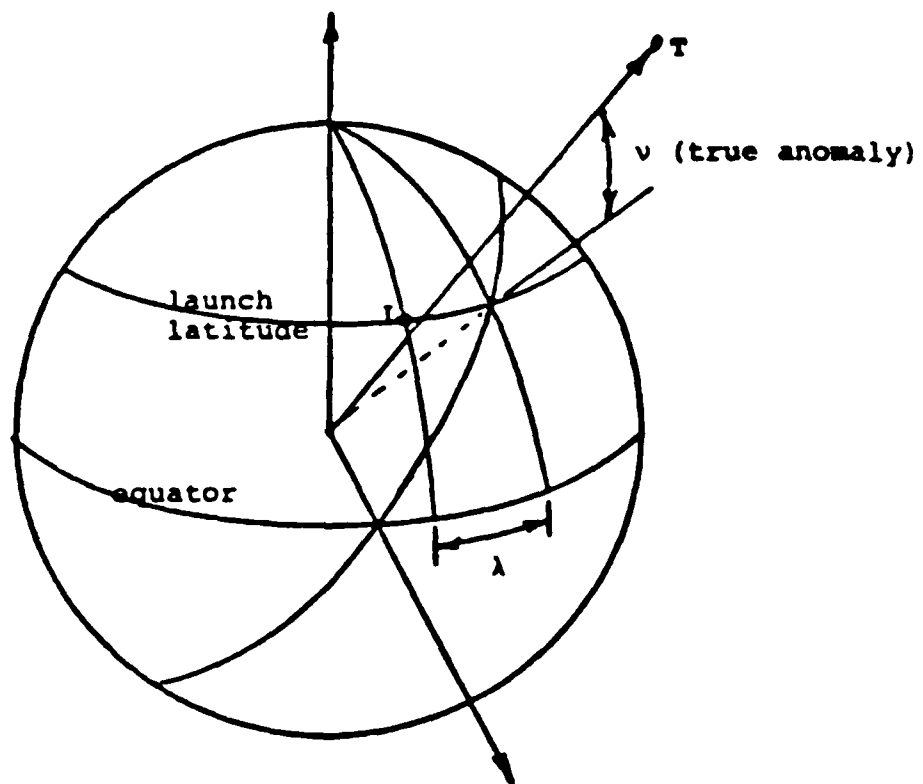
FIGURE 3.1 Problem Geometry
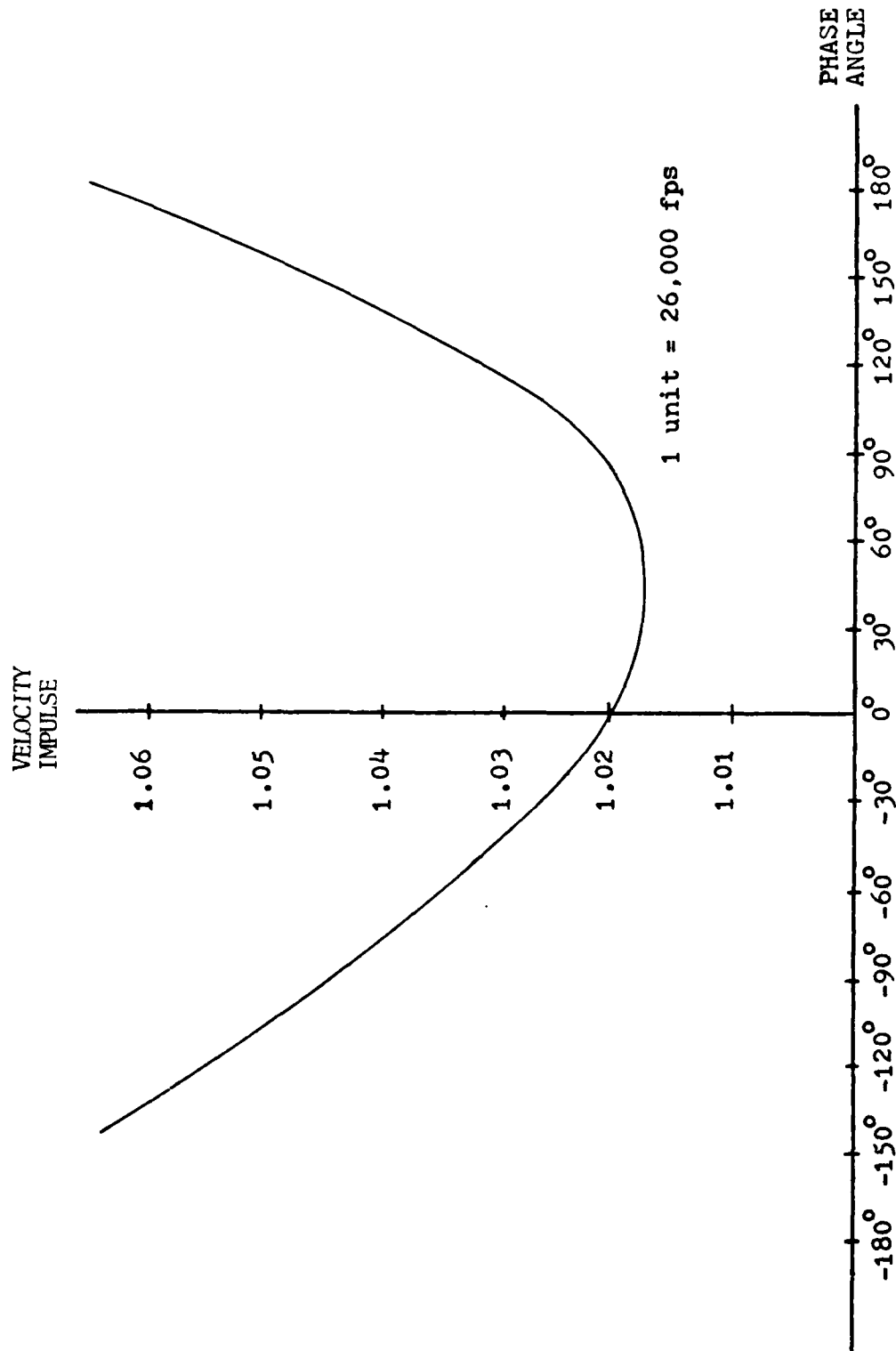
FIGURE 3.2 Minimum - Propellant Required
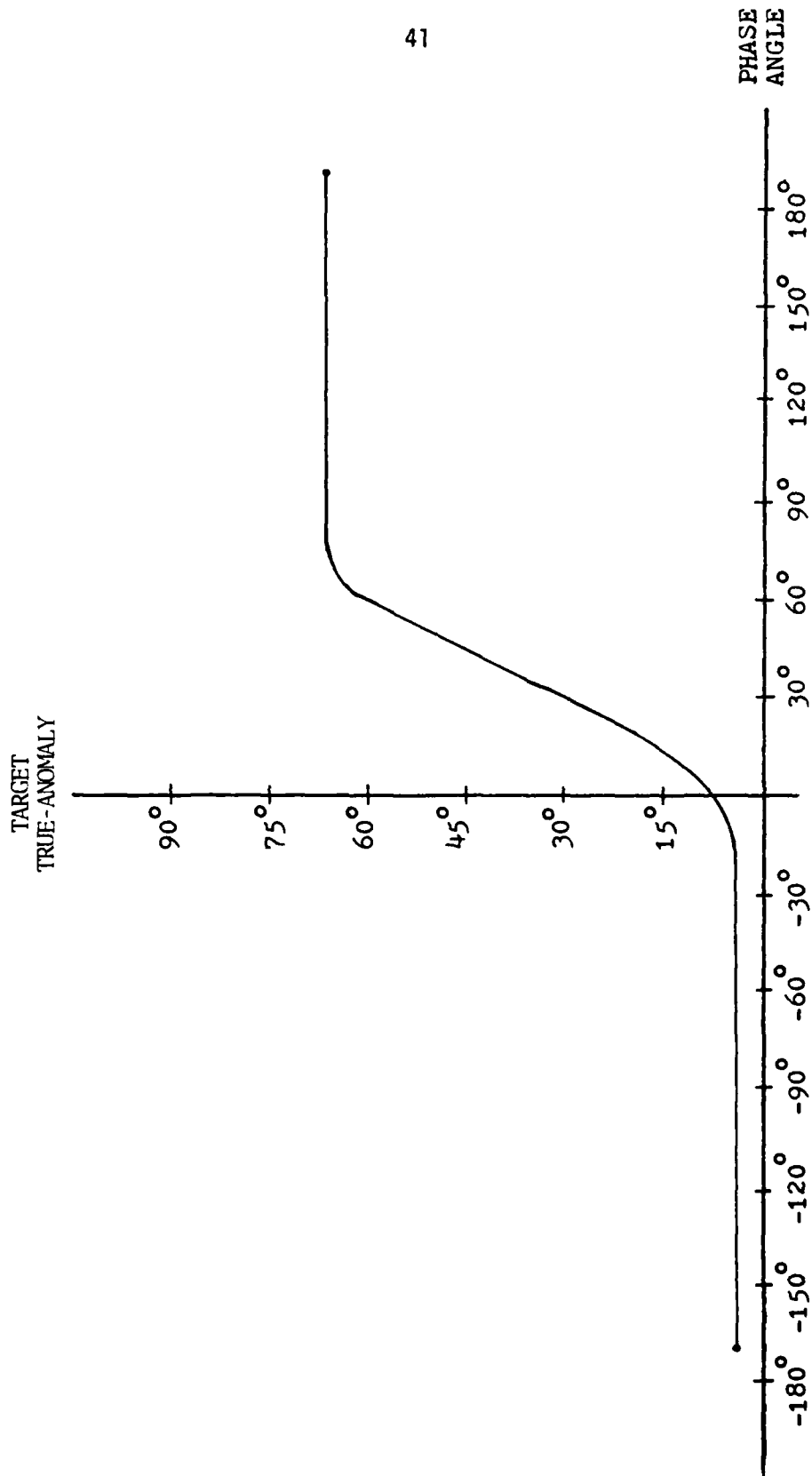
FIGURE 3.3 Target True-Anomaly at Launch
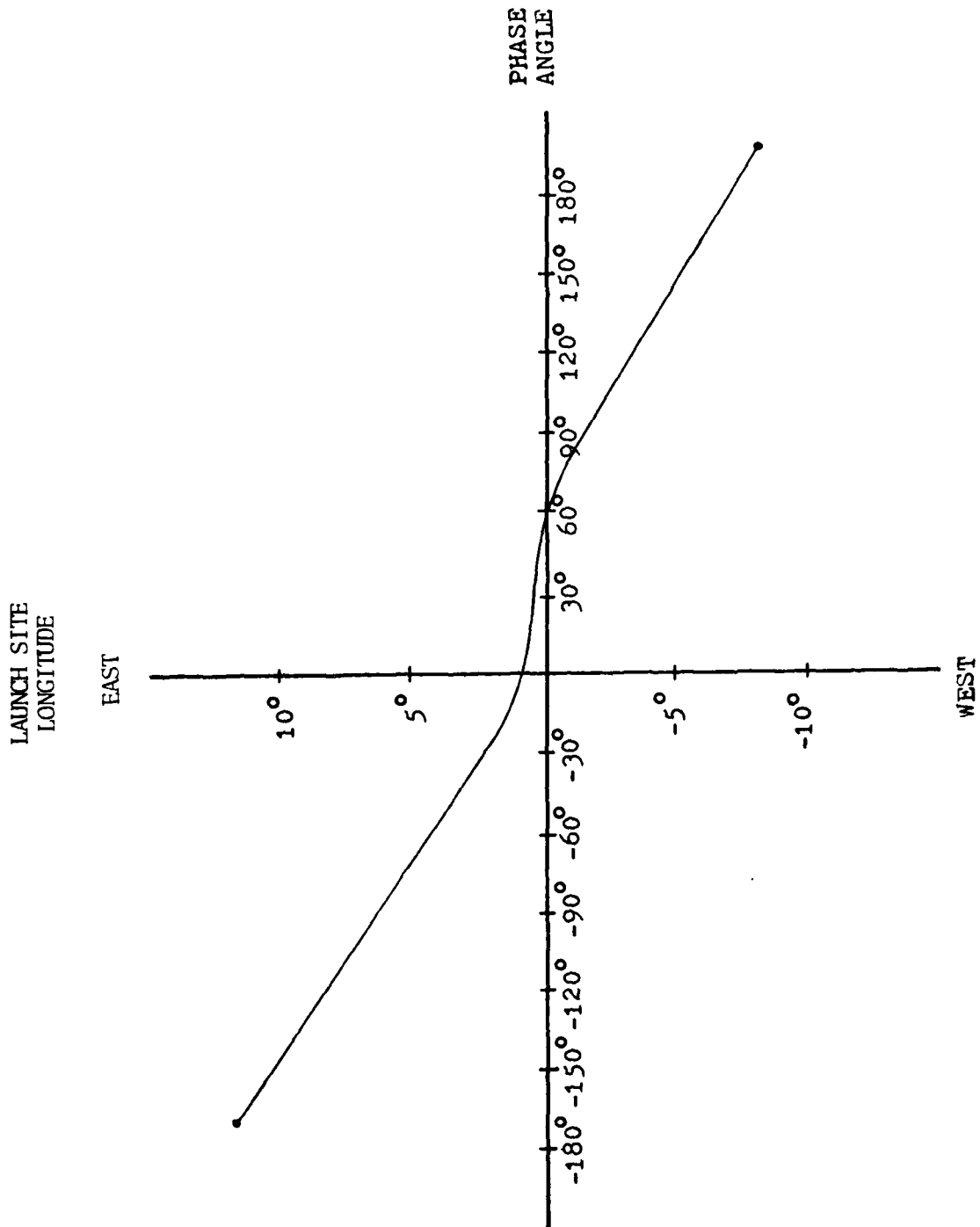
FIGURE 3.4 Launch Site Location Relative to Target's Orbit Plane
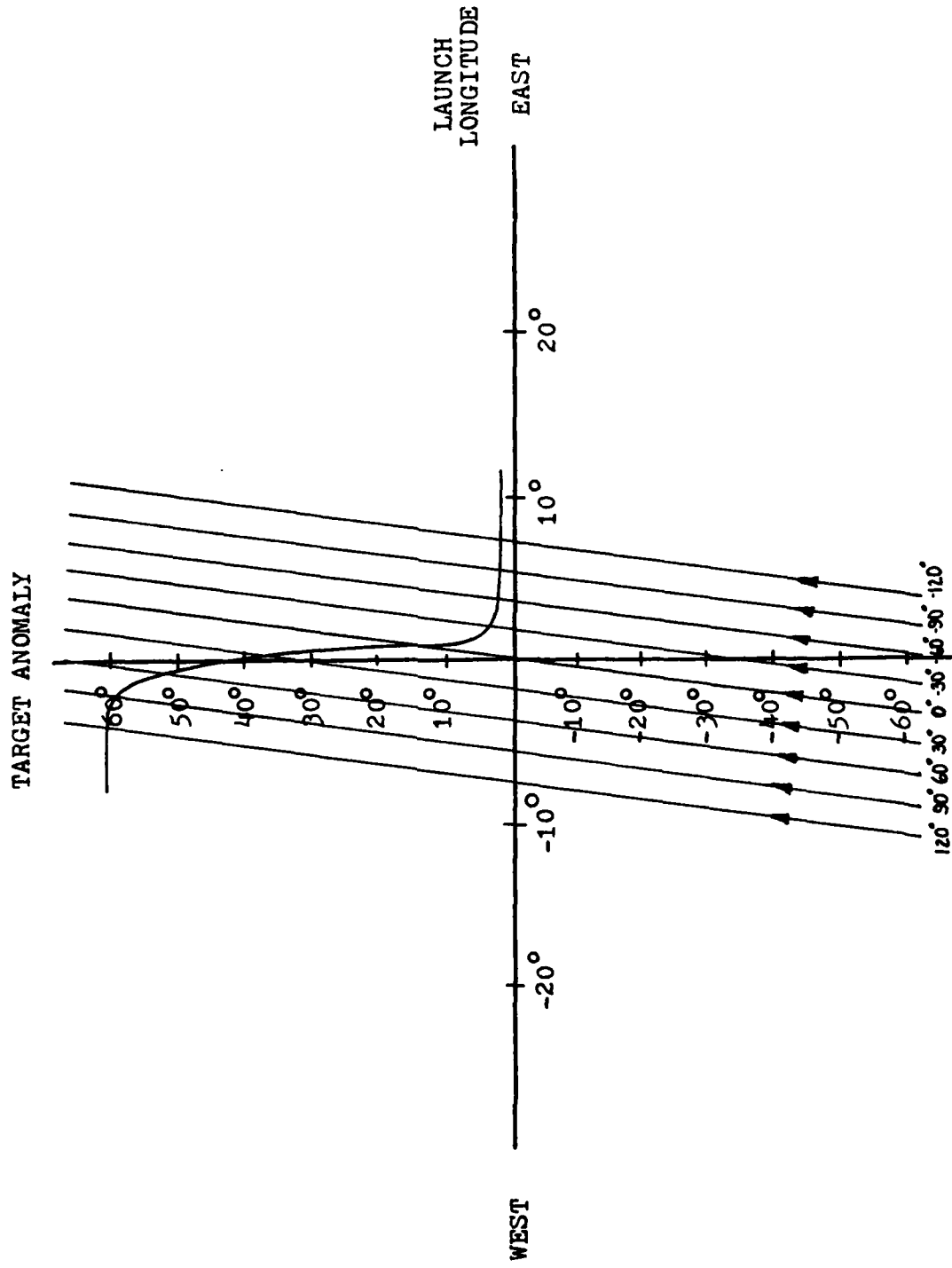
FIGURE 3.5 Launch Doctrine for Minimum - Propellant Intercepts
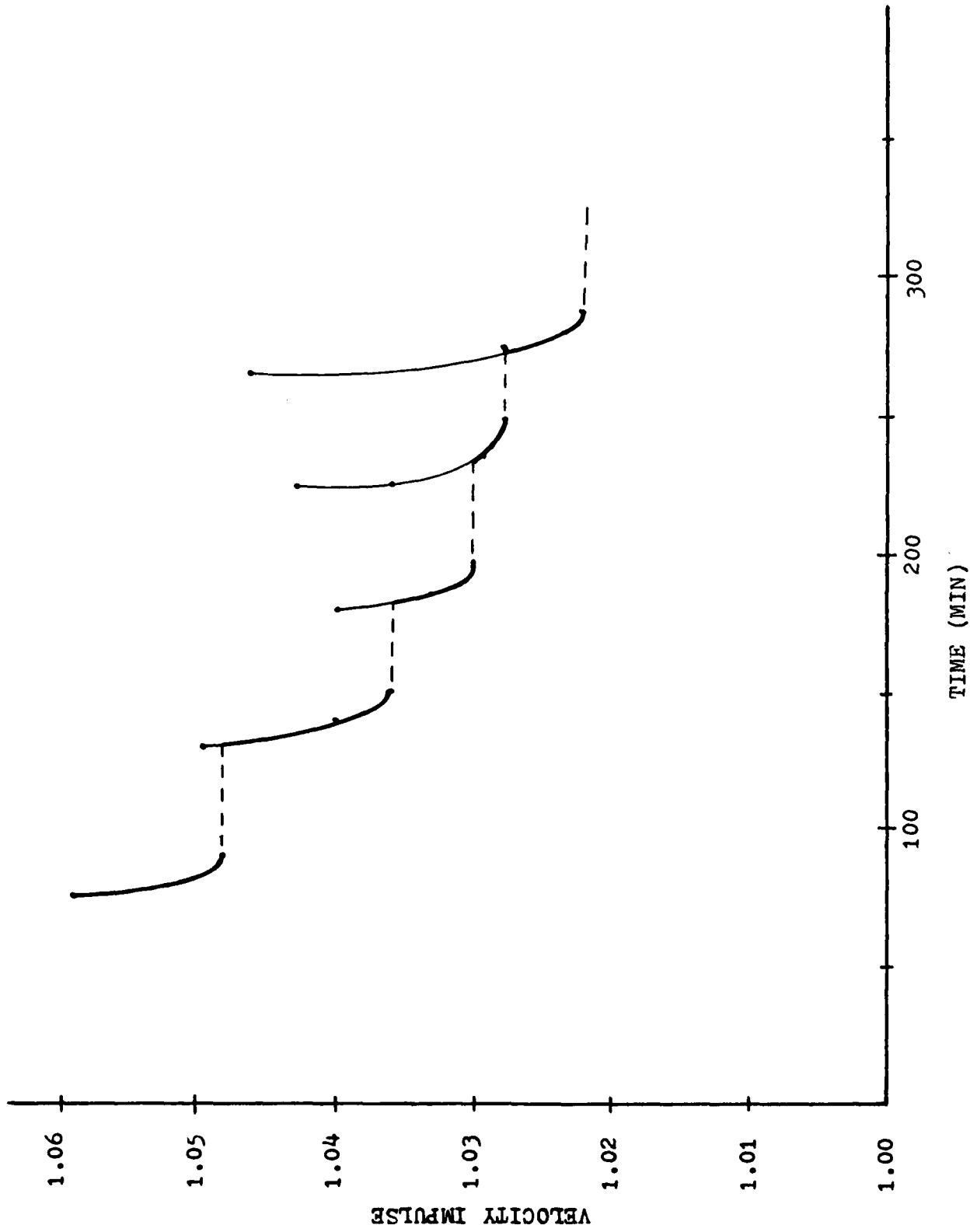
FIGURE 3.6 Minimum Propellant Required for Time Constrained Intercept   (90° Phase)
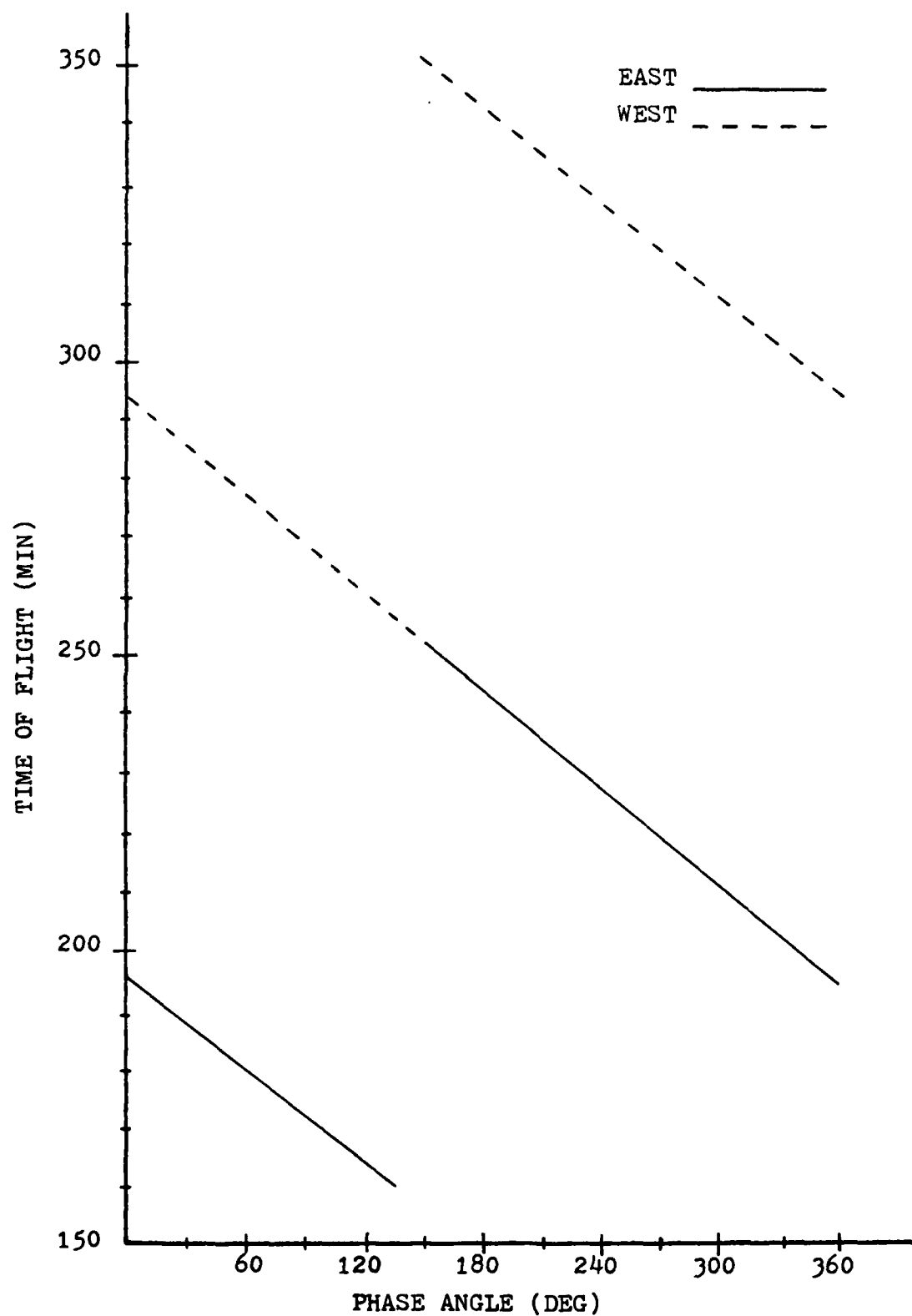
FIGURE 3.7 Time for Close-Approach to Moscow
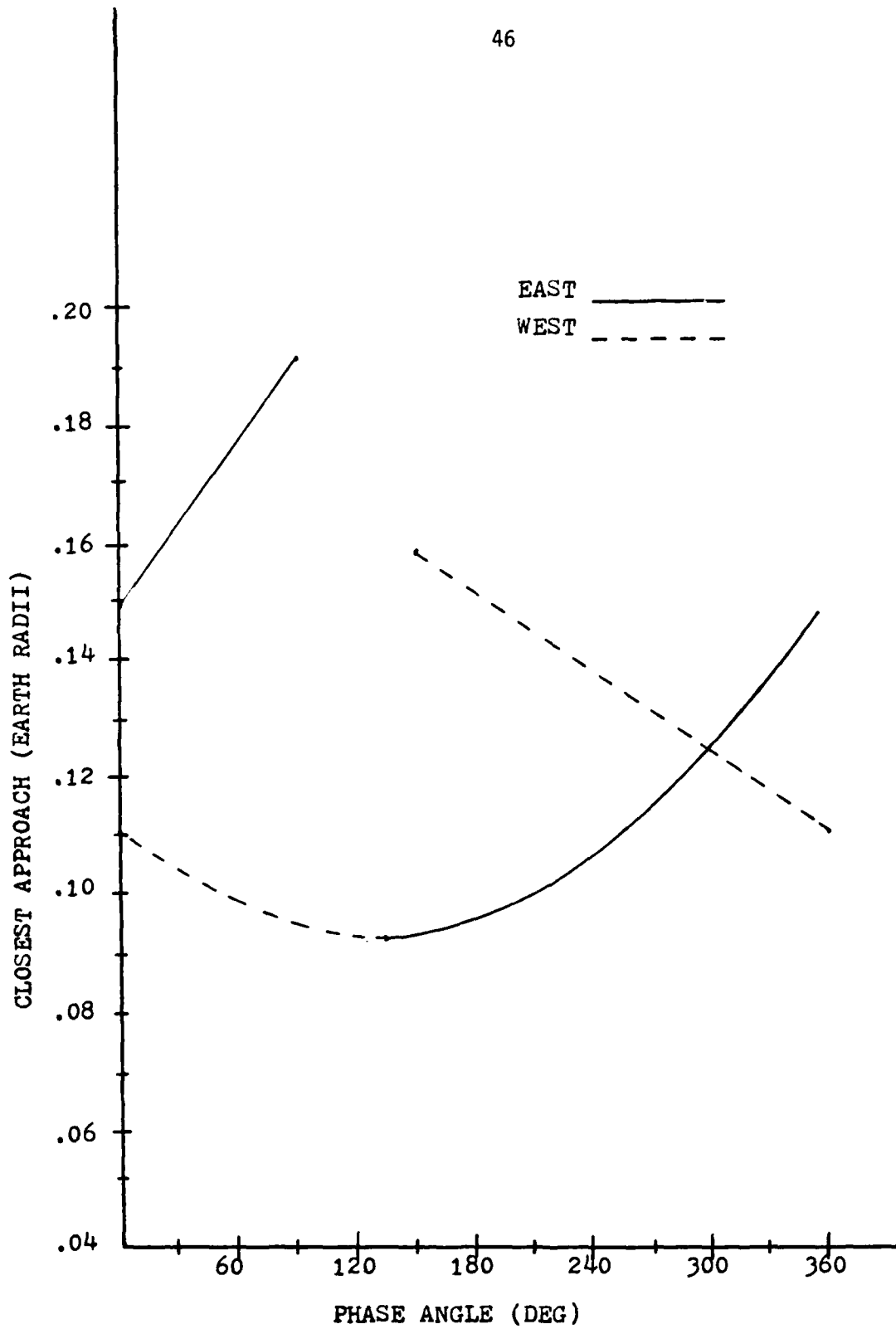
FIGURE 3.8   Close-Approach Distance

4. EVASIVE MANEUVERING

A satellite in an orbit which permits it to carry out some strategic function would best have the capability of maneuvering away from its location to avoid threats. In addition, it would be desirable to be able to return to the same orbit or, for some missions, to return to the same position in orbit the satellite would have occupied if no evasive maneuver had taken place, that is, return-on-station. In order to extend the lifetimes of such satellites, these evasive maneuvers should consume minimum fuel. This section evaluates various evasive-maneuvering sequences as to their effective-ness in avoiding the threat, returning on orbit or on station, and in minimizing fuel-consumption.

In order to complete a successful evasion, the closest approach between the pursuer and evader must exceed some minimum distance dictated by lock-on capability of the ASAT search sensors. In general this minimum miss distance will be small compared to the nominal orbit radius. Furthermore studies of typical interceptor ascent trajectories show that the final orbit segment which approaches the target is generally in-plane or nearly in-plane with the target orbit. These observations indicate that the linearized analysis of Clohessy and Wiltshire [1] is adequate for a preliminary investigation. In addition the simplified analysis will give a better insight to the problem.

The solution to the CW equations was presented earlier in the form of position and velocity of the satellite as a function of time.

Because of the simplicity of this solution certain evasive maneuvering results can be obtained analytically. For example the direction of thrust to maximize the distance from the "on-station" location for a given impulse (delta-V) can be determined analytically as a function of evasion (or warning) time. On the other hand maneuver sequences such as an evasion and return-to-orbit or return-on-station are too complex to handle in an analytic manner. For these sequences the analytic trajectory solutions of the CW equations are used in conjunction with the optimization code to establish minimum-fuel maneuvering sequences. In the following sections various optimum maneuver sequences are presented.

Before examining these maneuver sequences in more detail we should note that the CW solutions given by eqs. (2.30) and (2.31) reveal that the in-plane motion is uncoupled from the out-of-plane motion. Further, the out-of-plane motion is oscillatory in nature with respect to the orbital plane. Hence any evasive maneuver which occurs over a substantial amount of time would not include an out-of-plane component of motion since such efforts would eventually be wasted as the vehicle returns to the plane. These observations were verified in Reference 3. Consequently the remaining discussion will be restricted to in-plane maneuvers only, which are governed by eq. (2.30).

Equations (2.30) and (2.32) allow one to gain considerable insight into the problem because of their simplicity. Further, some manipulation of these equations allows certain results to be obtained analytically. For actually describing trajectories in space, these

equations are limited in accuracy depending on the distance from the origin and length of time considered. However, for the purposes of this study (comparisons, trends, etc., as opposed to detail trajectory calculations) these equations can be used for quite long time periods of interest. The results presented can be scaled up or down directly. Both distances and velocities scale the same, doubling the velocity will double the corresponding size of the maneuver.

Evasive Maneuvering Away from Origin

There are several strategies which may serve as bases for evasive maneuvering. The most elementary strategy is that of moving as far from the starting point (the origin) in a given time for a given amount of fuel (or delta-V). Here it is assumed that the interceptor is attempting to get to a specific point in space at a specific time (intercept time). The maneuver of interest maximizes the distance from that point at a given time (evasion or warning time). One should note that the maneuver only considers the position of the threat at the intercept time and not the trajectory taken to arrive at that position. Consequently it is possible that during (or after) the approach the interceptor and target may be closer than the distance calculated at intercept time [3]. This aspect of the problem is discussed in a later section.

Of additional interest is the maneuvering the evader does after the threat is past. Typically, he can remain in the new orbit into which the evasive maneuver placed him, he can return to the original orbit, or he can return to the original orbit at the same point he

would have occupied if no evasion was necessary (i.e., return on station). Obviously other scenarios are possible, but these are the ones which seem to have the most utility and are considered herein.

Maximum Distance from the Origin

The maneuver to be examined in this section is that of maximizing the distance from the origin at a given time for a specified amount of fuel or delta-V. It is useful to represent the initial velocity required for the maneuver in the form

$$x_0' = \Delta V_0 \cos\gamma$$
$$y_0' = \Delta V_0 \sin\gamma$$

$$(4.1)$$

where ΔV_0 = initial impulse required, assumed to be proportional to
                   the fuel required

       γ = thrust angle relative to the x axis

If x_0 and y_0 are zero, corresponding to starting at the origin, and eq. (4.1) is substituted into eq. (2.30), the square of the distance from the origin can be shown to be

$$R^2 = \Delta V_0^2 \ [A \cos^2\gamma + B \sin\gamma\cos\gamma + C \sin^2\gamma + D]$$

$$(4.2)$$

where $A = (4 \sin\tau - 3\tau)^2$

     $B = 12 \ (1 - \cos\tau)[\sin\tau - \tau]$

     $C = \sin^2\tau$

     $D = 4 \ (1 - \cos\tau)^2$

It is clear from eq. (4.2) that the distance from the origin achieved is directly proportional to the ΔV_0 applied. Furthermore the angle at which the optimal thrust should take place is independent

of the magnitude of the ΔV_o. It is easily shown that the angle for obtaining the maximum distance is given by

$$\text{Tan } 2\gamma = \frac{B}{A - C}$$

$$= \frac{4 (1 - \cos\tau)}{5 \sin\tau - 3\tau} \tag{4.3}$$

Equation (4.3) gives four possible angles for thrusting, only two of which yield <u>maximum</u> distance from the origin. The two angles are those which occur nominally in the second and the fourth quadrant. Although the distance from the origin is the same for both quadrants, the solution which gains energy has been shown to be better when some consideration of the threat trajectory is included [3]. Hence only results for thrust (or impulse) directions in the second quadrant are presented.

Equation (4.3) was evaluated for several warning or evasion times and the results are presented in Figure 4.1. These results are independent of orbit altitude and represent the best angle for an initial impulse in order to achieve the maximum distance from the origin in the specified time.

The distance achieved by the above maneuver depends directly on the magnitude of the initial impulse (ΔV) as indicated by eq. (4.2). Consequently we can select one of two methods to normalize and compare our later results. For comparing the fuel costs of various maneuver sequences for a specific evasion time it is useful to compare against the fuel costs for the pure evasion maneuver which led to Figure 4.2. In this case the distance at the specified evasion time is held

constant at the value given in Figure 4.2. On the other hand, for
, comparing fuel costs for the same maneuver sequence over various
evasion times it is useful to hold the evasion distance constant over
all evasion times. If we pick that distance as unity, the ΔV for this
second normalization procedure is related to that of the first by
dividing the first ΔV by the non-dimensional distance associated with
each evasion time given in Figure 4.2. In the following, the tables
will show results normalized using method 1 while the graphs will dis-
play results normalized by both methods.

As indicated previously Figure 4.2 shows the distance from the
origin achieved by using the evasion strategy given in Figure 4.1.
Here the initial impulse is assumed to be unity. Also shown in
dimensional units is the distance that would be achieved using this
strategy in an orbit 100 miles above the earth's surface with an
initial impulse of 1 ft/sec. The information necessary for the
purposes of calculation is given as

$$R_{ref} = 2.146848 \times 10^7 \text{ ft}$$
$$V_{ref} = 25,600 \text{ ft/sec}$$
$$\omega = 1.19 \times 10^{-3} \text{ rad/sec}$$

Evasion from Origin and Return-to-Orbit

The strategy presented in the previous section provides a
maneuver which maximizes the distance from the origin for a given
amount of fuel (ΔV). Such a maneuver ignores the requirement that the
target vehicle may need to return to its original orbit once the "side-
step" evasion procedure has been carried out. In order to investigate

this problem and make meaningful comparisons, it is useful to describe the maneuver as that which uses the minimum fuel to take the target from the origin to a specified distance in a specified time and then return to orbit.

In the CW frame of reference a return to orbit maneuver brings the target back to the x axis only and not to the origin. At the x axis the velocity components must be nulled. The usual number of impulses necessary to do the maneuver is three, the evasive impulse, the return-to-orbit impulse, and the final impulse to null the velocity. With the distance from the origin specified at a given time, the object is to carry out this maneuver with minimum fuel.

Under these restrictions one might suspect that with unrestricted time the minimum-fuel maneuver would be to perform the evasive burn, remain in that orbit until apogee, and return to the original orbit using a Hohman-like transfer. That such a maneuver sequence is indeed optimal was confirmed computationally by the optimization algorithm and the CW model. The results of this activity are presented in Figs. 4.1, 4.3a, 4.3b, and 4.4.

Figure 4.1 compares the initial angle of thrust for this maneuver with that required for the purely evasive maneuver. It is shown that for all evasion times the angle required for the pure evasion is larger by about 20 degrees than that required for the evasion and return maneuver.

Figure 4.3a compares the initial ΔV and the total ΔV for the "round-trip" maneuver with that required for the purely evasive maneuver. The results indicate that the initial ΔV must be increased

by a small amount and that the total ΔV ranges from about 1.5 to 2.0 times the initial ΔV depending on the evasion time. The maximum value of 2.0 occurs when the evasion time corresponds to 180 degrees of orbit motion with the total maneuver occurring over one complete orbit. In this case the second ΔV goes to zero and the vehicle simply returns to the x axis in the course of moving along the initial evasion orbit. Upon returning to the x axis it has the same velocity as it started with which must be nulled. The initial ΔV for the 180 degree case is just the same as that for the purely evasive maneuver. Hence the initial ΔV curve starts at the value 1 for zero wait time and returns to the value 1 for the 180 degree case with values slightly greater than 1 between these.

Figure 4.3b gives the same information as Figure 4.3a. However, here the evasion distance is held constant at the value of 1 over all evasive times.

Figure 4.4 shows how the total maneuver time varies with the specified evasion time. All maneuvers take between three-quarters and one full orbit to complete. The bulk of this time is taken by the Hohman-like return orbit which requires half an orbit to complete.

The solution to the CW equations is characterized by a periodic motion, with the same period as the reference orbit, plus a secular drift in the x direction. Consequently a return to the x axis is made once each orbit period. Figure 4.4 shows only the time required for the first return to the x axis. Additional curves could be

generated by adding 2kπ (k an integer > 1) to the times indicated in

Figure 4.4. A vehicle could remain in its initial evasion orbit for

several orbital periods and then initiate the return-to-orbit impulse,

or the return-to-orbit impulse could be initiated at the first apogee,

but the final velocity nulling impulse could be delayed until several

orbits later. No additional cost in fuel is occasioned by these

types of maneuvers. As a result considerable flexibility in this

particular maneuver sequence is possible.

Several attempts were made to determie if sequences which in-

cluded more impulses would reduce the fuel consumption further. All

formulations reduced to a three burn sequence for minimum fuel con-

sumption.

Table 4.1 contains a summary of the results for pure evasion

from the origin and an evasion from the origin and return-to-orbit

maneuvers.

Evasion from the Origin and Return-on-Station

A more sophisticated maneuver sequence than those described in

the previous sections is that in which the target makes an evasive

"side step" maneuver and then returns back to the original orbit to

the same position where it would have been had no evasive maneuver taken

place, i.e., it returns-on-station. Several scenarios are presented

here which accomplish this task but which in turn consume various

amounts of fuel. On the other hand various features of each strategy

are attractive from the point of view of time and mission requirements,

as well as fuel considerations.

The first strategy to be examined is that which involves only two impulses to evade and return on station. Although it is not particularly fuel efficient, as we shall see, it has the feature of simplicity and is useful for purposes of comparison. If the CW equations (2.30) are examined for the case where the initial position and final position are at the origin, it is easily shown that such an orbit can occur only if the component of initial velocity in the x direction is zero. Furthermore the time to return to the origin for any amount of thrust in the y direction is exactly one orbit period. Hence the strategy is quite straightforward, thrust ninety degrees from the orbital path and in one orbital period (or any number of orbital periods) the satellite will pass through the origin. At this point a thrust equal in magnitude to the first will null the motion with respect to the original orbit. It is required that the distance from the origin at a specified evasion time must be the same as those shown in Figure 4.2 or Table 4.1 for the comparisons made in Figure 4.5a and Table 4.2, and that the distance from the origin be unity for the comparisons made in Figure 4.5b.

It is clear from these results that the simple two-impulse return-on-station strategy is costly fuel-wise. However the computational requirements are minimal, thrust 90 degrees to the orbit path, the magnitude depending upon how much warning time exists and how big a miss is required. The required radial velocity is given by

$$y_0' = R_{miss}/(5 - 8\cos\tau + 3\cos^2\tau)^{1/2} \tag{4.4}$$

where R_{miss} = desired miss distance

τ = warning time (radians)

An alternative scheme which is attractive from the operational as well as the fuel-consumption point of view is one where the previous sequence of evasion and return to orbit is used followed by a phasing maneuver to enable a return on station. The result would be a three-impulse evasion-and-return-to-orbit maneuver followed by a two-impulse phasing maneuver. This five-impulse sequence reduces to a four-impulse sequence by merging the first phasing impulse with the final return-to-orbit impulse. The resulting fuel cost is unchanged by such a merger. Furthermore, several orbits could be completed in the off-station position before the final phasing maneuver is completed. Finally, as shown below, the fuel consumption required for the final phasing maneuver is inversely proportional to the number of orbits over which the maneuver takes place. Consequently by taking several orbits to complete the phasing maneuver the fuel cost is only slightly more than that required for evasion and return-to-orbit.

In the context of the CW equations, a phasing maneuver is one which moves the satellite from any point on the x axis to the origin. An examination of the CW equations (2.30) indicates that such a maneuver is best carried out over some integral number of orbits. It includes two impulses of equal magnitude directed along the x-axis at the beginning and end of the maneuver. The magnitude is given by the simple expression

$$x_0' = \frac{x_0}{6k\pi} \qquad (4.5)$$

where k = number of orbits required for maneuver.

From eq. (4.5) it can be seen that x_0' can be made quite small by letting k become large. Hence if time is not a factor, this strategy appears to be one worth considering.

A comparison of the total fuel used to evade and return to orbit, to evade and return on station using a one-orbit phasing maneuver, and to evade and return on station using a two-orbit phasing maneuver is shown in Figures 4.6a and 4.6b. It is clear that if the time is available, the additional orbit used during the phasing maneuver reduces the fuel consumption significantly. In fact, from eq. (4.5), the additional phasing orbit reduces the fuel by the amount 1/2 of that for one phasing orbit.

The total maneuver times for the three cases shown in Figure 4.6 are shown in Figure 4.7. Here it is assumed that the last return-to-orbit impulse is merged with the first phasing impulse so that no unnecessary time is spent in the orbit off-station. It should be emphasized that if it is desirable to remain in the orbit off-station for some period of time, only the total time for the maneuver is affected and not the amount of fuel consumed. A summary of various parameters associated with these maneuvers is given in Table 4.3.

Although the above maneuver sequence for returning-on-station is a good candidate from both the operational and fuel-consumption viewpoints, the total maneuver time for best results becomes quite lengthy. However before discussing the time-constrained results in the next section, it is important to investigate some additional unconstrained-time maneuvers. These maneuvers are less flexible than

those discussed previously in that no waiting time is allowed in any of the intermediate orbits and consist of three impulses, the evasive impulse, the return-to-station impulse, and the final impulse to null the relative velocity. Using this scenario one finds several locally-fuel-optimal solutions which depend upon the total maneuver time. Several of these families of local-minimum solutions are discussed here.

The basic maneuver consists of an initial evasive impulse which moves the target away from the origin to be at a specified distance in a specified time. For the cases presented here this time and distance are either those established by the basic evasive maneuver presented in Figures 4.2 and Table 4.1 or a distance of unity for all times. Sometime after the specified distance is reached a second impulse is executed which starts the vehicle on a return orbit to the origin (i.e., "on station"). Upon arriving at the origin, the velocity is nulled. The maneuver can be done in any specified amount of time provided it is larger than that at the specified miss distance. However of interest in the present section is the behavior of the maneuver if unconstrained by time.

The results of this investigation are presented in Figures 4.8a, 4.8b and 4.9 where the total fuel consumed and the total maneuver time are shown for various evasion times respectively. Additional information is given in Table 4.4. Four families of curves are shown, each one corresponding to a local minimum in the range of total maneuver time indicated. Curve A in Figure 4.8 represents the minimum fuel expenditure for various evasion times for total maneuver times in the

neighborhood of fifteen radians or about two-and-a-half orbits. Curve
B gives similar information for total maneuver times in the neighbor-
hood of eight radians or one-and-a-half orbits. Curve C is for ten-
and-one-half radians or one-and-two-thirds orbits while Curve D is
for approximately six radians or one orbit.

The angles for the first impulse to carry out the maneuvers
associated with Curves A and B are about 100 and 92 degrees respective-
ly, both in the second (or fourth) quadrant. Those for Curves C and
D are in the first (or third) quadrant at about 81 and 88 degrees
respectively. In the case of Curve D, the initial impulse angle in-
creases to 90 degrees for an evasion time of 1.35 radians, at which
time the second impulse collapses to zero giving the two-impulse solu-
tion discussed earlier.

The significance of these families of local-minimum fuel consump-
tion is apparent when considering a time constraint on the overall
maneuver. For the time-unconstrained case a good strategy is to per-
form the optimum return-to-orbit maneuver followed by a phasing
maneuver which is completed over several orbits. Under these circum-
stances the total delta-V would approach that for a pure return-to-
orbit as the number of phasing orbits becomes large. However once a
time constraint is placed on the completed maneuver, the strategy
changes significantly, as shown in the next section.

It should be pointed out that additional four-impulse strategies
other than the return-to-orbit-phase sequence discussed above were
investigated. However in all attempts one of the impulse magnitudes
faded to zero with convergence of the optimization process, reducing

the result to one of the three-impulse strategies already discussed.

Time-Constrained Maneuvers--Return-to-Orbit

As discovered earlier, the strategy for optimal evasion and return-to-orbit consists of an evasive impulse, after which the target coasts to apogee, followed by a Hohman-like return-to-orbit. The time of flight takes somewhat less than one orbit to complete, the exact times for various evasion times given in Table (4.1). If however the total maneuver time is constrained, the return-to-orbit maneuver is altered and the fuel consumption is increased as shown below. Although the results presented are for evasion times of 1 and 2 radians, the general trends indicated are typical for all evasion times (a property which is not true when considering a time-constrained return-on-station).

The time-constrained return-to-orbit maneuver results for evasion times of 1 and 2 radians are presented in Fig. 4.10 and Table 4.5. Here it is seen that the fuel consumed increases rapidly as the total maneuver time approaches the evasion time. In addition we can note that eventually the total time of flight is so short that the second impulse to initiate the return to orbit occurs at the specified evasion time. Hence the maneuver is such as to just satisfy the evasion constraint when the return impulse is initiated.

Time-Constrained Maneuvers--Return-on-Station

In the previous section it was observed that as the overall maneuver time is reduced the fuel cost increases in a fairly smooth manner. However for the return-on-station problem a similar smooth curve is not found. The reason for this difference is the existence

of the local minima discussed earlier. As the total maneuver time is reduced the fuel cost for a given evasion strategy increases. Eventually as the time constraint is reduced further, the fuel costs increase to a value which is greater than that for an unconstrained local minimum of possibly less time. At this point the evasion strategy changes abruptly. Such an occurrence happens more than once as the total time for the maneuver is reduced. The actual behavior depends upon the specified evasion time.

As an example the strategy for an evasive maneuver is tracked as the total time allowable for the completed maneuver is reduced for a specified evasion time of one radian. It can be seen from Tables 4.1 and 4.4 that the cost for a return-on-station for strategy "A" using a three-impulse sequence is the same (to three decimal places) as the cost simply to return to orbit. Hence it is clear that a large number of phasing orbits would be required for the return-to-orbit-phasing maneuver to be better than strategy "A". Hence for an evasion time of one radian with the total maneuver time allotment greater than 14.5 radians (2.31 orbits) the fuel costs provided by strategy "A" is optimal.

It should be noted that this statement is clearly not true for different evasion times. From Figures 4.6 and 4.8 it can be seen that fuel cost associated with the return-to-orbit phase-maneuver with two phasing orbits approaches that of strategy "A" as the evasion time exceeds 3 radians. For more phasing orbits the fuel cost would become less than that for strategy "A" at some lower evasion time. On the other hand, for an evasion time of 0.5 radians it appears that

strategy "B" is the best for all total maneuver times exceeding 7.9

radians since the return-to-orbit-only fuel costs are about the same

as strategy "B".

Returning now to the case for the evasion time equal to 1 radian,

we can examine the effect of constraining the total maneuver time.

A summary of results is given in Figure 4.11 and Table 4.6. Here we

see that several strategies come into play as the total time for

maneuver is restricted. As indicated previously, for times greater

than 14.5 radians, strategy "A" is the minimum-fuel strategy. As the

total time is reduced to values below 14.5 radians the "constrained

strategy A" uses an increased amount of fuel as shown in Figure 4.11.

Eventually the amount of fuel consumed increases above that used by

strategy "B" for much less time. Here that situation occurs for

constrained time values slightly less than 14.0 radians. At this

point the best fuel strategy is "B" until the total maneuver time is

reduced to less than 7.96 radians. Here a "constrained strategy B" is

used until its fuel consumption exceeds that used by strategy "D".

In this case this occurs for times-of-flight less than approximately

6.3 radians. Further reduction in total maneuver time causes a

"constrained strategy D" to be the optimal with respect to fuel

consumption. As might be expected the fuel penalty for very short

maneuver times is quite severe. One notes a qualitative similarity to

families of time-constrained attack maneuvers seen in the preceding

section.

An additional characteristic of these constrained maneuvers can

be observed in Table 4.6. For the shorter maneuver times, the

return-to-station impulse (the second impulse) occurs at the specified time and distance from the origin for the evasion portion of the maneuver. Hence it just satisfies that constraint and then returns. This explains the nice even times-of-flight noted for the three shortest total maneuver times.

Evasive Maneuvering Away from Line

The previous results describe various strategies for moving away from the nominal target position (origin) and returning-to-orbit or returning-on-station. It was assumed that the threat occurred at a specific time (evasion time) and at a specific point (the origin). Little consideration was given for the possibility of a closer encounter either before or after the specified evasion time. It was observed in Reference 3 that the miss distance can be significantly less than the distance computed at the specified evasion time. It was also shown in Reference 3 that since the interceptor is near the apogee of its orbit when it encounters the target its velocity is generally slower than that of the target and that a good approximation of the interceptor orbit with respect to the target orbit is a straight line which passes through the origin. Consequently a reasonable strategy for evasion would be to move as far as possible from a given line in a specified time with a specified amount of fuel.

As in the case of the pure evasion away from the origin, the problem of pure evasion away from a line can be solved analytically. Using arguments similar to that for moving away from the origin, we will assume we have an initial impulse of unit magnitude of some angle γ.

The object is to move to the farthest distance from a line passing through the origin at some angle α with respect to the x axis, (see Fig. 2.1). Assuming α less than 90 degrees, an expression for an outward pointing unit vector perpendicular to the line is given by

$$\hat{n} = - \sin \alpha \, \hat{i} + \cos \alpha \, \hat{j} \tag{4.6}$$

The object is to maximize the distance perpendicular to the line given by

$$d = \hat{n} \cdot \bar{r} \tag{4.7}$$

where $\bar{r} = x \, \hat{i} + y \, \hat{j}$

and x and y are given by the CW solution (eq. 2.30) with the initial position at the origin. Equation (4.7) becomes

$$d = - [\cos\gamma \, (4\sin\tau - 3\tau) + 2\sin\gamma \, (1 - \cos\tau)] \sin\alpha$$
$$+ [-2\cos\gamma \, (1 - \cos\tau) + \sin\gamma \, \sin\tau] \cos\alpha \tag{4.8}$$

where τ = evasion time

The initial impulse angle which maximizes this distance is given by

$$\text{Tan } \gamma = \frac{2 \, (1 - \cos\tau) \, \sin\alpha - \sin\tau \, \cos\alpha}{(4\sin\tau - 3\tau) \, \sin\alpha + 2 \, (1 - \cos\tau) \, \cos\alpha} \tag{4.9}$$

This angle is shown in Figure 4.12 for various evasion times. The corresponding distances are displayed in Figure 4.13. Also shown for comparison purposes are the corresponding two curves for pure evasion from the origin calculated previously.

For low evasion times the distances from the origin and from the various lines are nearly equal although the initial impulse angle is significantly different, increasing in value as the line angle with

the x axis increases. As the warning time increases, the initial impulse required for the optimal evasion also increases to angles which are 20 to 30 degrees more than that required for evasion from the origin.

Another feature which is significantly different from that associated with evasion from the origin is that the maximum distance obtainable does not monotonically increase with evasion time. Hence the strategy for evasion from a line can include a waiting period if the evasion time is greater than that required to reach the maximum distance from the line. Consequently in the subsequent sections we are interested only in evasion times less than or equal to those which provide the maximum miss. From Figure 4.13 these times are given by 3.1, 2.8, 2.6, 2.3 and 2.1 radians for lines at angles 0, 5, 10, 15 and 20 degrees respectively.

A summary of the results for pure evasive maneuvers from a line are presented in Table 4.7.

Evasion from Line and Return-to-Orbit

The maneuver discussed in this section is analogous to the evasion from the origin and return to orbit discussed previously. As in that case the proper maneuver is to make the evasive impulse, remain in the evasion orbit until apogee is reached, and then perform a Hohman-like return. Although the complete maneuver takes just under one orbit to complete, there is some flexibility in that the vehicle could remain in the evasion orbit until the second (or more) apogee, pass before initiating the Hohman-like return. Consequently some

multiple of 2π can be added to the total maneuver time without changing the fuel cost.

Results for a line at 5 degrees with respect to the x axis are given in Figures 4.14, 4.15a, and 4.15b and in Table 4.8. In Figure 4.14 we can note that the initial impulse angle for evasion from a line and return-to-orbit approaches that for pure evasion from a line at larger evasion times and in fact becomes the same in this case when the evasion time is 2.8 radians. At the same point we can note from Figure 4.15a that the total delta-V approaches the value of 2. For this value of evasion time (2.8 radians) the pure-evasion-orbit coincides with the evasion-and-return-orbit so that the second impulse decreases to zero and the vehicle returns to the original orbit with the same velocity as it left. Hence the nulling impulse equals the original impulse for a total value of 2. We can also note that the initial impulse is along the negative x axis (180°).

Figure 4.16 shows the total maneuver time as it depends on evasion time. A complete maneuver can always be carried out in less than one orbit. However as indicated previously any multiple of 2π can be added to the total maneuver time without changing the initial angle of impulse or the total fuel consumption.

Several attempts were made to search for minimum-fuel solutions with four impulses. However all four impulse solutions reduced to three when coupled with the optimization algorithm.

Evasion from Line and Return-on-Station

The strategies for returning to the original position in orbit for the case of evasion from a line are analogous to those considered for evasion from the origin. They include: 1) a two-impulse maneuver sequence in which the initial impulse injects the vehicle into an evasion orbit which coincides with a return orbit, 2) a four (or five) impulse maneuver which consists of a return-to-orbit maneuver discussed in the previous section, followed by a phasing maneuver taking place over one or more orbits, and 3) a three-impulse maneuver consisting of an evasive impulse, an intercept or return-to-station impulse, and a velocity-nulling impulse to complete the maneuver. Each of these is discussed below.

As observed previously, the simple two-impulse return-on-station is possible only if the first impulse is along the y axis (in the radial direction). Under these circumstances the evasion orbit appears as an ellipse which is tangent to the y axis and whose major axis lies along the x axis. If the impulse is outward, the ellipse lies on the positive x axis. Consequently the vehicle in the evasion orbit will return to the origin in one orbit period (or in any number of orbit periods) at which time a velocity-nulling impulse is required which is equal in magnitude and opposite in direction to the initial evasive impulse.

For the purposes of comparison it is necessary to constrain the motion so that the vehicle is at least the specified distance from the line for the specified evasion times as shown in Figure 4.13 and Table 4.7, or at a distance of unity. However, because of the relation

of the evasion-orbit ellipse and the straight line it is clear that there is a point (actually two points) on the evasion orbit which is the furthest from the line. Consequently for any evasion times greater than the time it takes to get to this point, the best strategy is to wait, deferring action until the evasion time equals the time it takes to reach that point. Two calculations must be made, the time it takes to get to the farthest distance from a line, and the fuel necessary to equal the distances specified in Figure 4.13 up to and including that time.

A general expression for the fuel required to meet the specifications of Figure 4.13 for the special case of a 90 degree initial impulse can be obtained from eq. (4.8) by setting $\gamma = 90°$ and rearranging. The resulting delta-V requirement is given by

$$y_0' = \Delta V_1 = R_{perp}/[2 (\cos\tau - 1) \sin\alpha + \sin\tau \cos\alpha] \qquad (4.10)$$

where R_{perp} = desired distance from line

τ = evasion time (radians)

Equation (4.10) is valid for evasion times up to and including that required for reaching the maximum distance from the line. This time is determined by differentiating eq. (4.8) with respect to τ and setting the result equal to zero. The result is expressed in terms of the following equation for evasion time for maximum distance from a line at angle α for the special case of a 90° first impulse:

$$\text{Tan } \tau = \frac{1}{2} \cot \alpha \qquad (4.11)$$

The results of these calculations are shown in Figures 4.17a and 4.17b and Table 4.9 for evasion times up to those determined by

eq. (4.11). For evasion times beyond this value the fuel consumption
is constant because the vehicle waits. Although not very fuel-
efficient, this strategy is easy to implement. Once the relative
orbit line angle is known, one thrusts immediately at 90 degrees if
the evasion time is less than the maximum distance time for that line
angle. If the warning time is greater than that value wait, and
thrust at 90 degrees when the appropriate evasion time is left.

By adding a phasing maneuver to the return-to-orbit strategy, the
vehicle can be made to return-on-station. Details of this phasing
operation were discussed previously where the extra fuel cost was
found to be related to eq. (4.5). If that equation is used with the
return-to-orbit results just developed for evasion from a line, the
total fuel and total time requirements for a return-on-station maneuver
can be determined. These results are displayed in Figures 4.18a,
4.18b and 4.19 and in Table 4.10.

The results here are very similar in nature to the results ob-
served for the evasion-from-the-origin cases discussed previously.
Again the extra fuel used for phasing is reduced for each additional
phasing orbit. In the limit as the number of phasing orbits grows
large, the total fuel to return on-station appraoches that for return-
to-orbit. The price, however, is paid in time. The cost in time is
shown for the first two phasing orbits in Figure 4.19.

The reader should be reminded that the return-to-orbit final
impulse can be merged with the initial phasing impulse to result in a
four-impulse maneuver sequence. On the other hand these impulses may
be kept separate allowing the vehicle to remain in orbit but off-station

for any desired amount of time before initiating the phasing impulse without any additional cost in fuel. The resulting five-impulse maneuver is the most flexible of all since the return-on-station can occur at any specified time as long as it is greater than that required for one phasing orbit with no wait as shown in Figure 4.19.

The final strategy to be discussed is the three-impulse evasion-from-a-line and return-on-station. There are several locally optimum solutions similar in nature to those observed for the case of evasion from the origin and return-on-station. Two of these are shown in Figures 4.20 and 4.21. Additional details concerning these solutions are given in Table 4.11.

If we examine Figure 4.20 with concern for fuel consumption only we can see that the return-to-orbit with a large number of phasing orbits is the best strategy with fuel consumption approaching that for the return-to-orbit case. For evasion times less than 1.2 radians, the three-impulse maneuver associated with strategy "A" uses less fuel than the return-to-orbit with a two-phasing-orbit strategy. In all cases strategy "A" uses less fuel than a return-to-orbit with one phasing orbit maneuver. The factor which ultimately lets one pick a particular strategy is the time allotted for the maneuver. The three-impulse strategy "A" takes about the same time as the return-to-orbit-with-one-phasing-orbit procedure for long evasive times (2.5 radians) but take significantly less time for short evasive times (0.5 radians). On the other hand the three-impulse strategy "B" requires significantly less time than both of the above maneuvers at the price of using considerably more fuel. However at low evasion times strategy "B"

uses less than the one orbit phasing maneuver, hence it has both a time and fuel advantage.

An interesting characteristic of maneuver "B" is that the intercept impulse to return the vehicle on-station occurs at the specified evasion time indicating that this strategy is most likely the fastest three-impulse optimal maneuver possible.

Time-Constrained Maneuvers--Return-to-Orbit

Although some discussion concerning time was included in the previous evasion-from-a-line results, the main purpose was to present the time-open strategies. In this section the return-to-orbit maneuver is examined subject to a constraint on the overall maneuver time. For the purposes of discussion only one case will be considered, evasion from a line angled at 5 degrees with respect to the x axis with an evasion time of 1 radian. We will examine the behavior of the minimum-fuel solutions as the maneuver time is reduced below the values indicated in Figure 4.19.

The results are presented in Figure 4.22 and in Table 4.12. As expected, the fuel cost increases as the total maneuver time is reduced. The best maneuver consists of a three impulse sequence until an evasion time of slightly less than 3.0 radians is encountered. At this point the middle impulse fades out to zero and a two-impulse maneuver-sequence results. In addition we can note from Figure 4.23 that, as the constraint on the maneuver time is reduced, the initial impulse angle also is reduced until the two-impulse solution is reached with an initial impulse angle of 90 degrees. At this point a further

reduction in total maneuver time again requires a three-impulse
maneuver sequence to minimize the fuel consumption. For these tra-
jectories, however, an additional constraint enters into the problem
as indicated by the time-of-flight for the first orbit (see Table
4.12). Here we see the first orbit just satisfies the distance-from-
the-line condition when the impulse to return to orbit occurs. The
effect of this constraint is to make the initial impulse angle increase
as the time is reduced further. The curves for a continued two-impulse
strategy as time is reduced are shown as dashed lines in Figures 4.22
and 4.23 for comparison purposes.

Time-Constrained Maneuvers--Return-on-Station

The final strategy to be investigated is that which includes an
evasive maneuver from a line and a return-on-station with the total
maneuver time constrained. The problem examined in the previous section
is continued here. The results for an evasion time of 1 radian are
presented in Figures 4.24 and 4.25 and in Tables 4.13 and 4.14.

The longer maneuver times favor the return-to-orbit-phase-maneuver
strategy with more phasing orbits with increasing time. Beyond 4 or 5
phasing orbits the decrease in fuel is small. For example the total
fuel used for a 4-phasing-orbit procedure is 2.108 while for 5 phasing
orbits it is 2.042, an improvement of about 3 percent. The data of
Table 4.14 are obtained from the constrained return-to-orbit results
of Table 4.12 and the use of eq. (4.5).

The fuel costs for the various maneuvers are shown in Figure
4.24 from which a constrained-time strategy can be developed. For
large maneuver times greater than about 30.0 radians one uses a

return-to-orbit with a 4-phase-orbit procedure. For times between
24.4 and 30.0 radians one uses an unconstrained 3-phase-orbit maneuver,
switching to the constrained return-to-orbit-3-phase maneuver as times
decrease to 23.6 radians. For times between 8.5 and 24.4 an un-
constrained three-impulse maneuver "A" is desired, with the "constrained
maneuver A" used for times between 6.3 and 8.5 radians. Finally the
"constrained strategy B" should be used for short warning times less
than 6.3 radians. The corresponding initial impulse angles are shown
in Figure 4.25.

Summary

The strategies for minimum-fuel evasion-from-the-origin and
evasion-from-a-line have been investigated for the cases of pure
evasion, evasion and return-to-orbit and evasion and return-on-station.
The pure evasion results consist of initial impulse angles which
maximize the appropriate distance for a given amount of fuel. The
results are independent of orbit altitude. For the case of evasion-
from-a-point, the greater the warning time, the greater the distance
achievable (at least within the warning time considered). For the
case of evasion-from-a-line, however, there is an evasion time which
gives the maximum distance. Warning times greater than this value
are not needed.

The return-to-orbit strategies are basically the same for the
evasion-from-the-origin or evasion-from-a-line scenarios. They
consist of the evasive maneuver, a coast out to apogee and a Hohman-
like return to orbit. The feature here is the flexibility of the

maneuver, allowing the return-to-orbit after one or more orbit periods.

Return-on-station strategies generally can be considered to be one of two forms, a return-to-orbit maneuver followed by a phasing procedure which can take one or more orbits, or a three-impulse maneuver which consists of an evasive impulse followed by an intercept impulse and concluded by a velocity-nulling impulse. In general for shorter evasive times the three-impulse maneuver is most efficient.

Finally time-constrained maneuvers were considered with the general result indicating that fuel costs increase as the total maneuver time allowed is reduced. Additionally, as the total maneuver time is reduced, discontinuities in strategy are encountered to keep the fuel costs minimal.

TABLE 4.1

Pure Evasion from Origin

Evasion Time	Angle	Distance	Delta-V		Time-of-Flight
			ΔV_1	ΔV_{total}	
0.5	104.3	0.542	1.0	-	-
1.0	118.3	1.338	1.0	-	-
1.5	131.3	2.628	1.0	-	-
2.0	142.2	4.560	1.0	-	-
2.5	151.0	7.102	1.0	-	-
3.0	158.1	10.038	1.0	-	-

Evasion from Origin and Return to Orbit

0.5	92.5	0.542	1.004	1.508	4.800
1.0	101.0	1.338	1.027	1.568	5.084
1.5	112.3	2.628	1.046	1.672	5.399
2.0	124.3	4.560	1.046	1.778	5.651
2.5	135.7	7.102	1.035	1.860	5.830
3.0	145.9	10.033	1.023	1.917	5.955

TABLE 4.2

Two-Impulse Evasion from Origin and Return-on-Station

Evasion Time (rad)	Minimum Distance	ΔV_1	ΔV_{total}
0.5	0.542	1.001	2.002
1.0	1.338	1.073	2.146
1.5	2.628	1.246	2.492
2.0	4.560	1.533	3.066
2.5	7.102	1.945	3.890
3.0	10.038	2.521	5.042

TABLE 4.3

Evasion from Origin and Return-on-Station Parameters

Evasion Time	ΔV_{total} Return-to-Orbit	x Position on Return	ΔV_1 Phasing Maneuver 1 Orbit (2 Orbits)	ΔV_{total} Return-to-Station	Total Maneuver Time
0.5	1.508	4.805	0.255 (0.127)	2.018 (1.763)	11.083 (17.366)
1.0	1.568	6.635	0.352 (0.176)	2.274 (1.920)	11.367 (17.650)
1.5	1.672	9.444	0.501 (0.250)	2.674 (2.173)	11.682 (17.966)
2.0	1.778	12.398	0.658 (0.329)	3.093 (2.438)	11.934 (18.218)
2.5	1.860	14.801	0.785 (0.393)	3.431 (2.645)	12.113 (18.396)
3.0	1.917	16.491	0.875 (0.488)	3.667 (2.792)	12.237 (18.520)

TABLE 4.4

Three-Impulse Return-on-Station Parameters

Evasion Time	Angle of Initial Impulse	Delta-V		Time of Flight		
		ΔV_1	ΔV_{total}	Orbit 1	Orbit 2	Total
Maneuver A						
0.25	100.63	1.000	1.526	5.085	9.387	14.464
0.5	100.64	1.000	1.527	5.084	9.382	14.466
1.0	100.72	1.028	1.568	5.074	9.427	14.501
1.5	100.95	1.124	1.717	5.049	9.543	14.589
2.0	101.63	1.279	1.969	4.989	9.802	14.791
2.5	104.98	1.411	2.289	4.918	10.492	15.410
3.0	117.54	1.306	2.588	5.169	11.461	16.630
Maneuver B						
0.25	91.07	1.000	1.501	4.752	3.136	7.888
0.5	91.11	1.006	1.509	4.745	3.154	7.900
1.0	91.40	1.066	1.601	4.706	3.257	7.963
1.5	92.01	1.220	1.840	4.635	3.460	8.095
2.0	93.81	1.447	2.222	4.531	3.815	8.346
2.5	97.14	1.638	2.715	4.447	4.475	8.922
3.0	107.23	1.560	3.208	4.699	5.247	9.946

TABLE 4.4 (cont.)

Evasion Time	Angle of Initial Impulse	Delta-V		Time of Flight		
		ΔV_1	ΔV_{total}	Orbit 1	Orbit 2	Total
Maneuver C						
0.25	80.78	1.002	1.523	7.557	3.091	10.648
0.5	80.82	1.018	1.546	7.564	3.073	10.637
1.0	80.93	1.129	1.715	7.590	3.002	10.592
1.5	81.10	1.390	2.116	7.624	2.915	10.539
2.0	81.26	1.835	2.802	7.656	2.827	10.484
2.5	81.43	2.535	3.886	7.688	2.743	10.431
Maneuver D						
0.25	68.40	1.007	1.827	0.912	4.616	5.528
0.5	72.68	1.031	1.879	1.034	4.615	5.649
1.0	82.91	1.116	2.114	1.374	4.627	6.001
1.3	88.84	1.175	2.326	1.596	4.641	6.237
1.35	89.81	1.184	2.365	1.633	4.643	6.276
1.40	90.00	1.202	2.404	-	6.283	6.283
2.0	90.00	1.533	3.066	-	6.283	6.283
2.5	90.00	1.945	3.890	-	6.283	6.283
3.0	90.00	2.521	5.042	-	6.283	6.283
Maneuver E						
1.5	100.43	1.129	1.720	11.330	15.767	27.097
2.0	100.58	1.297	1.981	11.298	15.884	27.182

TABLE 4.5

Time-Constrained Evasion and Return-to-Orbit
Evasion Time = 1 Radian

Constraint Time	Angle of Initial Impulse	Delta-V		Time of Flight		
		ΔV_1	ΔV_{total}	Orbit 1	Orbit 2	Total
6.000	101.04	1.027	1.568	1.943	3.142	5.085
5.000	99.79	1.031 ·	1.569	1.948	3.052	5.000
4.500	93.20	1.057	1.609	1.910	2.590	4.500
4.000	87.50	1.087	1.690	1.798	2.202	4.000
3.500	82.24	1.120	1.806	1.647	1.853	3.500
3.000	77.12	1.158	1.956	1.474	1.526	3.000
2.500	71.98	1.201	2.140	1.291	1.209	2.500
2.000	66.92	1.248	2.360	1.108	0.892	2.000
1.500	61.78	1.299	2.598	1.028	0.472	1.500

Evasion Time = 2 Radians

6.000	124.33	1.046	1.778	2.510	3.142	5.651
5.000	117.20	1.172	1.898	2.623	2.377	5.000
4.000	94.93	1.409	2.366	2.343	1.657	4.000
3.000	85.54	1.672	3.162	2.000	1.000	3.000

TABLE 4.6

Fuel Consumption in the Presence of Time Constraints

Time Constraint	Strategy	Angle of Initial Impulse	Delta-V		Time-of-Flight		
			ΔV_1	ΔV_{total}	Orbit 1	Orbit 2	Total
14.501	A	100.72	1.028	1.568	5.074	9.427	14.501
14.000	A	100.38	1.029	1.589	5.220	8.780	14.00
13.000	A	99.24	1.033	1.829	5.477	7.523	13.00
13.000	B	91.40	1.066	1.601	4.706	3.257	7.963
7.000	B	89.79	1.074	1.742	5.173	1.827	7.000
6.500	B	89.77	1.074	1.989	5.334	1.166	6.500
6.300	B	89.98	1.073	2.134	5.356	0.944	6.300
6.300	D	82.88	1.112	2.114	1.374	4.627	6.001
6.000	D	82.88	1.112	2.114	1.374	4.626	6.000
5.000	D	70.84	1.211	2.289	1.239	3.761	5.000
4.300	D	64.08	1.275	2.523	1.001	3.299	4.300
4.000	D	62.02	1.296	2.646	1.000	3.000	4.000
3.000	D	55.03	1.369	3.267	1.000	2.000	3.000
2.000	D	47.52	1.446	4.846	1.000	1.000	2.000

TABLE 4.7

Pure Evasion from Line

Evasion Time	α = 0		α = 5		α = 10	
	Angle	Distance	Angle	Distance	Angle	Distance
0.5	117.05	0.538	121.56	0.535	136.59	0.531
1.0	137.53	1.246	141.34	1.214	145.38	1.177
1.5	151.78	2.109	155.28	1.989	159.26	1.862
2.0	162.20	2.975	165.86	2.697	170.37	2.413
2.5	170.57	3.652	174.87	3.156	180.78	2.661
3.0	177.97	3.982	183.65	3.236	192.68	2.516

	α = 15		α = 20	
0.5	130.76	0.528	135.48	0.523
1.0	149.67	1.138	154.29	1.098
1.5	163.82	1.732	169.14	1.601
2.0	176.09	2.129	183.53	1.857
2.5	189.32	2.187	202.23	1.770
3.0	208.28	1.886	235.17	1.497

TABLE 4.8

Evasion from Line and Return to Orbit

$\alpha = 5°$

Evasion Time	Angle	Perpendicular Distance	Delta-V		Time of Flight	
			ΔV_1	ΔV_{total}	Orbit 1	Total
0.5	107.74	0.535	1.030	1.612	2.140	5.282
1.0	125.00	1.214	1.042	1.777	2.521	5.663
1.5	142.23	1.989	1.026	1.897	2.772	5.914
2.0	157.70	2.697	1.010	1.964	2.939	6.081
2.5	171.81	3.156	1.001	1.996	3.163	6.211

TABLE 4.9

Two Impulse Evasion from Line and Return-on-Station

Evasion Time	Minimum Perpendicular Distance	Delta-V	
		ΔV_1	ΔV_{total}
$\alpha = 0°$			
0.5	0.538	1.122	2.244
1.0	1.245	1.480	2.960
1.5	2.109	2.114	4.228
1.571	2.236	2.236	4.472
$\alpha = 5°$			
0.5	0.535	1.172	2.344
1.0	1.214	1.602	3.204
1.398	1.830	2.186	4.372
$\alpha = 10°$			
0.5	0.531	1.236	2.472
1.0	1.177	1.759	3.518
1.232	1.500	2.152	4.304
$\alpha = 15°$			
0.5	0.528	1.321	2.642
1.0	1.138	1.980	3.960
1.079	1.238	2.141	4.282
$\alpha = 20°$			
0.5	0.523	1.426	2.852
0.942	1.031	2.156	4.312

TABLE 4.10

Evasion from Line and Return-on-Station Parameters

Evasion Time	ΔV_{total} Return-to-Orbit	x Position on Return	ΔV_1 Phasing Maneuver 1 Orbit (2 Orbits)	ΔV_{total} Return to Station	Total Maneuver Time
0.5	1.612	8.200	0.435 (0.218)	2.482 (2.047)	11.565 (17.848)
1.0	1.777	12.506	0.663 (0.332)	3.104 (2.440)	11.946 (18.229)
1.5	1.897	15.930	0.845 0.423	3.587 (2.742)	12.197 (18.480)
2.0	1.964	17.910	0.950 0.475	3.864 (2.914)	12.364 (18.647)
2.5	1.996	18.765	0.996 0.498	3.987 (2.992)	12.494 (18.777)

TABLE 4.11

Evasion from Line and Return-on-Station Parameters

Evasion Time	Angle of Initial Impulse	Delta-V		Time of Flight		
		ΔV_1	ΔV_{total}	Orbit 1	Orbit 2	Total
Maneuver A $\alpha = 5°$						
0.5	91.94	1.150	1.734	4.642	3.440	8.082
1.0	94.23	1.400	2.295	4.488	4.013	8.501
1.5	105.08	1.562	3.074	4.626	5.137	9.764
2.0	130.24	1.230	3.690	5.413	5.823	11.236
2.5	162.89	1.022	3.966	6.051	6.228	12.174
Maneuver B $\alpha = 5°$						
0.5	90.00	1.172	2.344	6.282	-	6.282
1.0	95.66	1.437	3.194	1.000	5.296	6.296
1.5	125.48	1.152	4.228	1.500	5.101	6.601
2.0	154.14	1.021	5.095	2.000	4.996	6.996
2.5	184.58	1.014	5.677	2.500	4.901	7.401

TABLE 4.12

Effect of Maneuver Time Constraints on Evasion from Line and Return-to-Orbit Maneuver

$\alpha = 5°$ $\qquad$ $\tau = 1.0$ $\qquad$ $d(\tau) = 1.214$

Three Impulse

| Constraint Time | Angle of Initial Impulse | Delta-V | | x Final | Time-of-Flight | |
		ΔV_1	ΔV_{total}		Orbit 1	Orbit 2
5.663*	125.00	1.042	1.777	12.506	2.521	3.142
5.000	110.01	1.171	1.910	9.700	2.678	2.322
4.500	102.10	1.291	2.130	8.199	2.582	1.918
4.000	96.01	1.422	2.432	7.128	2.423	1.577
3.500	91.13	1.563	2.830	6.407	2.244	1.256
3.000	87.31	1.702	3.351	6.056	2.065	0.935
2.800	101.89	1.295	3.486	3.782	1.000	1.800
2.500	103.80	1.261	3.850	3.080	1.000	1.500
2.000	108.64	1.188	4.830	2.114	1.000	1.000
1.500	120.45	1.070	7.498	1.184	1.000	0.500

Two Impulse

Constraint Time	Angle of Initial Impulse	ΔV_1	ΔV_{total}	x Final	Orbit 1	Orbit 2
2.8	85.07	1.801	3.602	5.878	2.800	-
2.5	80.57	2.048	4.096	5.564	2.500	-
2.0	72.20	2.809	5.617	5.545	2.000	-

*unconstrained time-of-flight

TABLE 4.13

Effect of Maneuver Time Constraint on Evasion-from-Line
and Return-on-Station Maneuver

$\alpha = 5°$ $\qquad \tau = 1.0$ $\qquad d(\tau) = 1.214$

Constraint Time	Strategy	Angle of Initial Impulse	Delta-V		Time-of-Flight		
			ΔV_1	ΔV_{total}	Orbit 1	Orbit 2	Total
8.501*	A	94.23	1.470	2.295	4.488	4.013	8.501
8.000	A	92.06	1.533	2.319	4.646	3.353	8.000
7.500	A	90.67	1.578	2.409	4.888	2.612	7.500
7.000	A	89.94	1.603	2.604	5.144	1.855	7.000
6.500	A	89.84	1.606	2.976	5.316	1.184	6.500
6.000	A	86.82	1.723	3.429	2.255	3.745	6.000
6.296*	B	95.66	1.431	3.194	1.000	5.296	6.296
6.000	B	103.53	1.266	3.318	1.000	5.000	6.000
5.000	B	118.37	1.086	3.862	1.000	4.000	5.000
4.000	B	134.68	1.007	4.429	1.000	3.000	4.000
3.000	B	157.41	1.041	4.950	1.000	2.000	3.000
2.000	B	166.79	1.107	5.744	1.000	1.000	2.000

*unconstrained time-of-flight

TABLE 4.14

Effect of Maneuver Time Constraints on Evasion-from-
Line, Return-to-Orbit and Phasing Maneuver

$\alpha = 5°$	$\tau = 1.0$	$d(\tau) = 1.214$	
Constraint Time	Phasing Orbit	Angle of Initial Impulse	ΔV_{total}
30.796*	4	125.00	2.108
30.133	4	110.01	2.167
29.633	4	102.10	2.347
24.512*	3	125.00	2.219
23.850	3	110.01	2.253
23.350	3	102.10	2.420
18.229*	2	125.00	2.440
17.566	2	110.01	2.425
17.066	2	102.10	2.565
11.946	1	125.00	3.104
11.283	1	110.01	2.939
10.783	1	102.10	3.000

*unconstrained time-of-flight

Evasion from origin only

Evasion from origin and
Return-to-orbit

EVASION TIME (RADIANS)
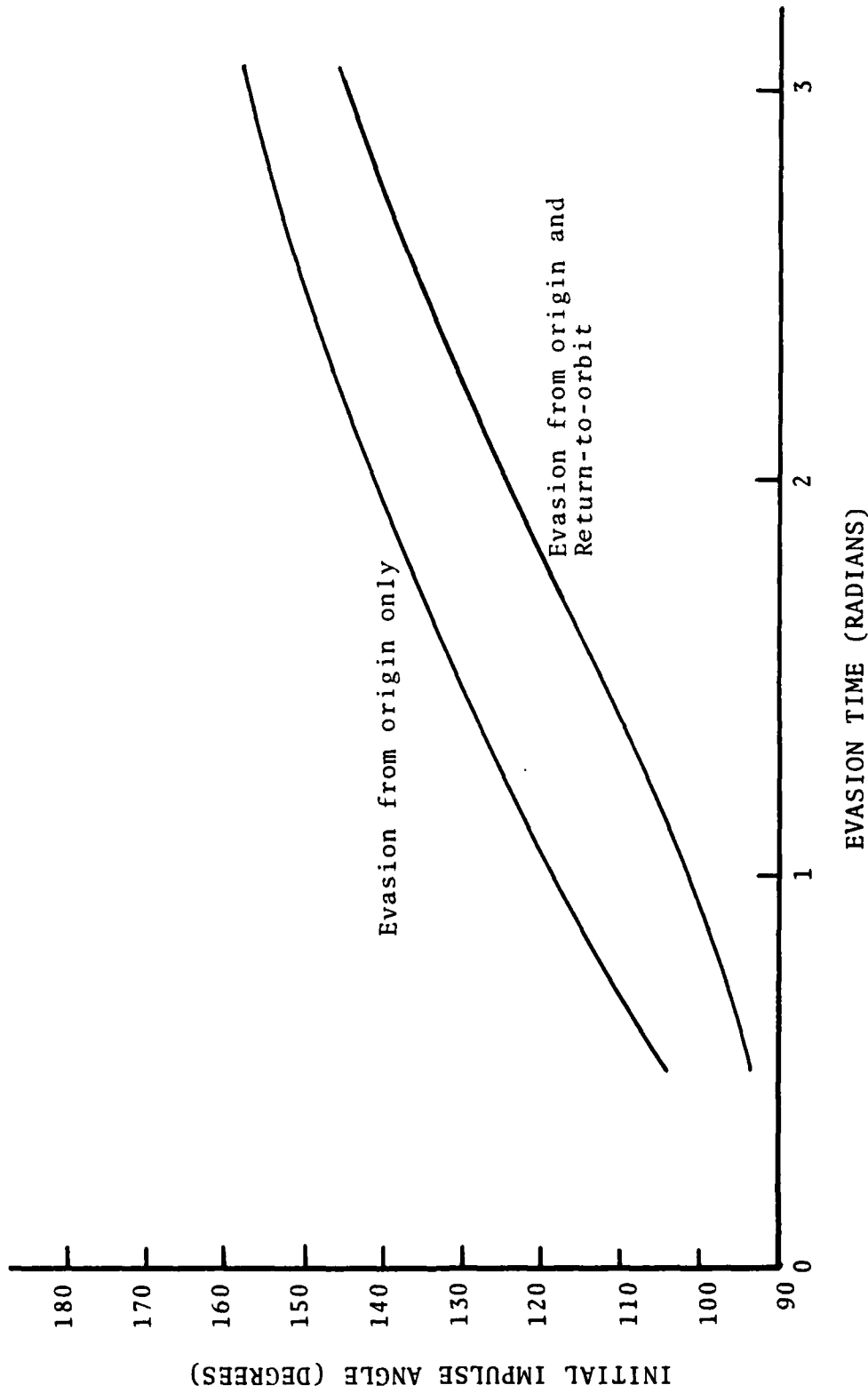
FIGURE 4.1 Initial Impulse Angle

INITIAL IMPULSE ANGLE (DEGREES)

180
170
160
150
140
130
120
110
100
90

0
1
2
3
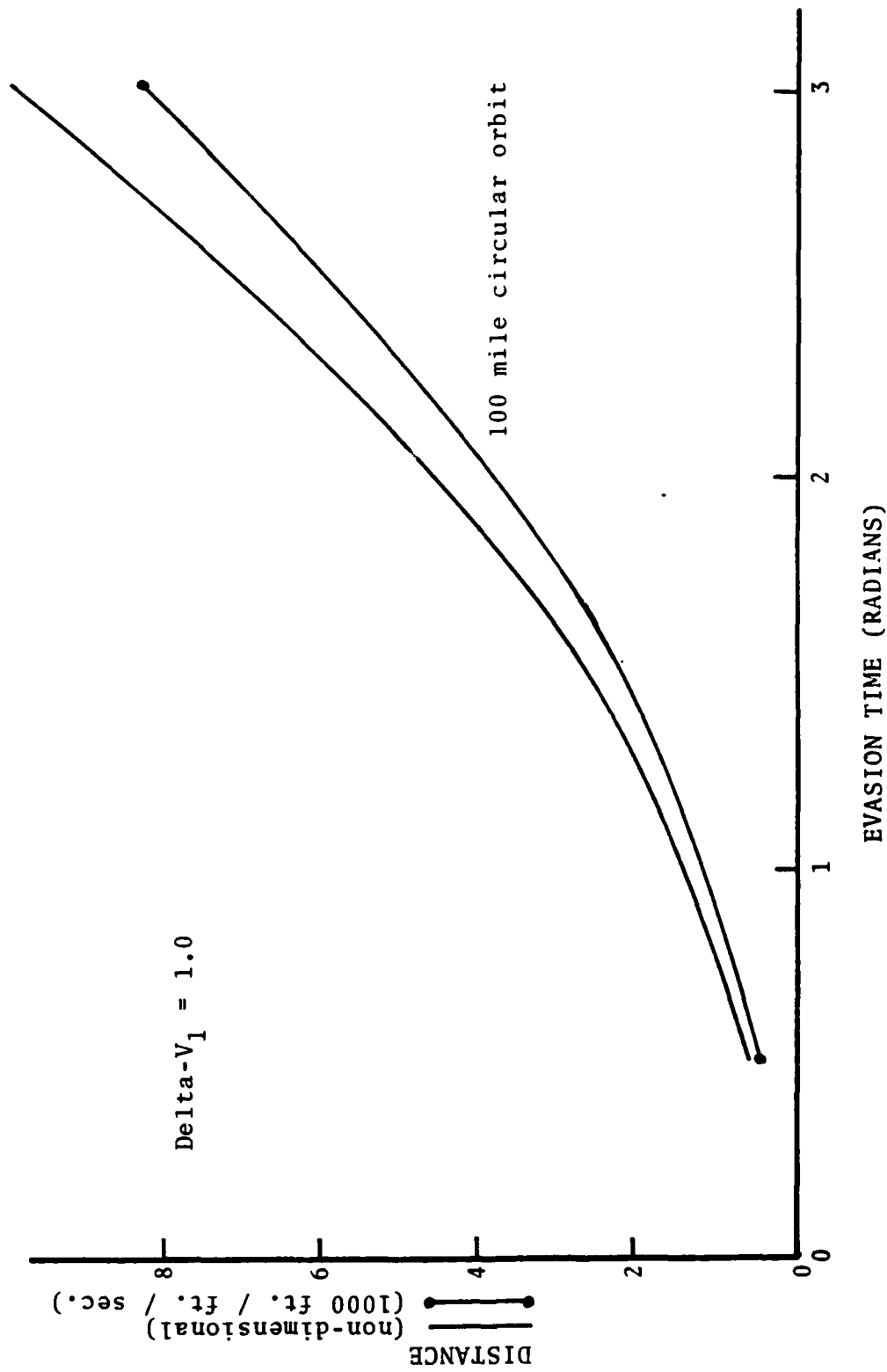
FIGURE 4.2 Distance from Origin

Delta-V$_{Ref}$ = Delta-V required using optimal evasion from origin strategy to achieve same distance in specified time as current maneuver of interest

Delta-V$_{Total}$

Delta-V$_1$

2

1

DELTA-V / DELTA-V$_{Ref}$

0

1

2

3

EVASION TIME (RADIANS)
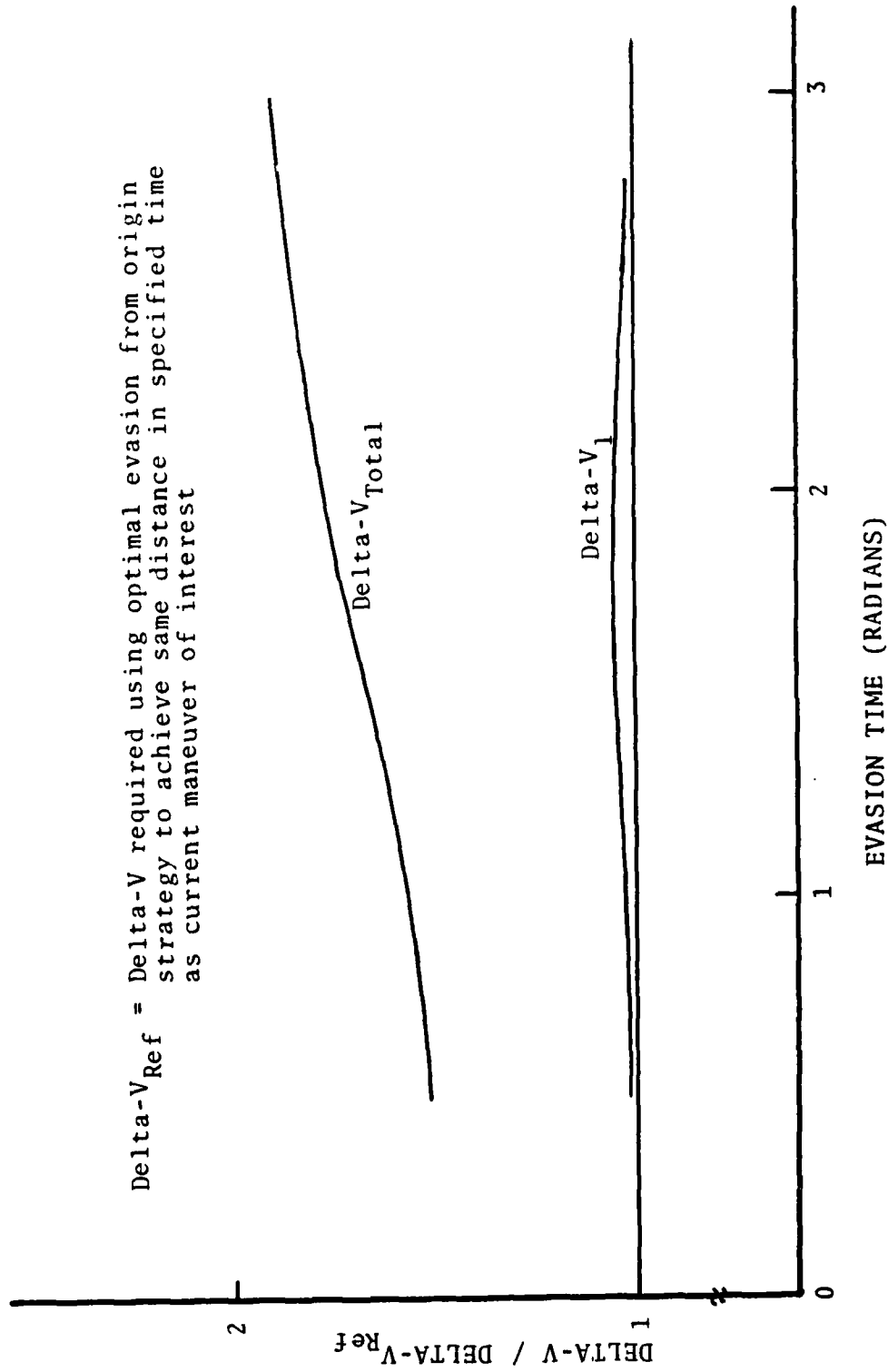
FIGURE 4.3a Delta-V Requirements for Evasion and Return-to-Orbit
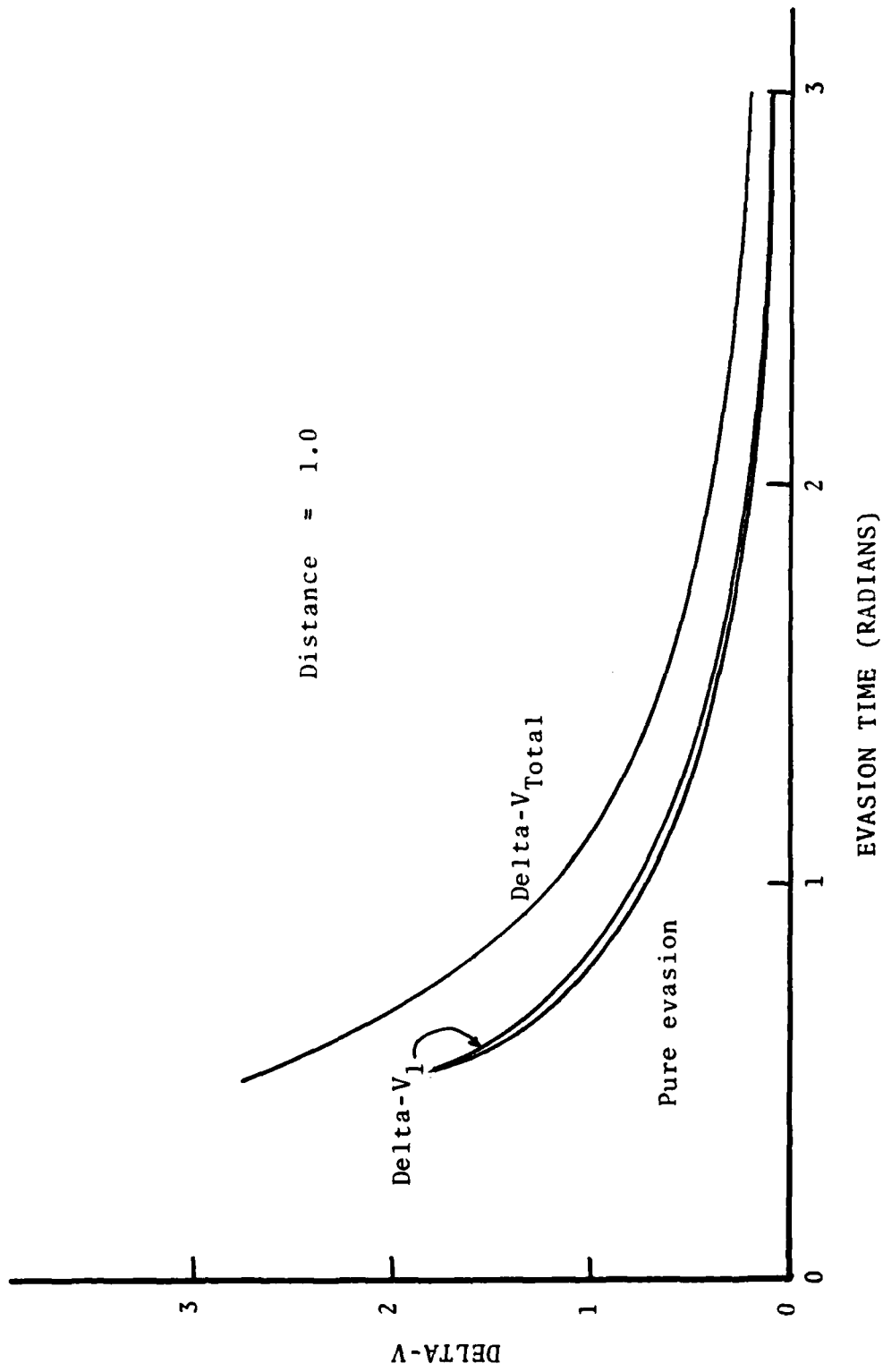
FIGURE 4.3b Delta-V Requirements for Evasion and
              Return-to-Orbit
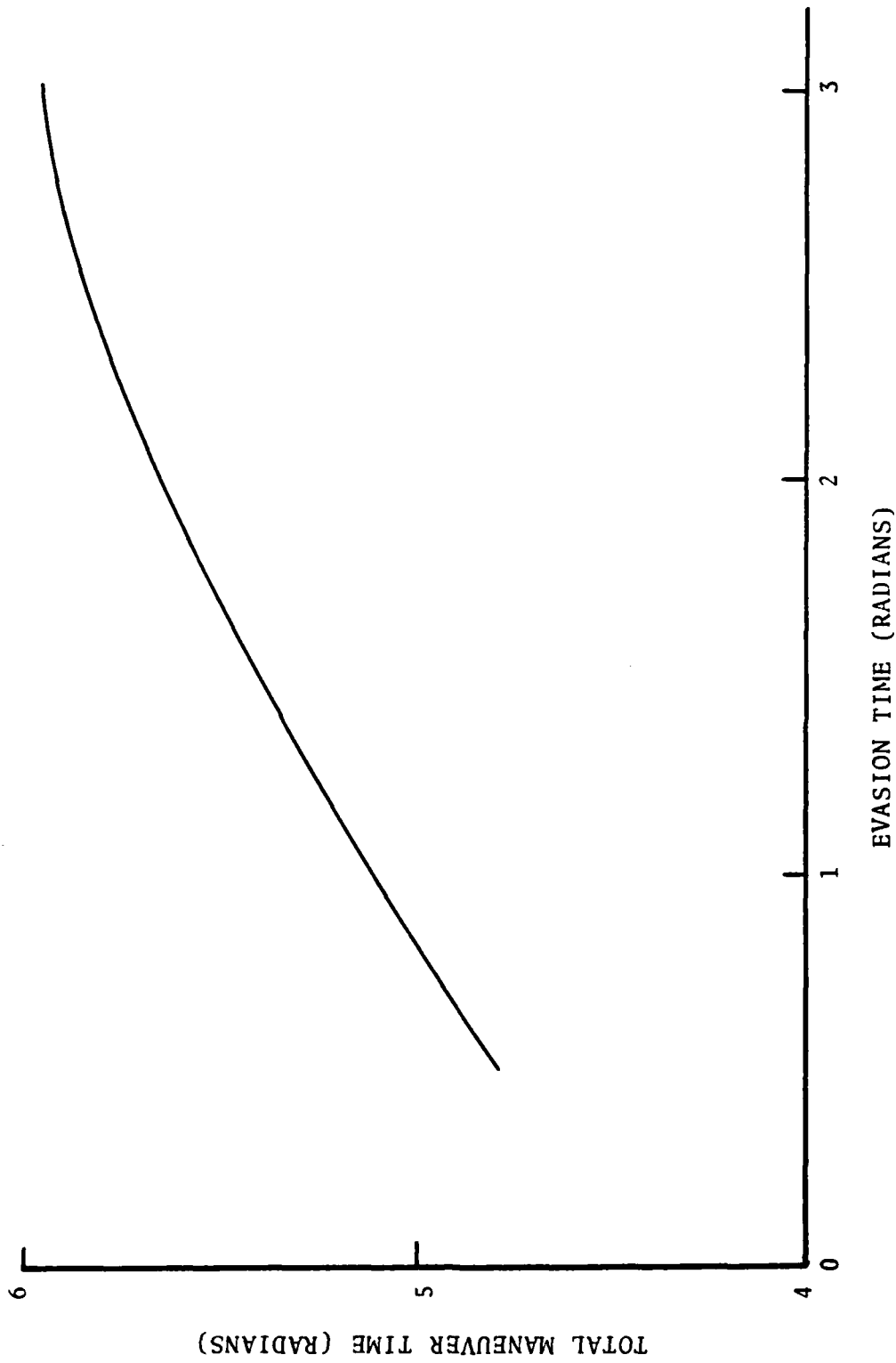
FIGURE 4.4   Total Maneuver Time to Evade from Origin and Return-to-Orbit

EVASION TIME (RADIANS)

TOTAL MANEUVER TIME (RADIANS)

Delta-V_1 angle = 90 degrees
Total maneuver time = 2π radians

Delta-V_{Total}

Delta-V_1

EVASION TIME (RADIANS)
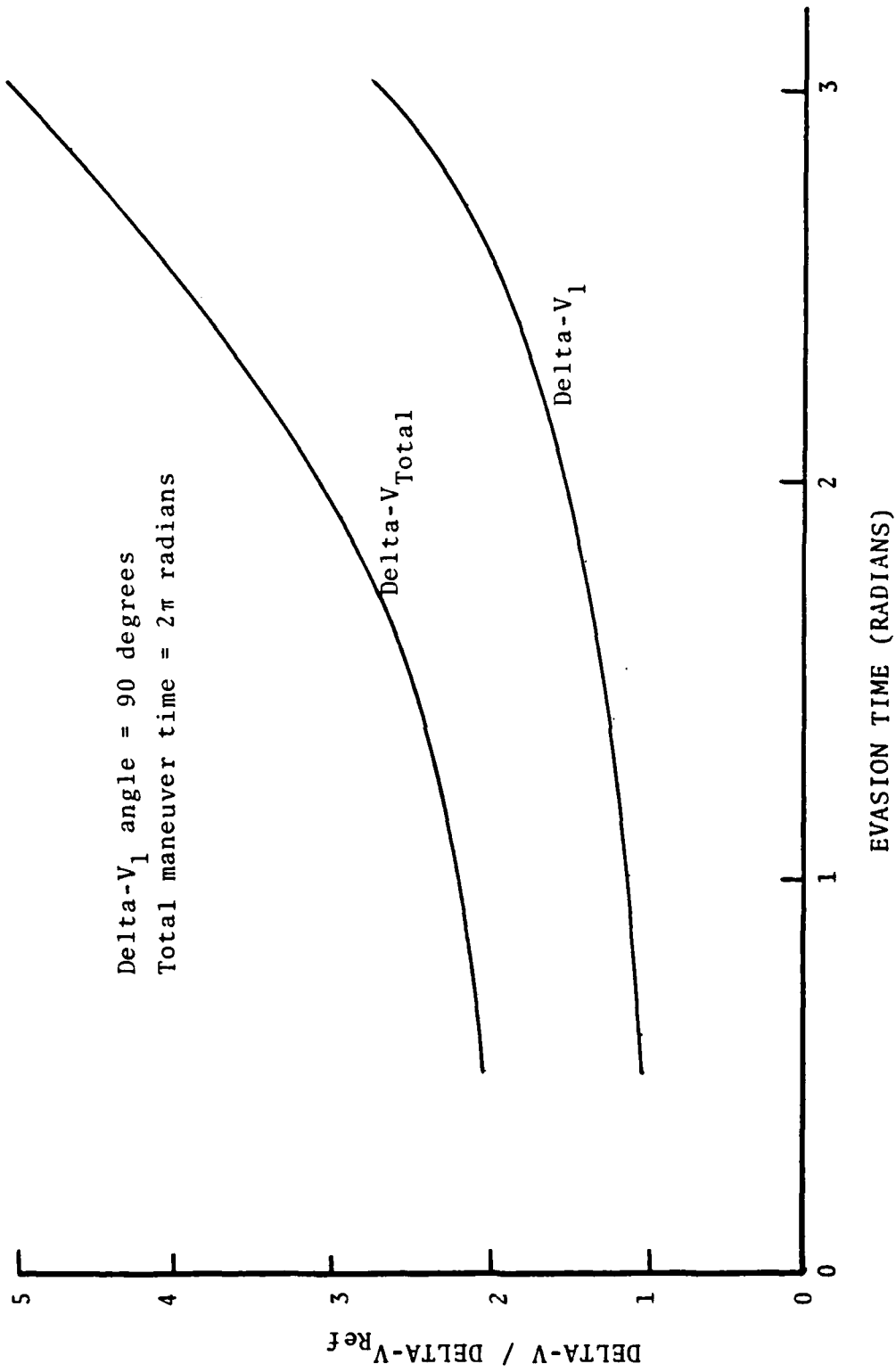
DELTA-V / DELTA-V_{Ref}

FIGURE 4.5a Delta-V Requirements for Two-Impulse Evasion
and Return-on-Station

Distance = 1.0

Delta-V$_{Total}$

Delta-V$_1$

DELTA-V

EVASION TIME (RADIANS)
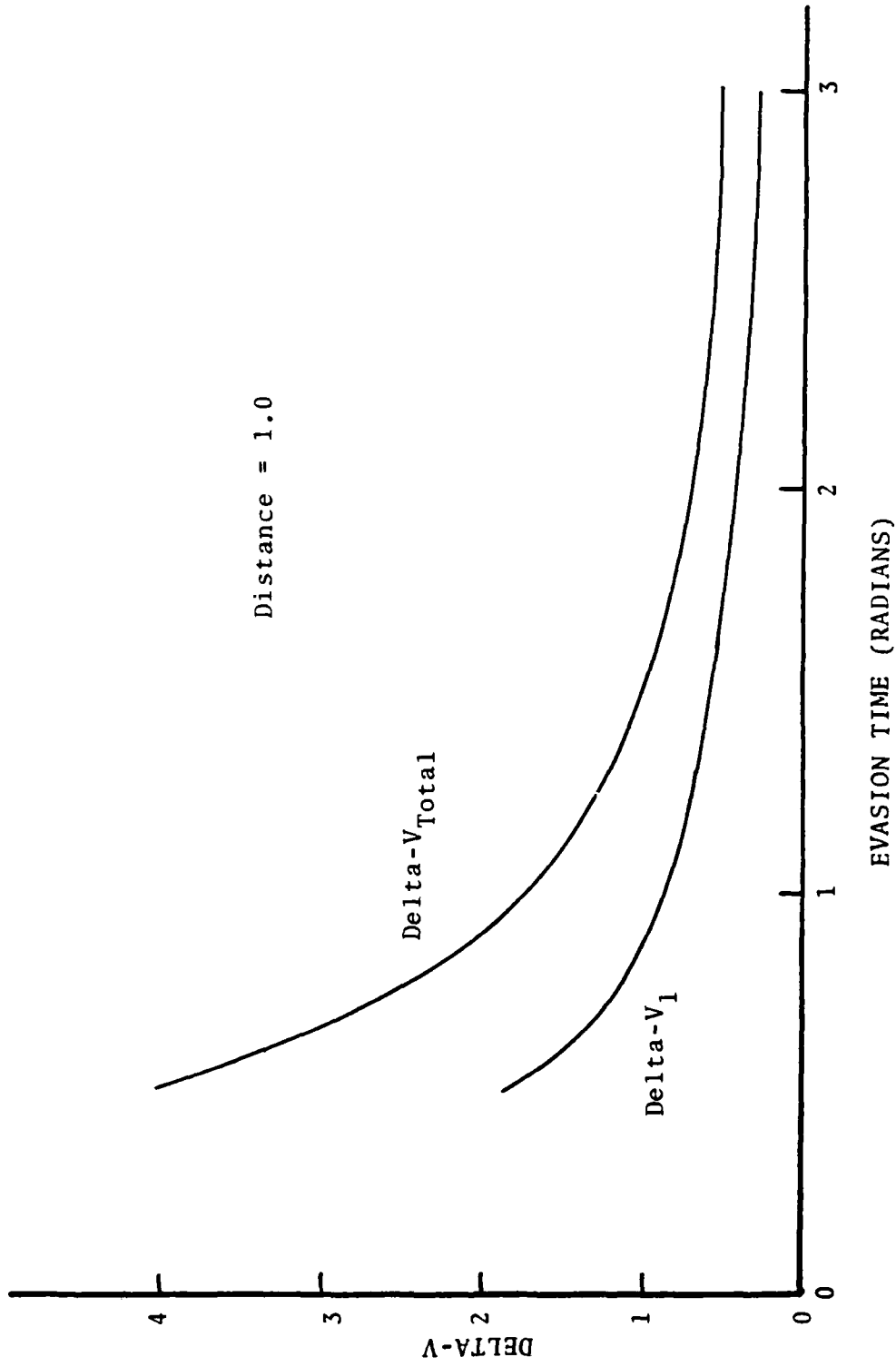
FIGURE 4.5b   Delta-V Requirements for Two-Impulse Evasion
and Return-on-Station
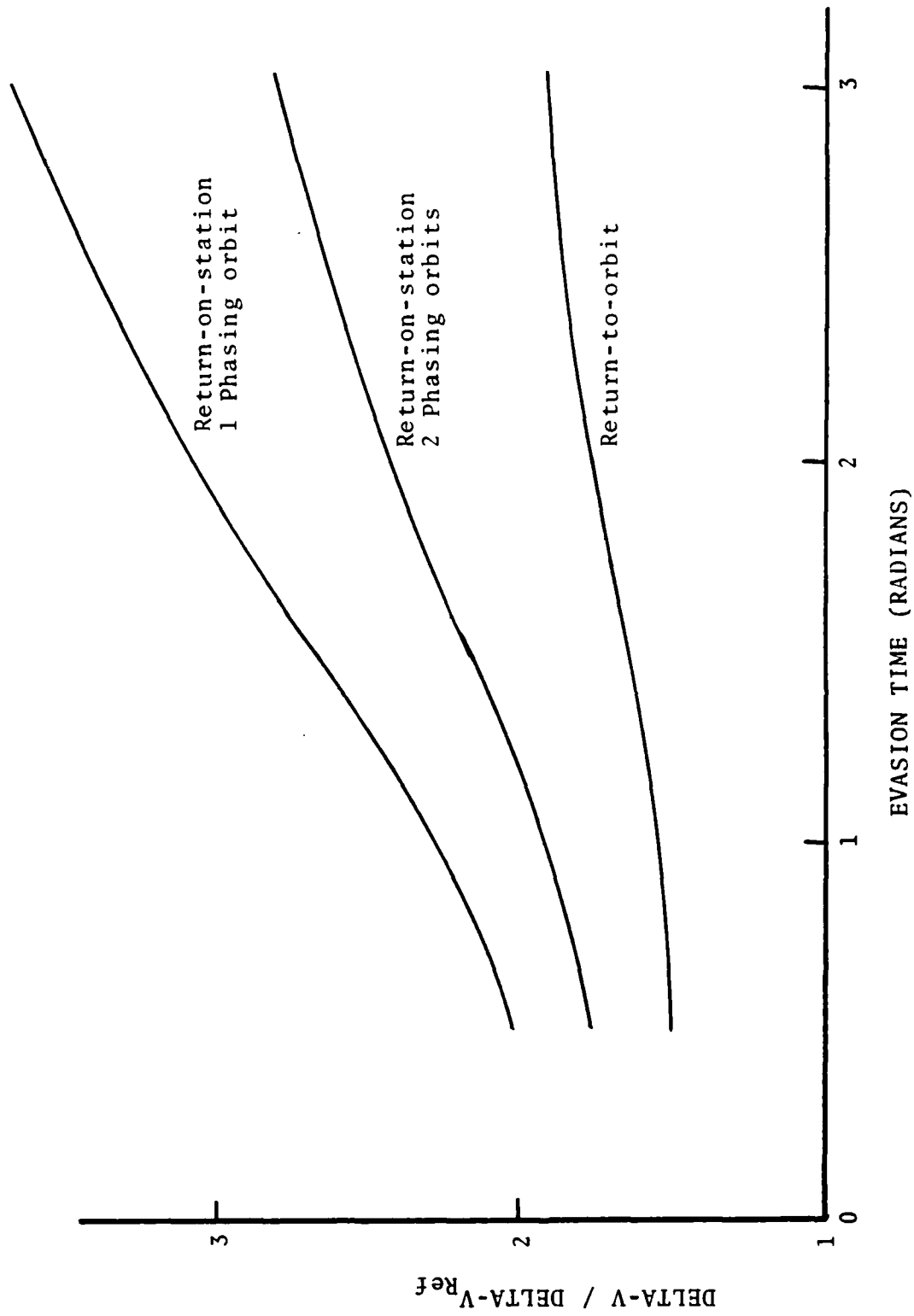
FIGURE 4.6a   Fuel Requirements for Evasion from Origin
and Return-on-Station
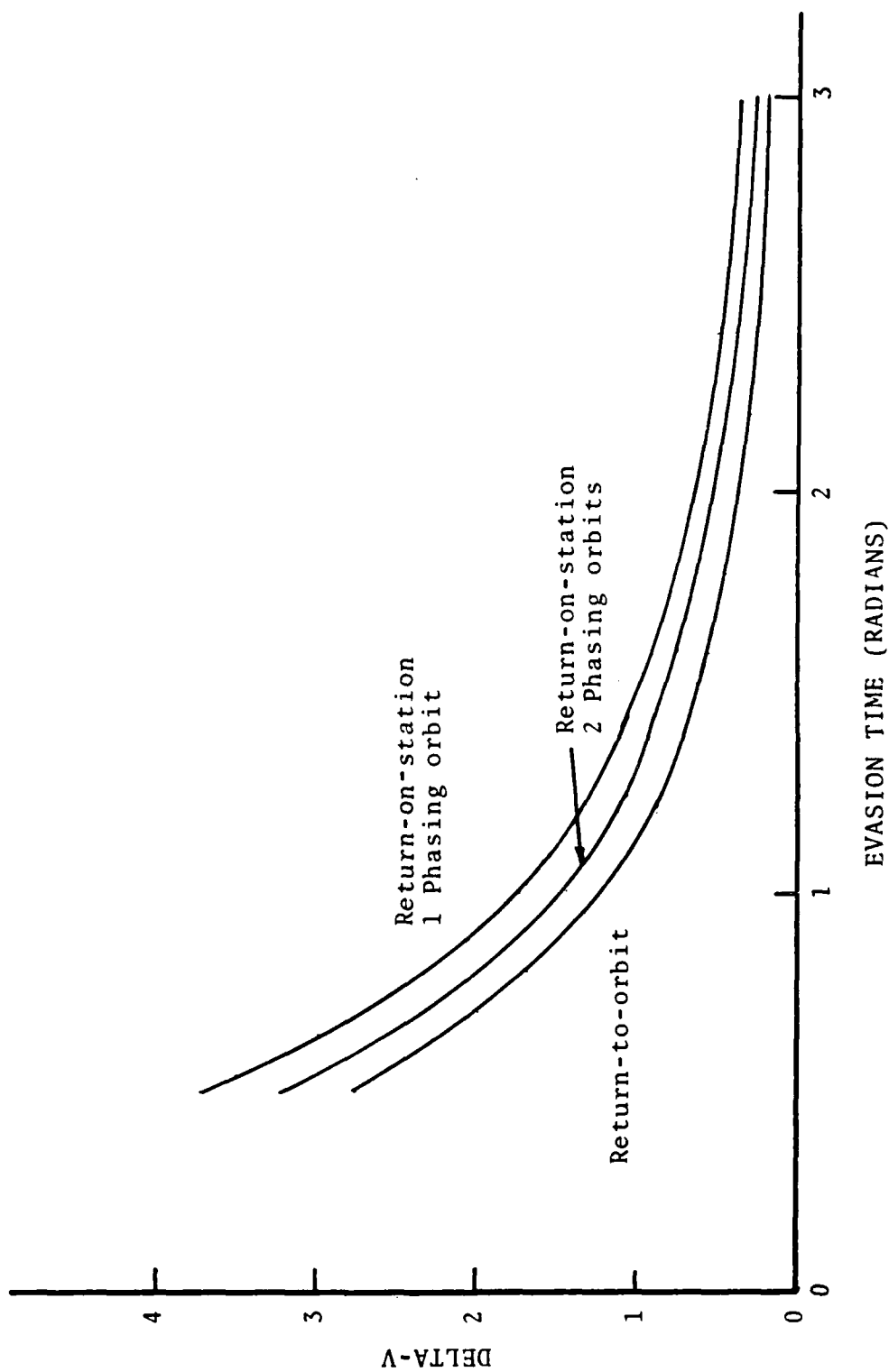
FIGURE 4.6b Fuel Requirements for Evasion from Origin
and Return-on-Station
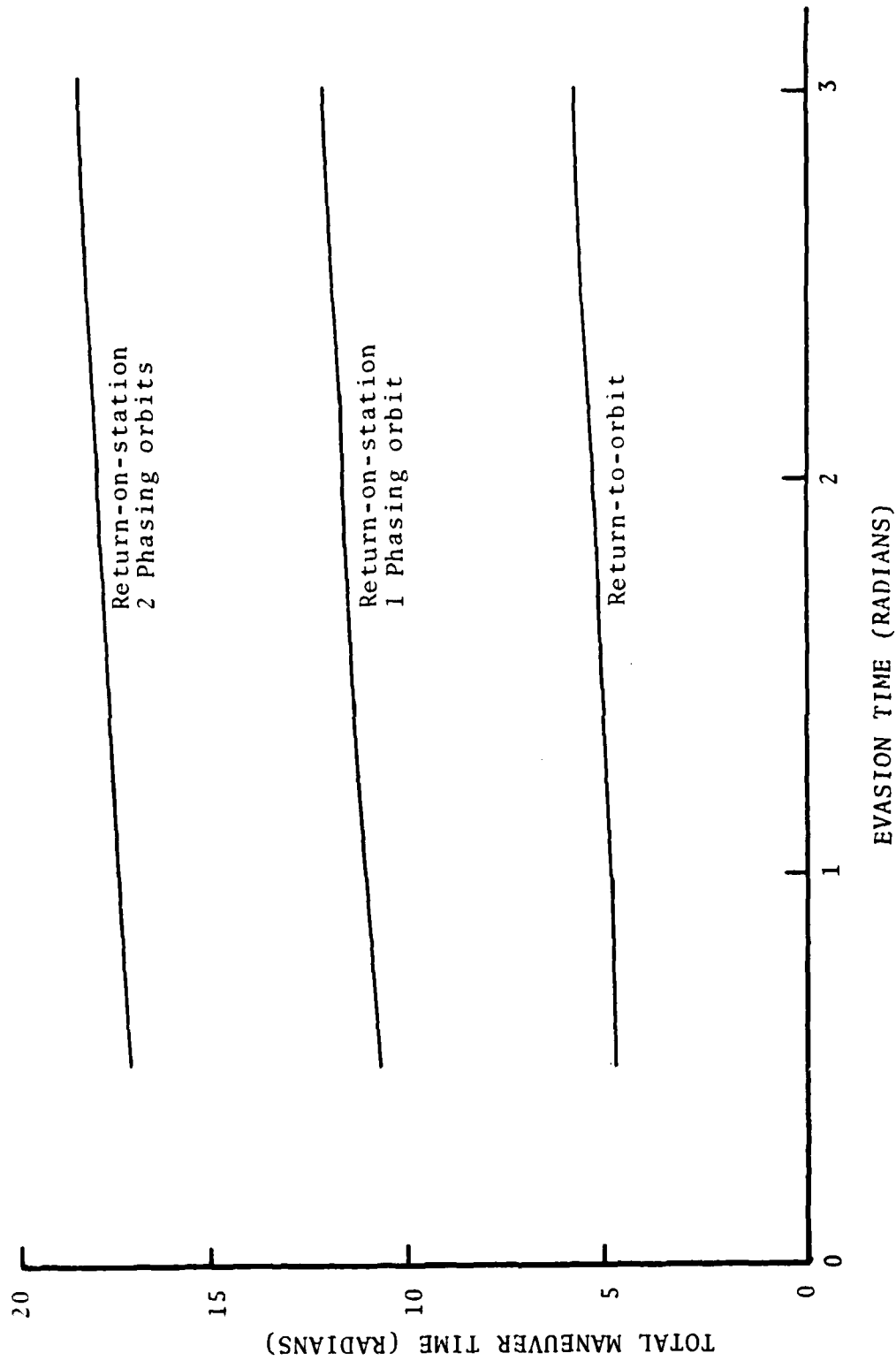
FIGURE 4.7 Maneuver Time Requirements for Evasion from Origin and Return-on-Station
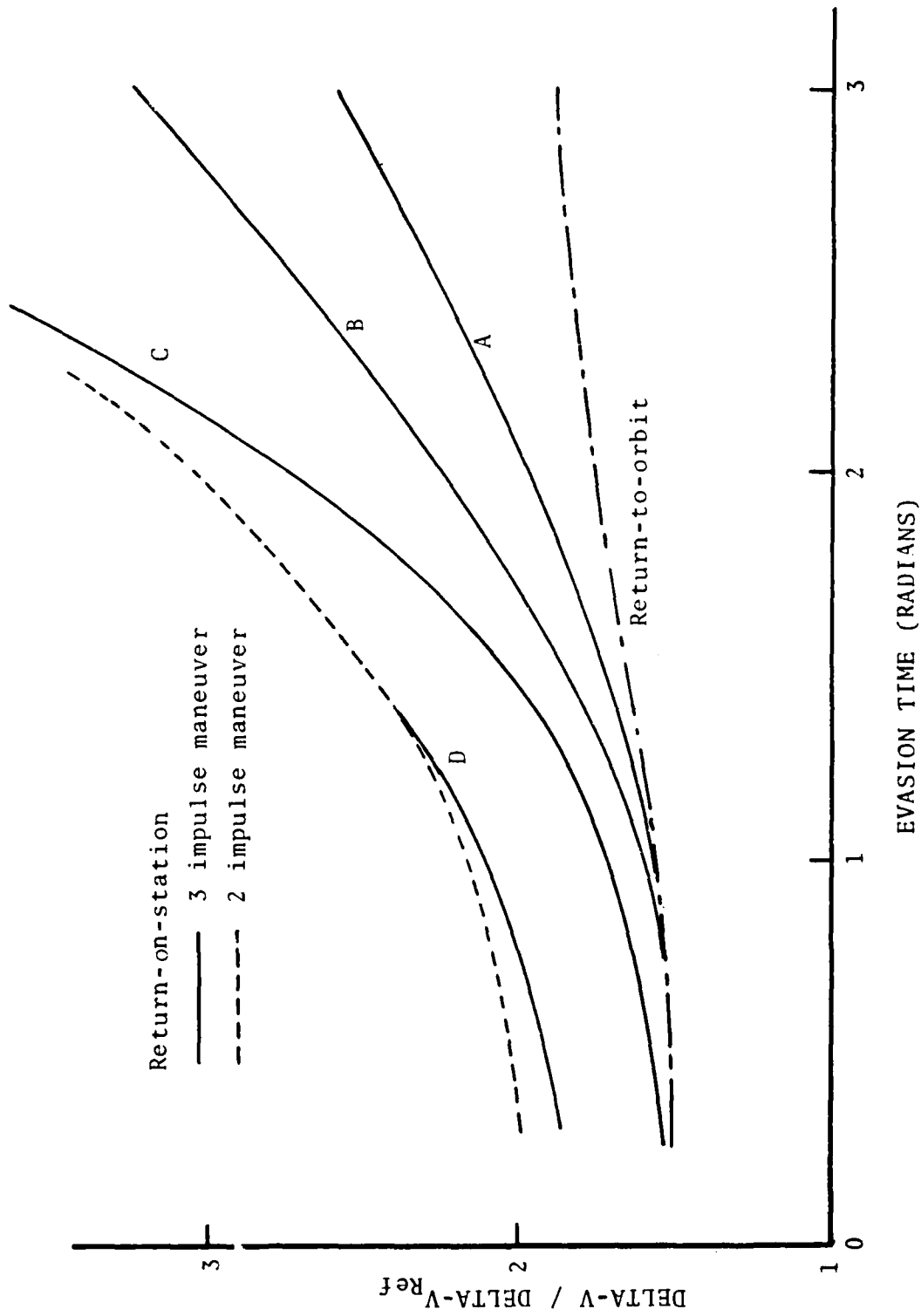
FIGURE 4.8a Time Open Return-on-Station Fuel Consumption
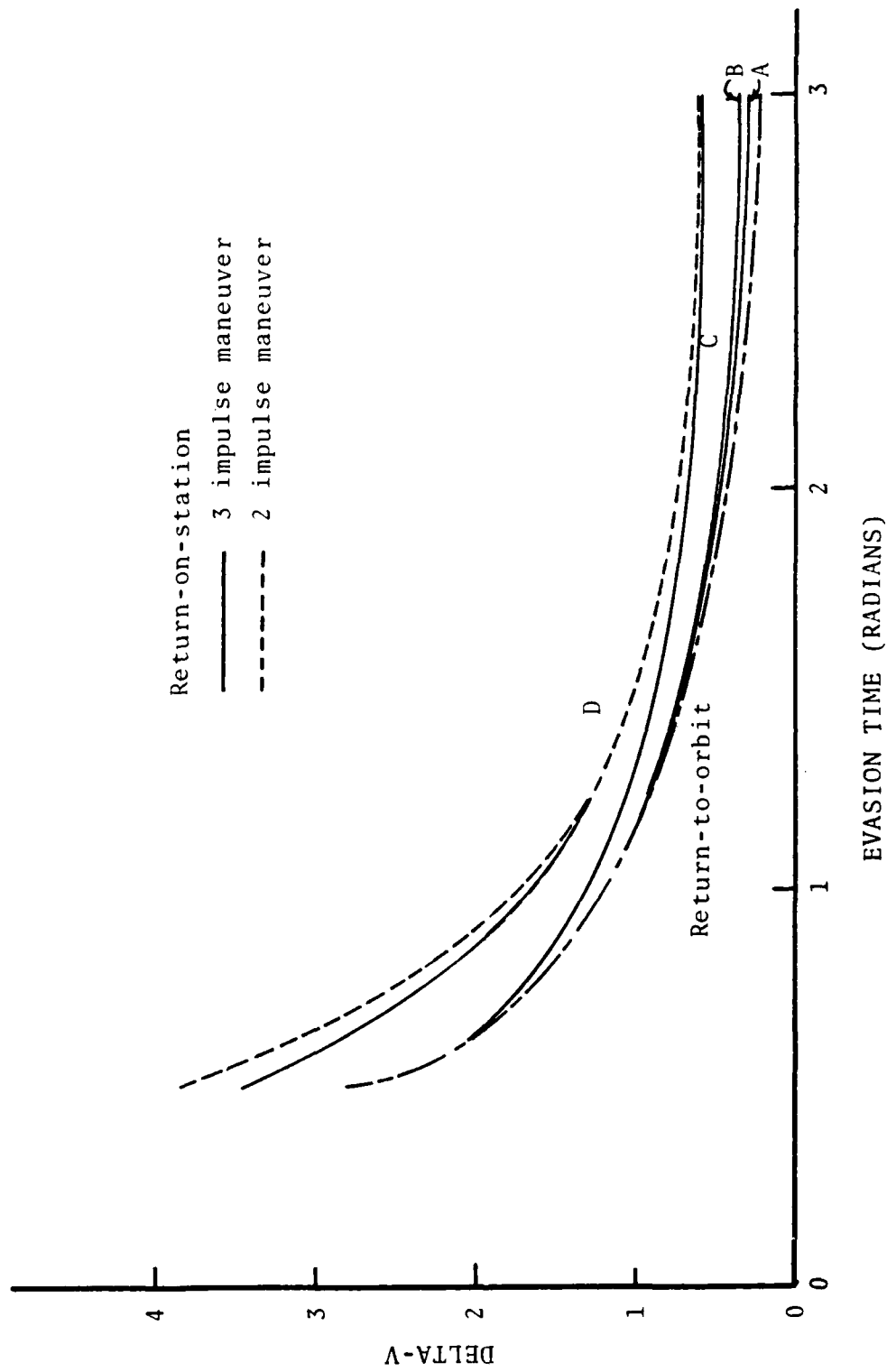
FIGURE 4.8b Time Open Return-on-Station Fuel Consumption
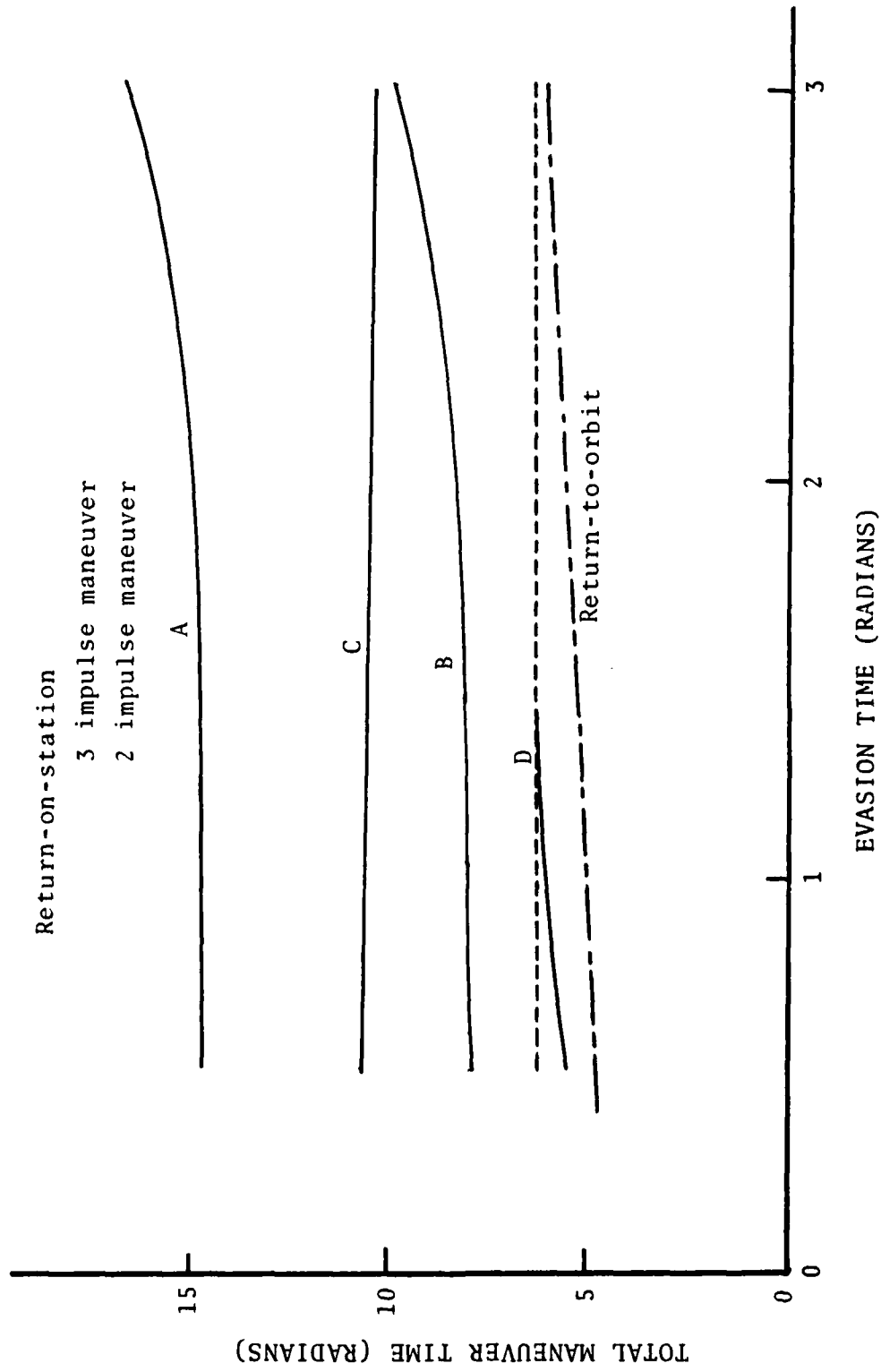
FIGURE 4.9   Time open Return-on-Station Manuever Times
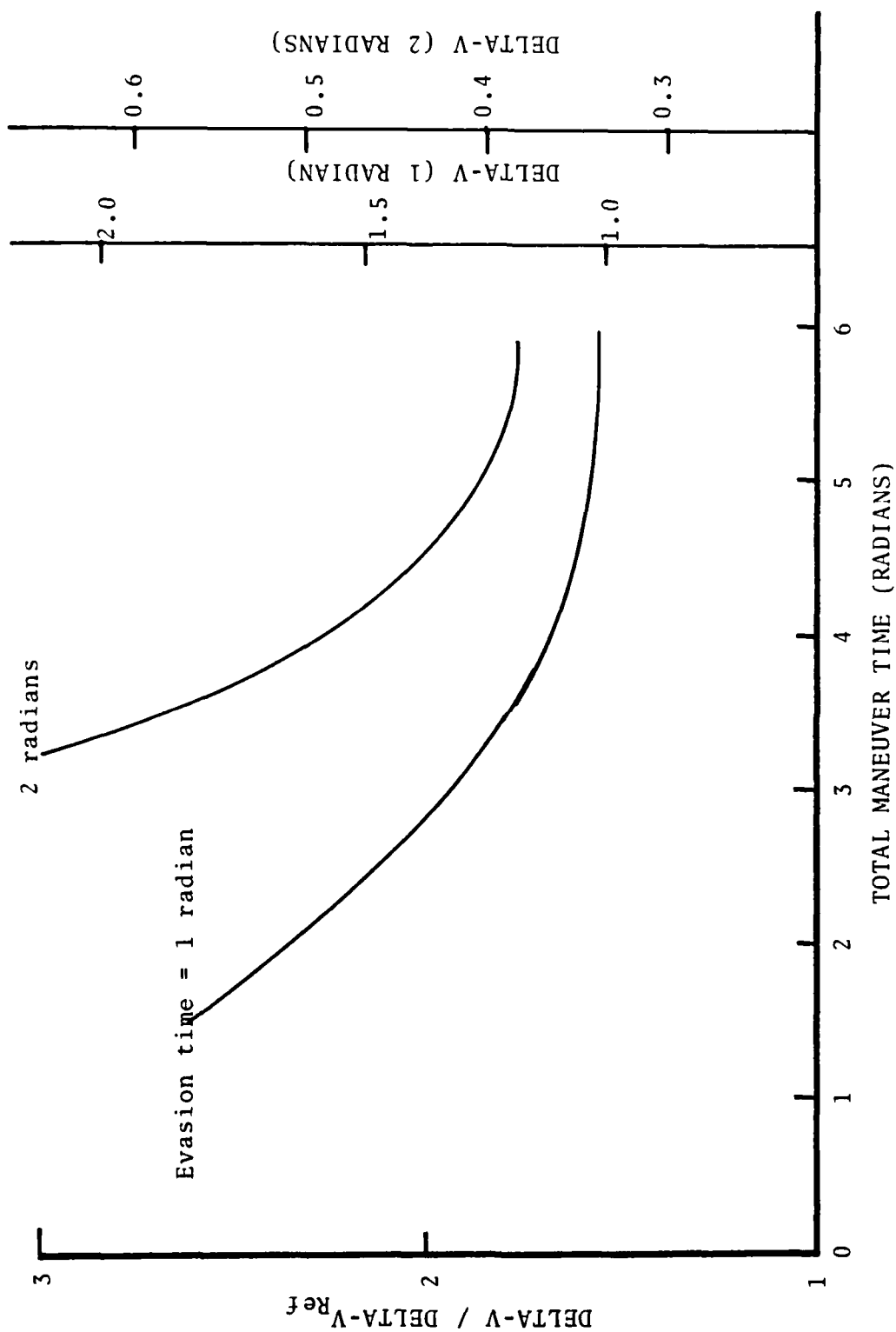
FIGURE 4.10 Effects of Time Constraint on Fuel Consumption
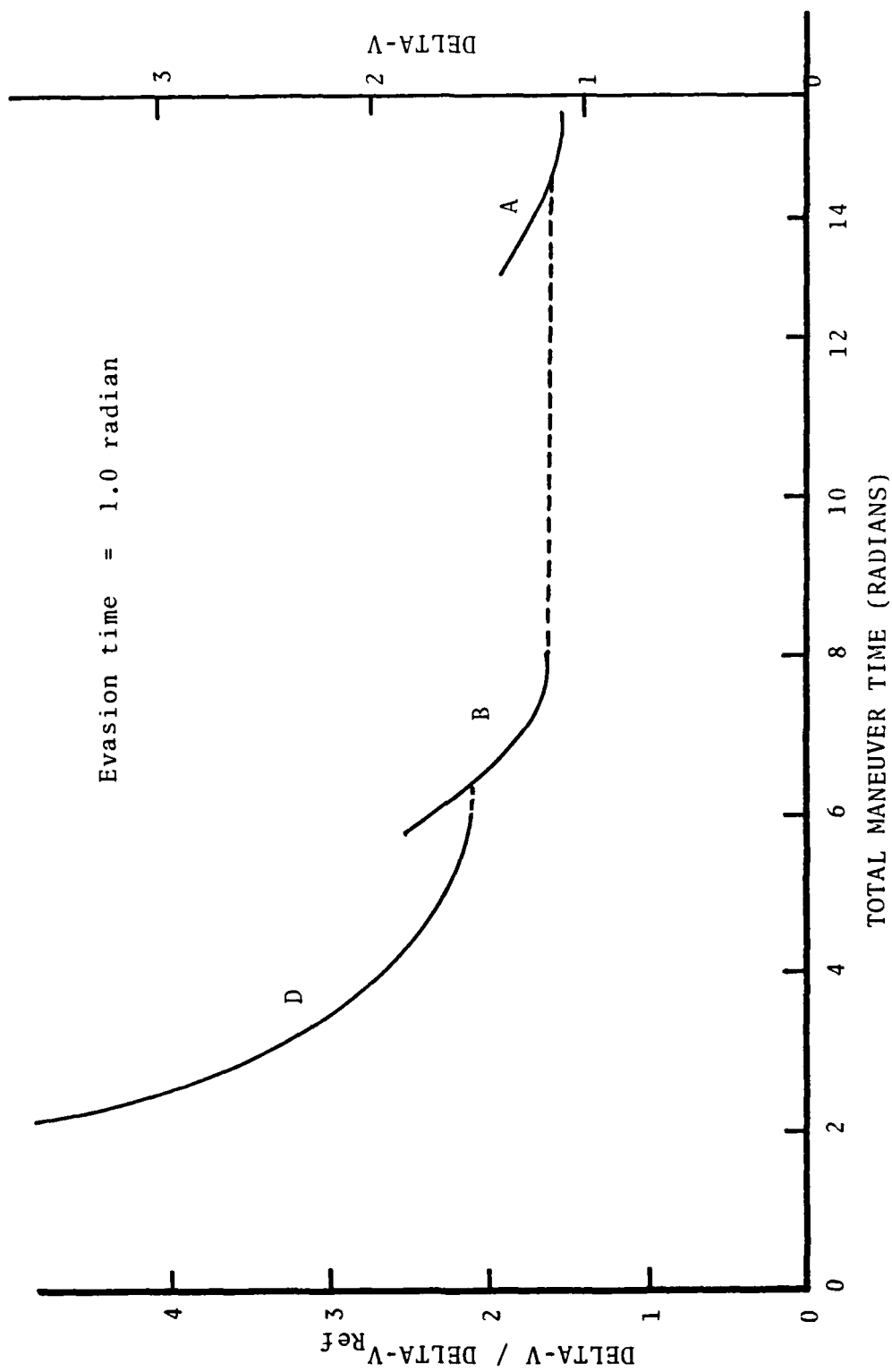
FIGURE 4.11 Effect of Time Constraint on Fuel Consumption

EVASION TIME (RADIANS)

INITIAL IMPULSE ANGLE (DEGREES)
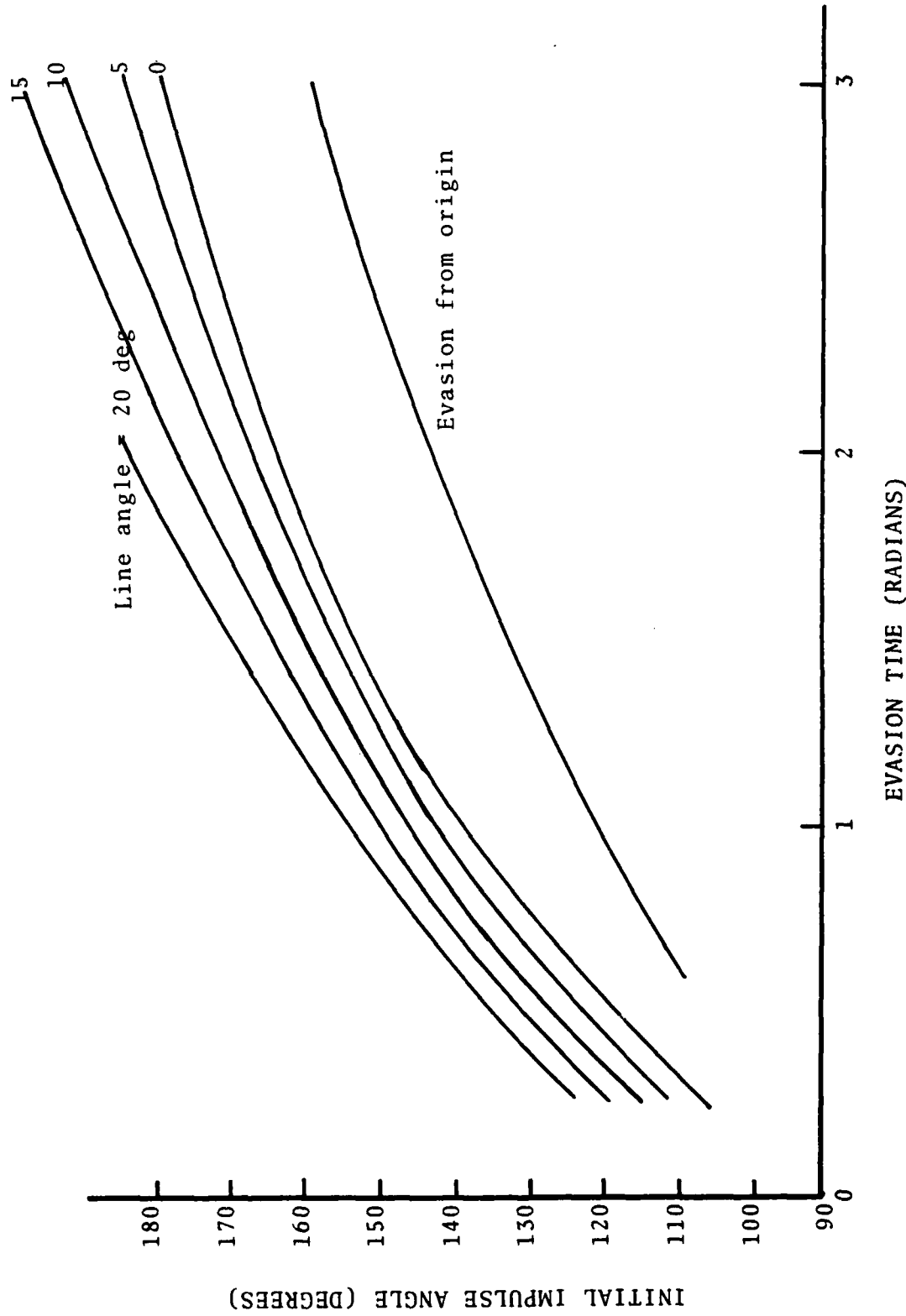
FIGURE 4.12   Initial Impulse Angle for Evasion From-a-Line
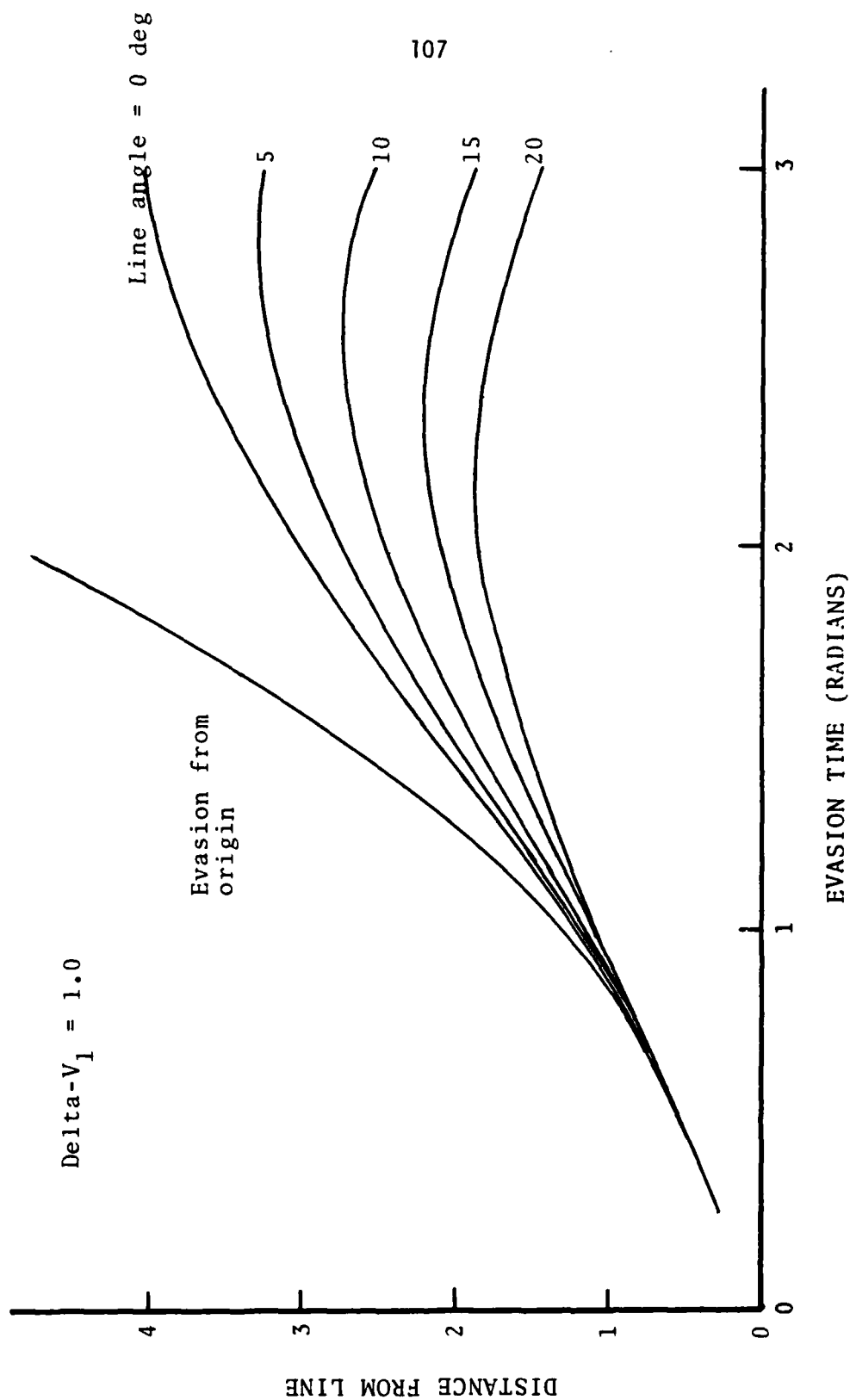
FIGURE 4.13 Distance Achieved for a Pure Evasion From Line
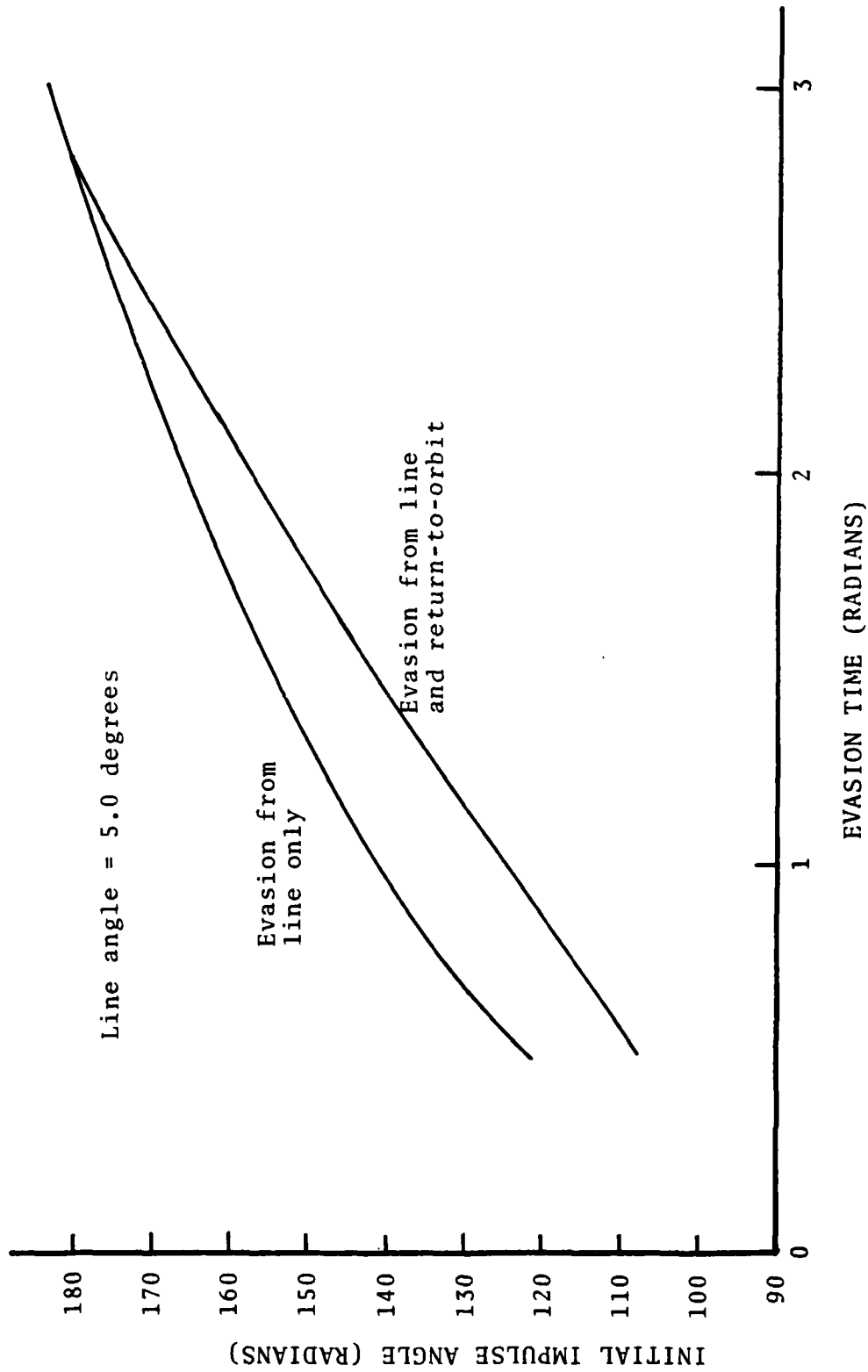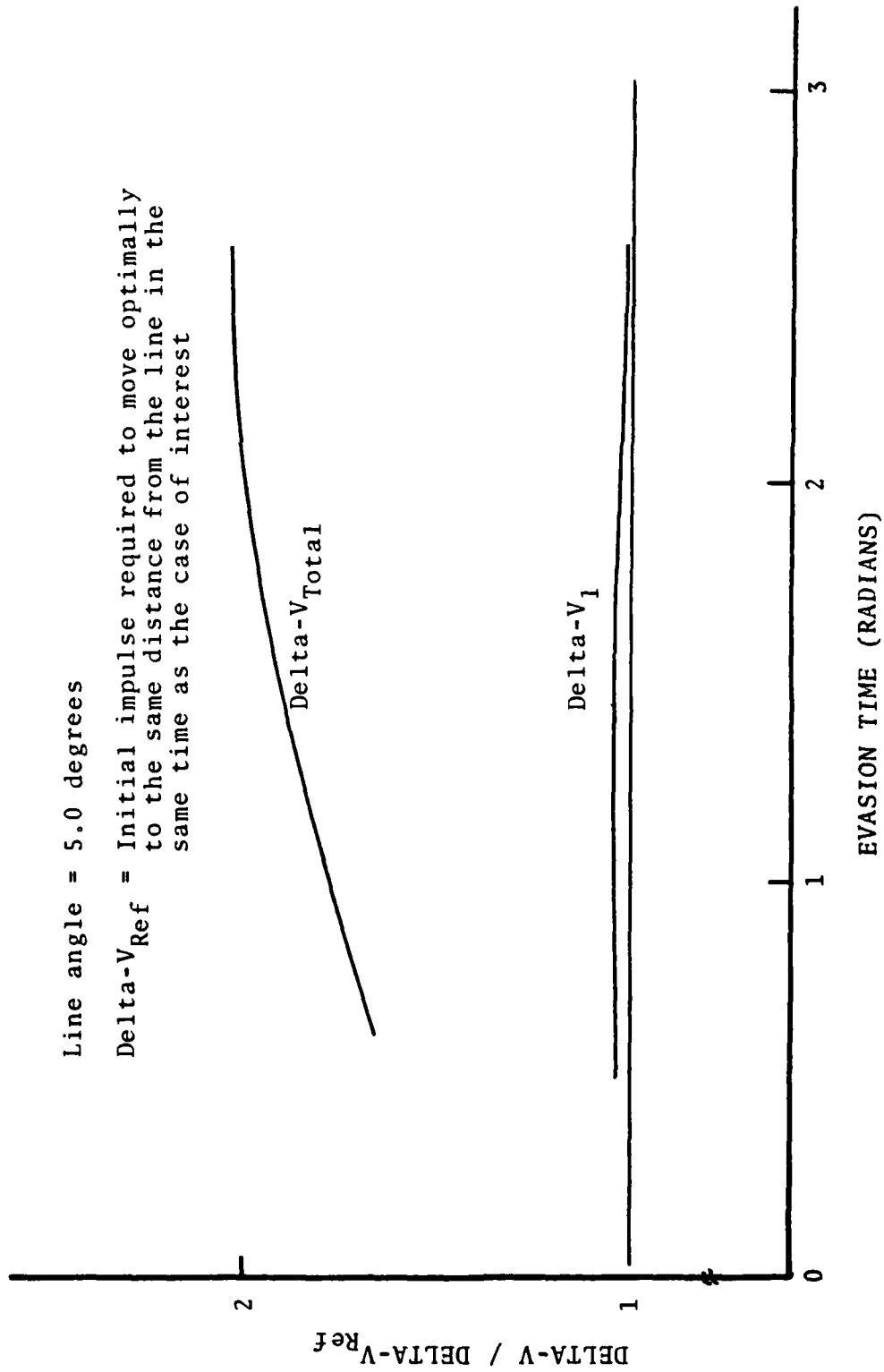
FIGURE 4.14 Initial Impulse Angle

Line angle = 5.0 degrees

Delta-V$_{Ref}$ = Initial impulse required to move optimally
to the same distance from the line in the
same time as the case of interest

Delta-V$_{Total}$

Delta-V$_1$

EVASION TIME (RADIANS)

DELTA-V / DELTA-V$_{Ref}$

FIGURE 4.15a   Fuel Consumption for Evasion From Line
and Return-to-Orbit
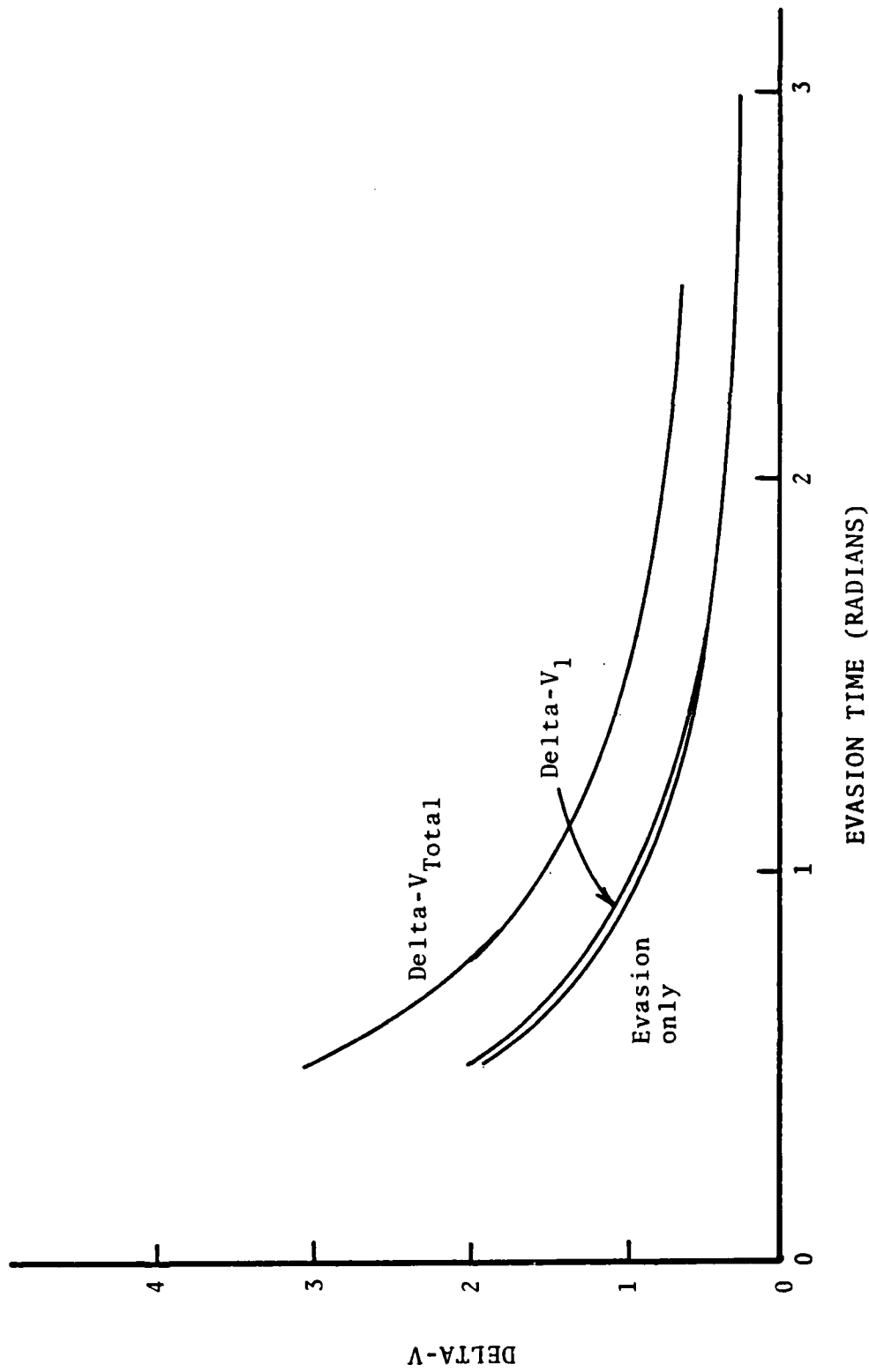
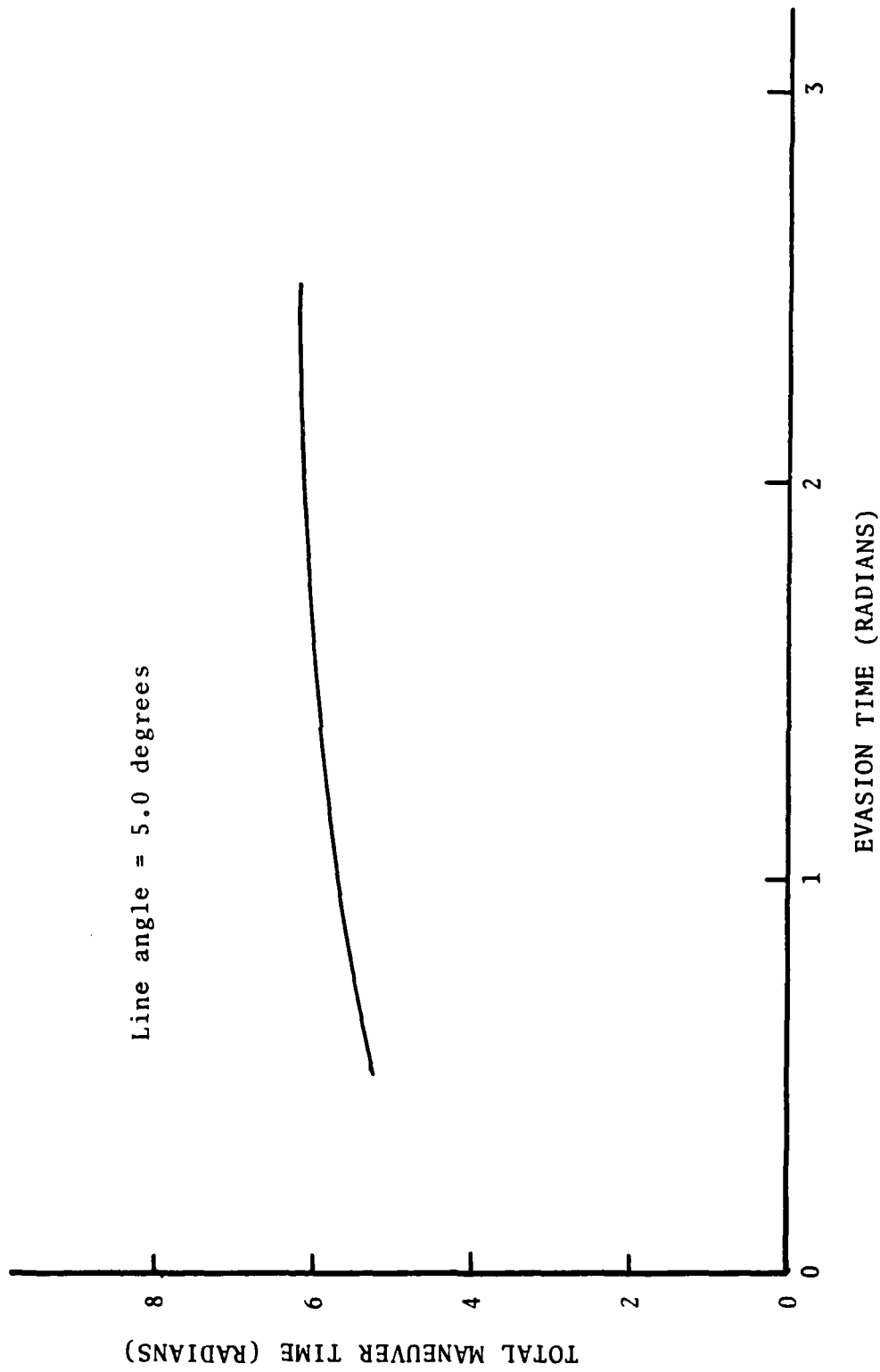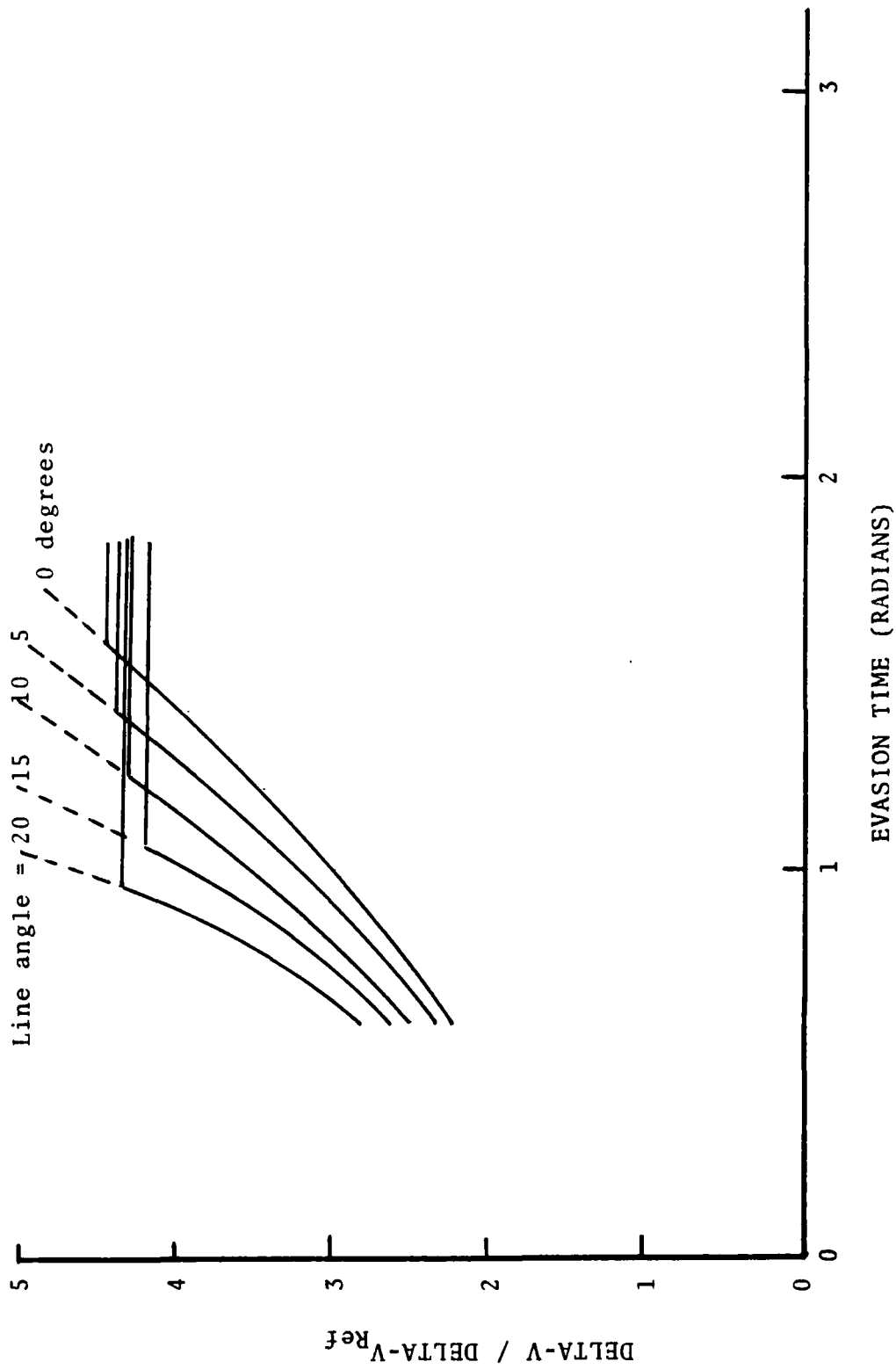FIGURE 4.15b Fuel Consumption for Evasion From Line
and Return-to-Orbit

Line angle = 5.0 degrees

EVASION TIME (RADIANS)

TOTAL MANEUVER TIME (RADIANS)

FIGURE 4.16   Manuever Time for Evasion From Line
and Return-to-Orbit

Figure 4.17a Fuel Requirements for Two-Impulse Evasion
From Line and Return-to-Orbit

DELTA-V

Line angle = 0 degrees
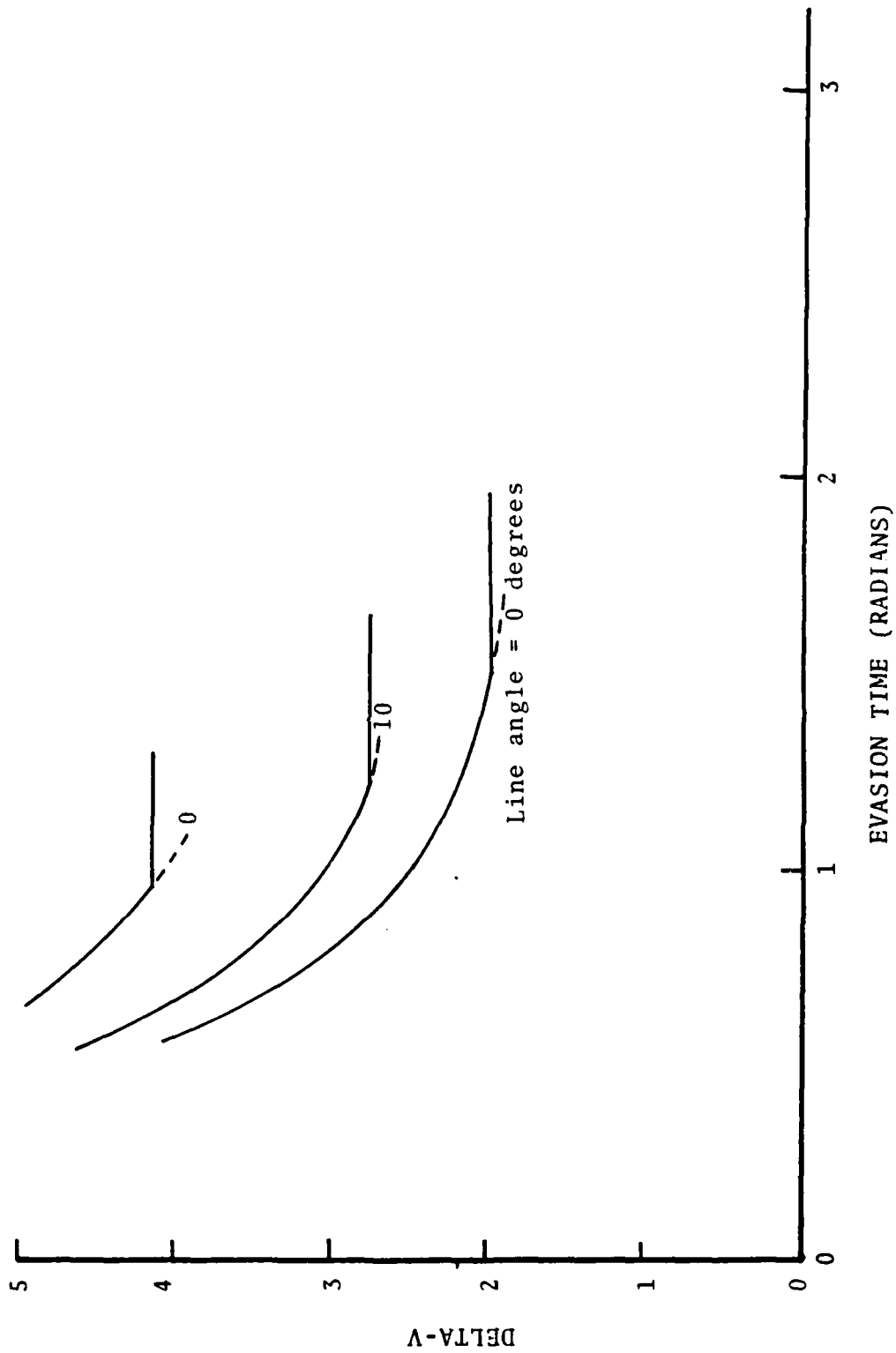
0

10

EVASION TIME (RADIANS)

FIGURE 4.17b Fuel Requirements for Two-Impulse Evasion
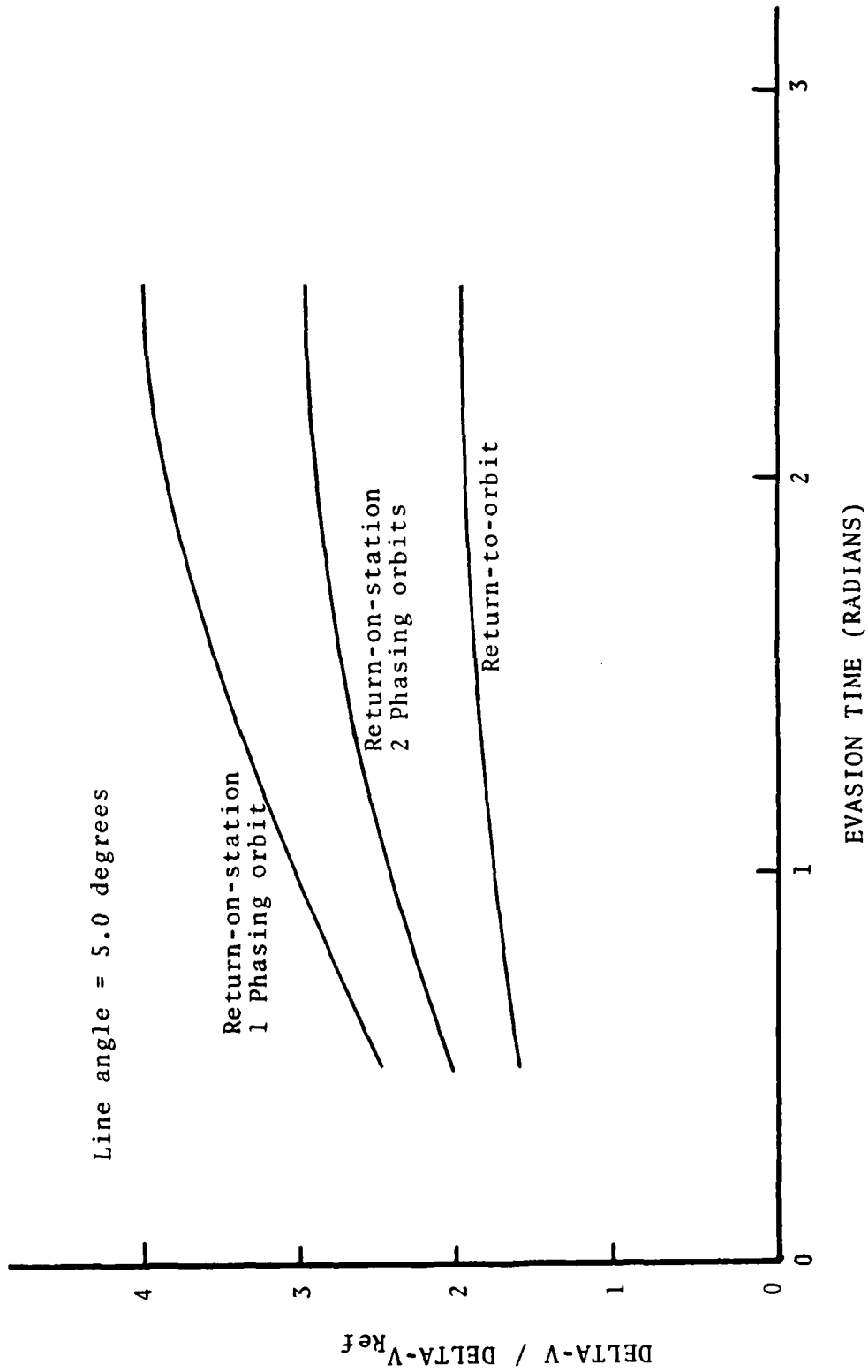From Line and Return-to-Orbit

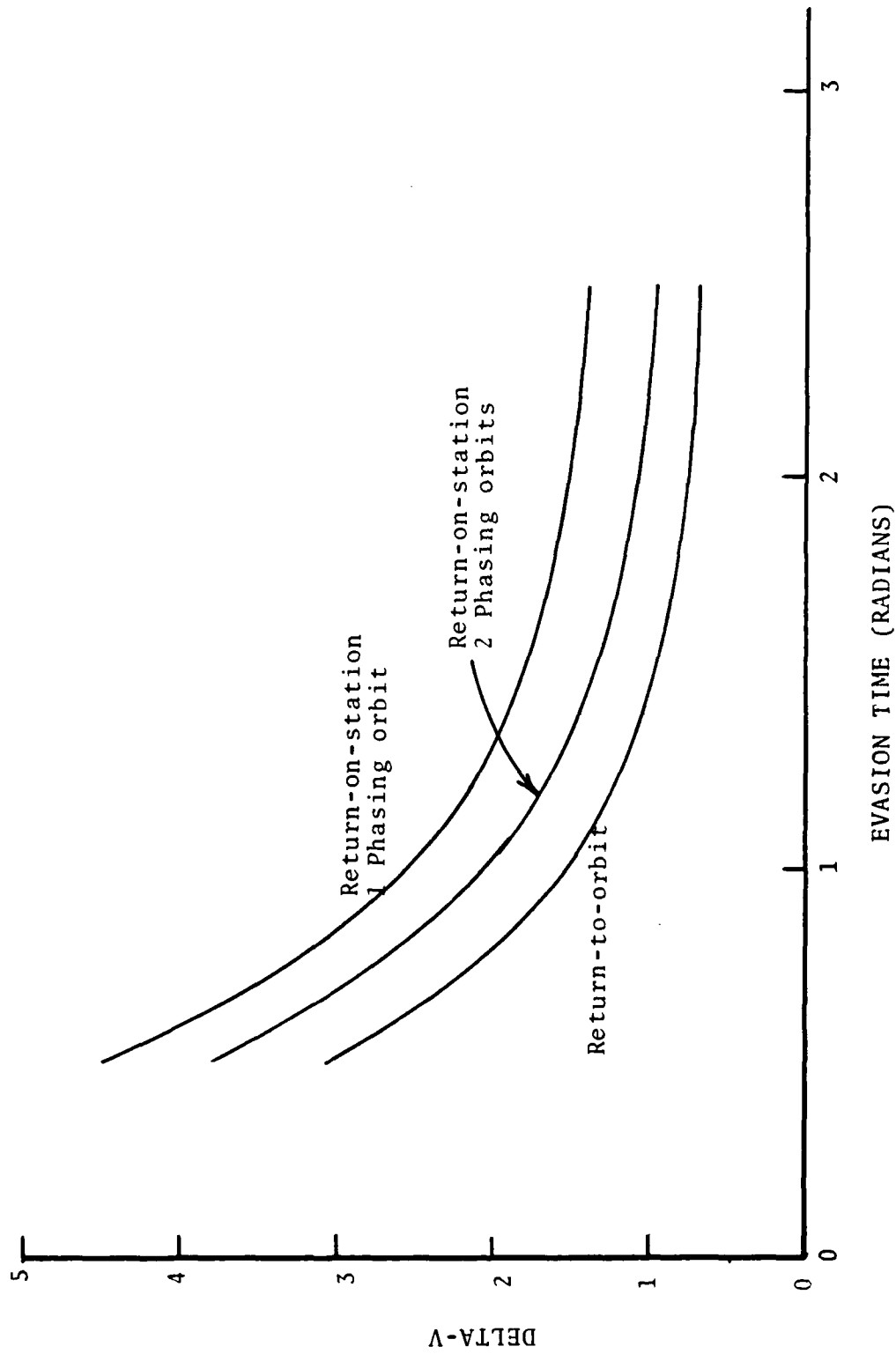FIGURE 4.18a Fuel Requirements for a Return-to-orbit-Phase Manuever

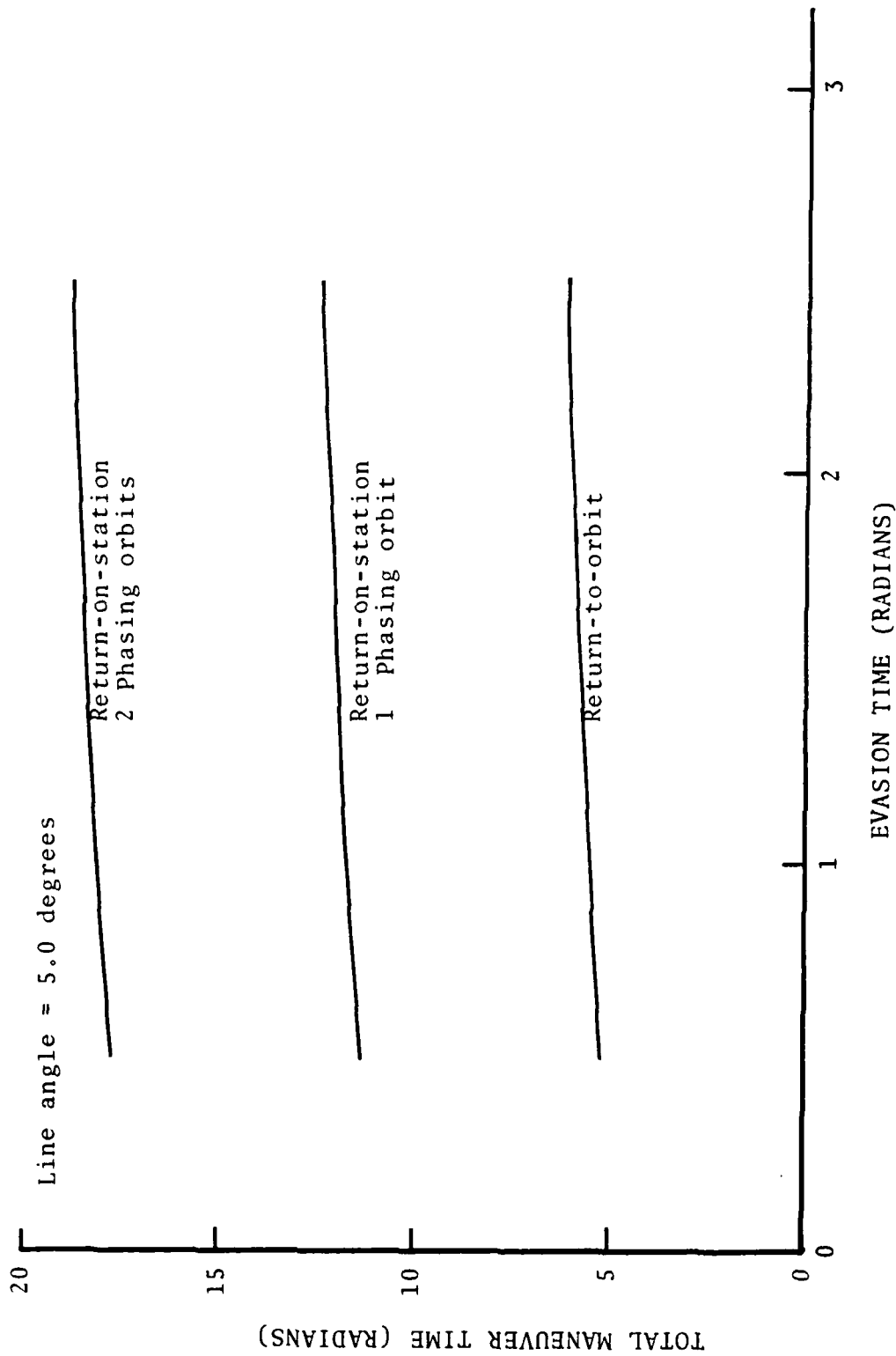FIGURE 4.18b   Fuel Requirements for a Return-to-orbit-
Phase Maneuver

FIGURE 4.19 Manuever Time for Return-to-Orbit-Phase Maneuver
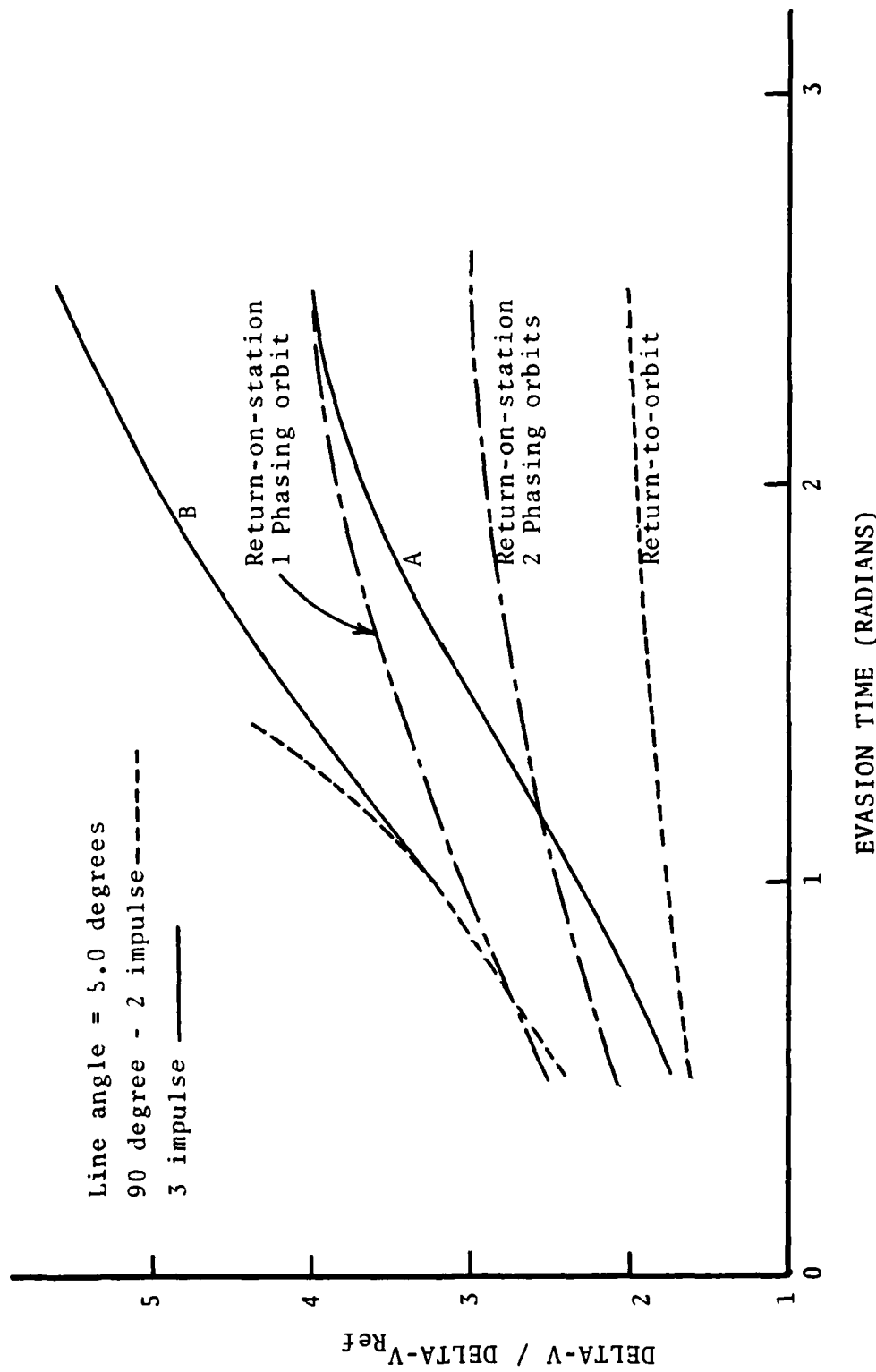
FIGURE 4.20a Fuel Requirements for Three-Impulse
Return-on-Station Maneuver
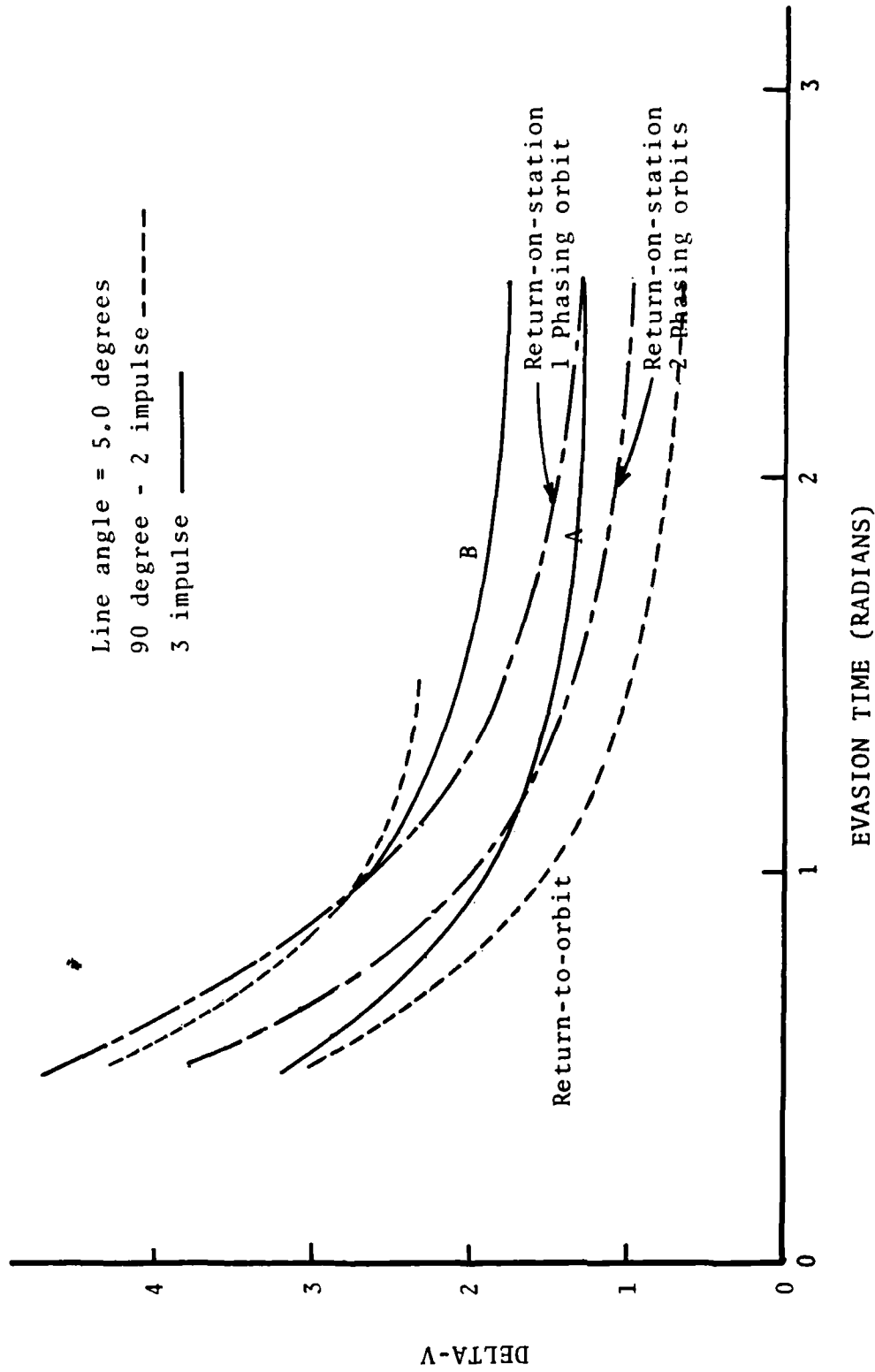
FIGURE 4.20b Fuel Requirements for Three-Impulse
Return-on-Station Maneuver

Line angle = 5.0 degrees

Return-on-station
1 Phasing orbit

A

B

Return-to-orbit

Return-on-Station

EVASION TIME (RADIANS)

TOTAL MANEUVER TIME
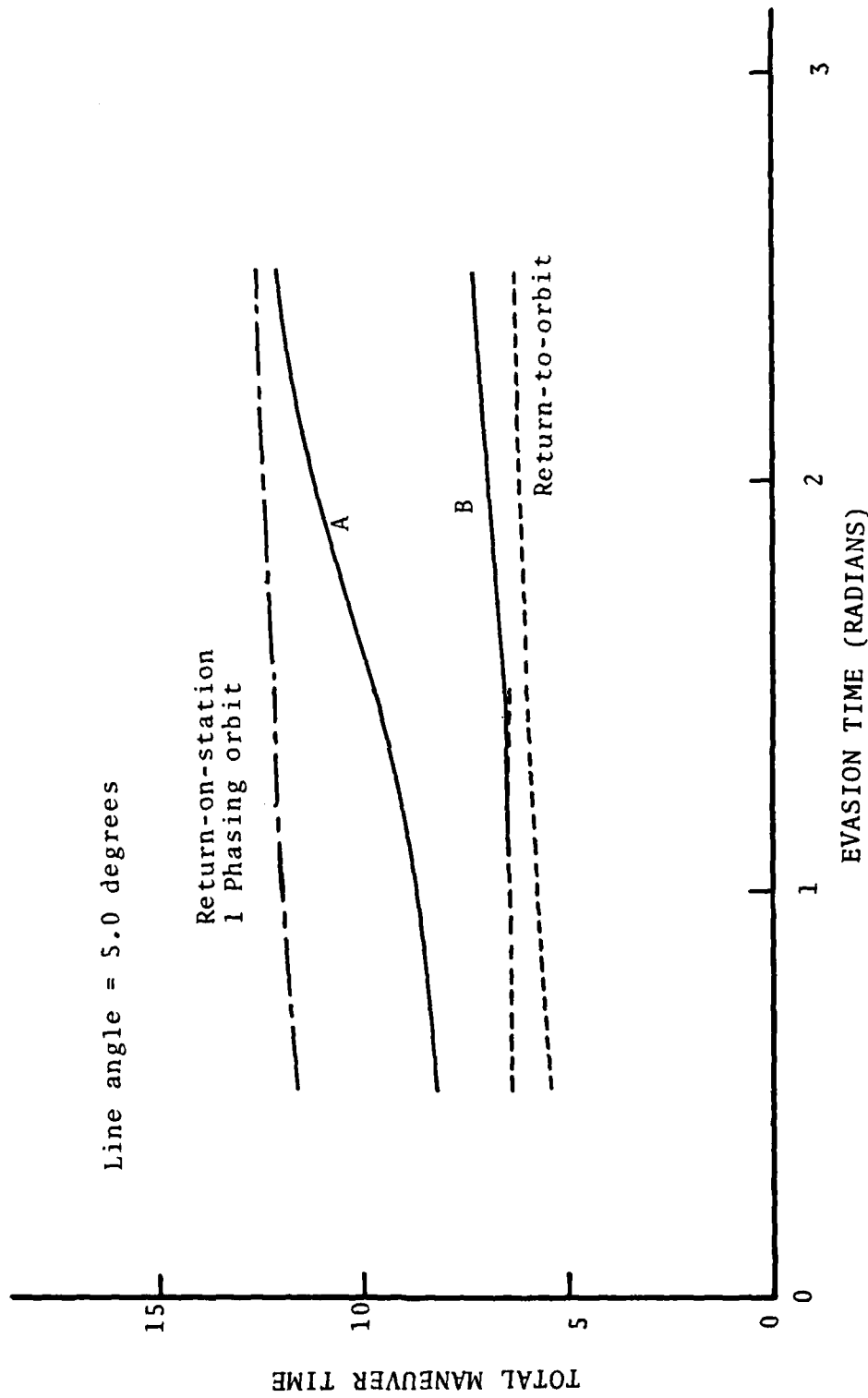
FIGURE 4.21 Manuever time for Three-Impulse
Return-on-Station

FIGURE 4.22 Effect of Maneuver Time Constraint on Fuel Consumption for Return-to-Orbit Maneuver

FIGURE 4.23 Effect of Maneuver Time Constraint on Initial
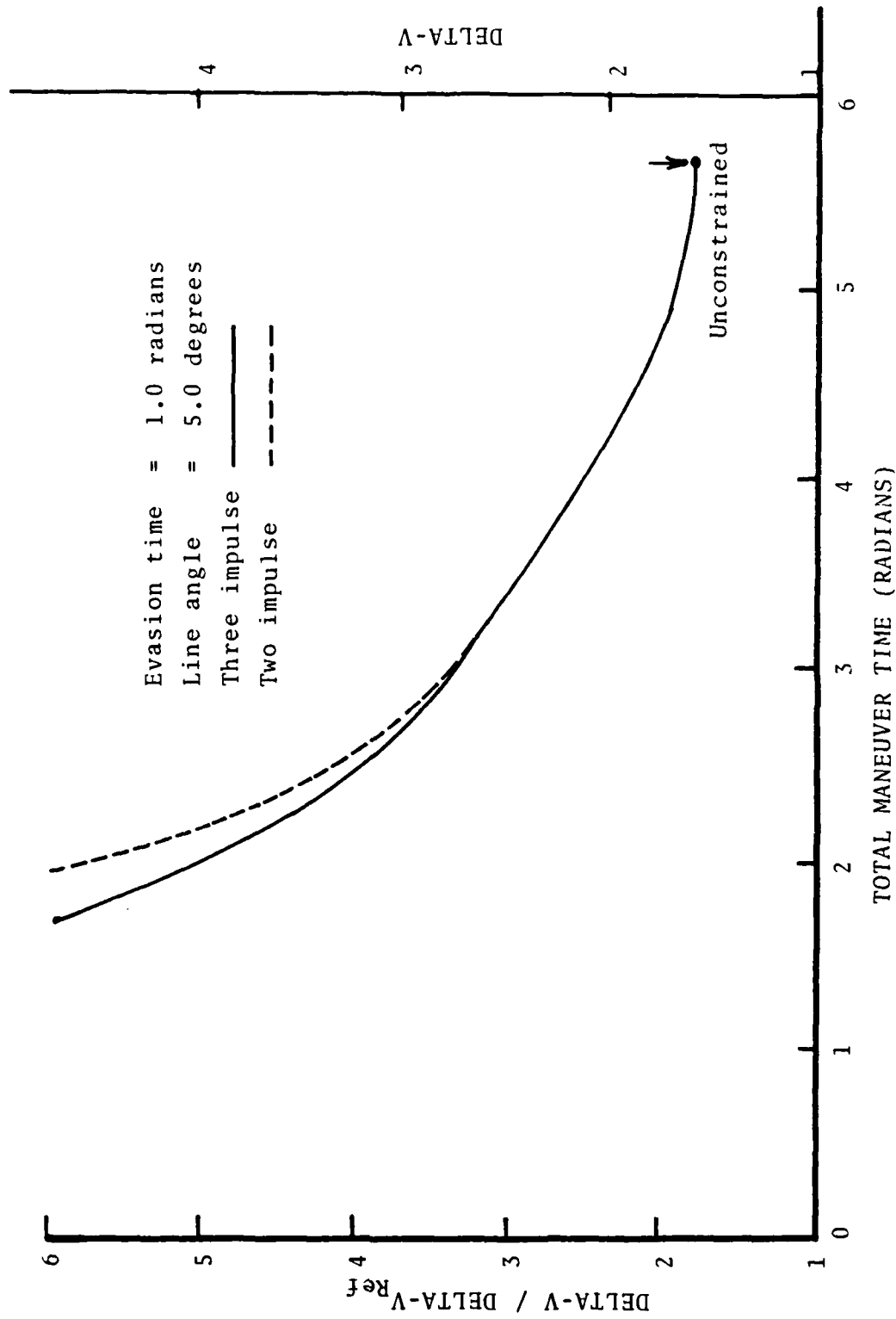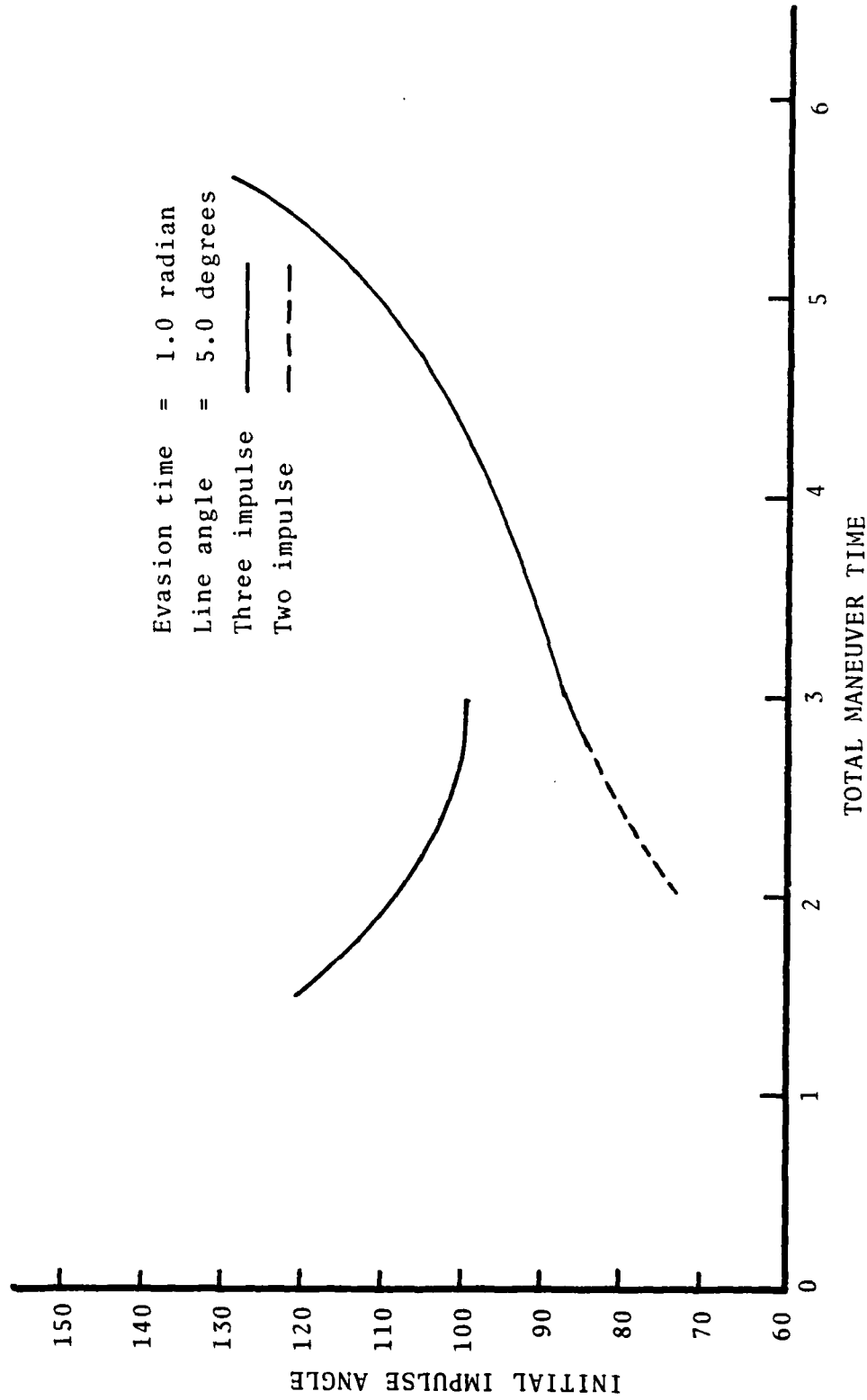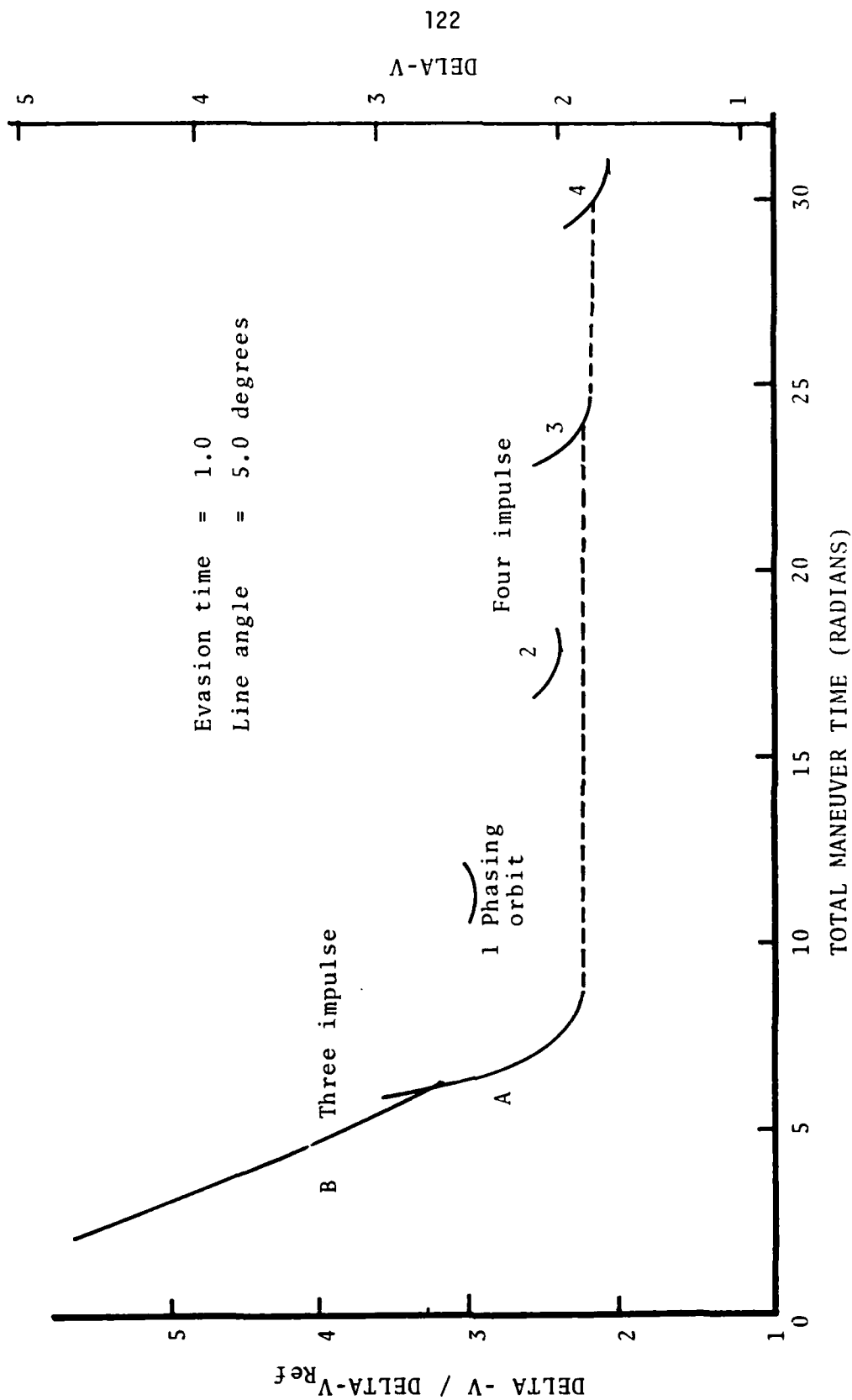Impulse Angle for Return-to-Orbit Maneuver

FIGURE 4.24 Effect of Maneuver Time Constraint on Fuel Consumption
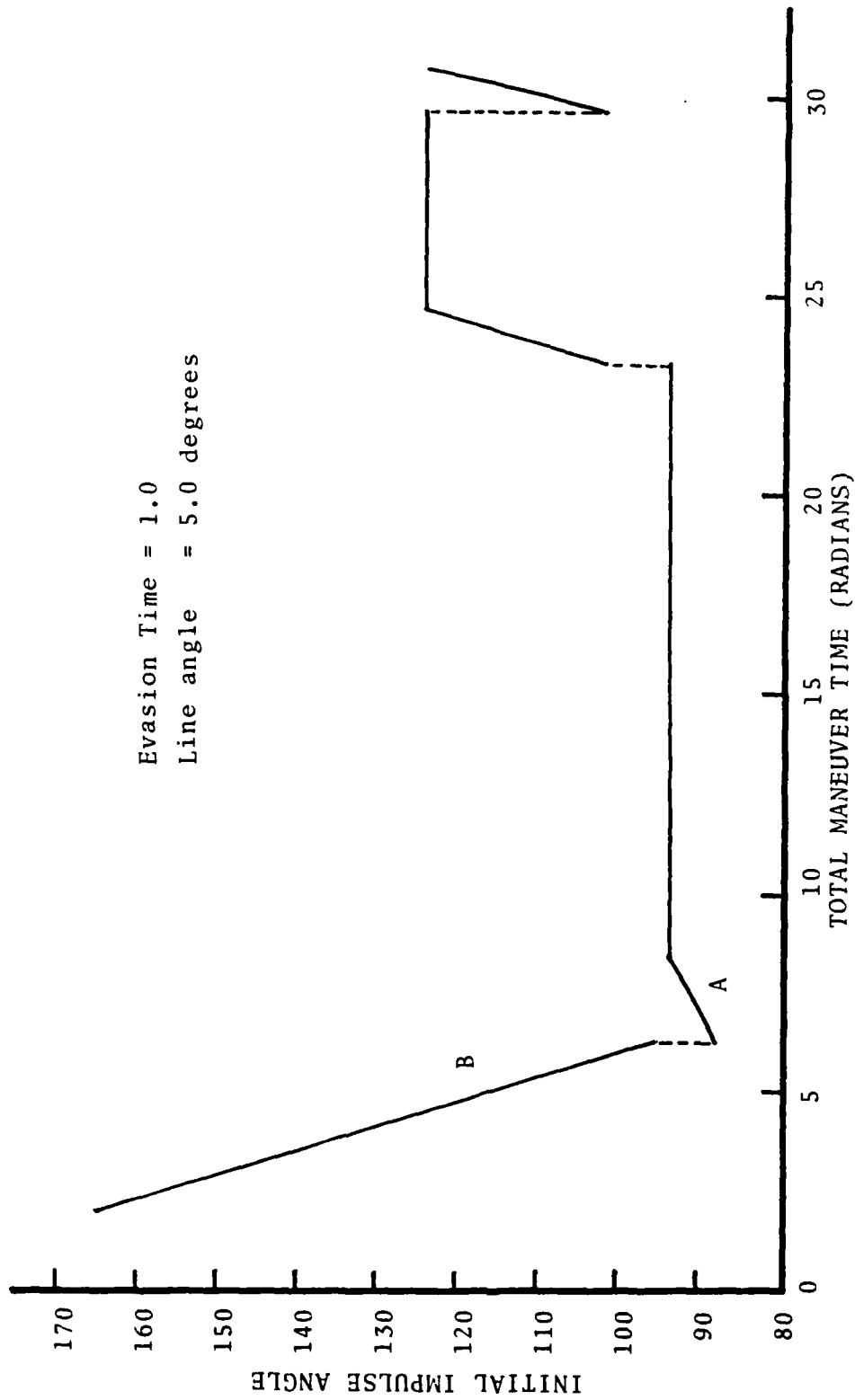for Return-on-Station Maneuver

FIGURE 4.25 Effect of Maneuver Time Constraint on Initial Impulse Angle for Return-on-Station Maneuver

5. CONCLUDING REMARKS

In conclusion, some suggestions for further work are offered.

The maneuver-sequence-optimization computer programs can be improved by a general restructuring and streamlining and the addition of various features. It is believed that with further development and systematic testing the programs have potential for real-time generation of optimal maneuver sequences in an operational setting. Robustness can be improved by tailoring various details of the nonlinear-programming package to the particular class of problems of interest. Greater user convenience can be provided by systematic generation of first-guess maneuver sequences for general combinations of constraints. Alterations in candidate sequences can also be mechanized gracefully to cope with the bothersome situations in which one or more impulses fade out to zero in the course of iterations and/or impulses coalesce into one. Auxiliary primer-vector calculations can also be added as a step towards validation of results and generation of alternative-candidate sequences.

It would be of interest to carry out detailed comparisons of observed Soviet ASAT maneuver sequences with optimized sequences incorporating various assumed combinations of operational constraints along the lines of the present exploration. To this end an improved launch-burn representation might be incorporated. Attention should be given to possible sensor constraints on approach to the target.

Further evasion-and-return studies should be mainly applications-oriented. Two one-parameter families of maneuver sequences (one up,

one down) could be pre-calculated and stored as a function of warning
time for operational in use in real time and, in some applications
(e.g., shuttle), on-board. Interactive alternating pursuit/evasion
maneuver sequences are of interest for future scenarios featuring
reduced tracking and communications delays.

APPENDIX A

THE OPTIMIZATION ALGORITHM

This chapter discusses an approach to numerical solution of minimum problems with nonlinear constraints which is motivated by the desire both (1) to avoid the evaluation of second partial derivatives necessary in second-variation procedures and (2) to improve upon the terminal-convergence behavior of first-order (gradient) methods. The basis of the approach is the variable-metric gradient method for finding an unconstrained minimum. This method employs a metric which is adjusted during the iteration cycles. As the metric approaches its limit, convergence to the minimum becomes quadratic. The Davidson-Fletcher-Powell (DFP) variable-metric algorithm and the Broyden-Fletcher-Goldfarb-Shanno (BFGS) algorithm are both incorporated in the program.

In one of the two approaches to the handling of constraints, the performance function is augmented by penalty terms which furnish a square-law measure of the constraint violations. The augmented function is minimized, yielding an approximation to the minimum of the original problem, with small violations of the constraints [10,11]. The second approach employs gradient projection. The history of the projection version of variable-metric optimization is somewhat checkered. Immediately successful with linear constraints, the seemingly obvious extension to the non-linear case encountered difficulty

in that one-dimensional searches may fail to terminate. The use of a
performance index augmented by a correction linear in the constraint
functions, however, in conjunction with a metric-update based upon
changes in the projected gradient vector, proved successful [4].
Subsequently, refinements in the projection algorithm have made it more
than a match for the penalty version [5,12].

In the interest of making the present account somewhat self-
contained, the three topics of unconstrained minimization via variable-
metric gradient method, penalty-function approximation, and projection
will be taken up each in turn. Much of the material is extracted from
previous work [4,5,12,13].

Unconstrained Minimization via Variable-Metric Processes

The DFP variable-metric method for numerically determining the
minimum of a function of several variables combines the best features
of the conventional gradient method and Newton's method; namely the
sureness of convergence of the former and the quadratic terminal con-
vergence of the latter. An excellent exposition of the method, in-
cluding convergence proofs, is given by Fletcher and Powell [14].

Denote the function to be minimized as $f(x)$. It is assumed that
f is smooth to the extent of possessing continuous second partial
derivatives. Any starting point may be chosen (although the best a
priori guess of the minimizing x is the obvious choice to keep the
number of iterations smallest). At the starting point the gradient
vector, f_x, as well as f itself, is evaluated. A change is then made
in x according to

$$\Delta x = -\alpha \, H \, f_x \; . \tag{A.1}$$

H is a positive-definite, symmetric matrix, defining the metric in the x-hyperspace.* Its initial selection is otherwise arbitrary. $\alpha > 0$ is a scalar step-size parameter.

In the DFP method, the one-dimensional minimum of f vs α is obtained. This requires an accurate and sure-footed numerical search algorithm [e.g. 15]. At the new x, the gradient vector f_x is again evaluated. The H matrix is updated according to

$$H + \Delta H = H + \frac{\Delta x \, \Delta x^T}{\Delta x^T \Delta f_x} - \frac{H \, \Delta f_x \, \Delta f_x^T \, H}{\Delta f_x^T \, H \, \Delta f_x} \; . \tag{A.2}$$

The procedure is begun again with the new values of x, f_x, H.

It is shown in [14] that H remains positive-definite and that, as x approaches the minimizing point, H approaches f_{xx}^{-1} evaluated at the minimum. For quadratic f the minimum is obtained in, at most, n steps (within round-off error); the method is quadratically convergent. For more general functions having the smoothness properties assumed, a Taylor expansion through quadratic terms provides a good representation of the function in some neighborhood of the minimum. With H converged, the minimum of f vs α then will occur for $\alpha = 1$. The Δx of eq. (A.1) will approach the value given by Newton's method, namely $-f_{xx}^{-1} \, f_x$.

A more general variable-metric formula is given by

$$H + \Delta H = H + \frac{\Delta x \Delta x^T}{\Delta f_x^T \Delta x} - \frac{H \Delta f_x \Delta f_x^T H}{\Delta f_x^T H \Delta f_x} + \phi \nu \nu^T \; , \tag{A.3}$$

---

*The inner product is given in matrix terms by $<X,Y> = X^T H Y$, and, as usual, $|| \, X \, || = <X,X>^{\frac{1}{2}}$.

where

$$
v = \left(\Delta f_x^T \; H \; \Delta f_x \right)^{\frac{1}{2}} \left[\frac{\Delta x}{\Delta x^T \; \Delta f_x} - \frac{H \; \Delta f_x}{\Delta f_x^T \; H \; \Delta f_x} \right] \quad , \tag{A.4}
$$

which first appeared in [16]. The update is the same as DFP when the scalar ϕ taken as $\phi = 0$. For $\phi = 1$, it is the same as BFGS (Broyden-Fletcher-Goldfarb-Shanno), the designation denoting simultaneous dis-covery by the four investigators named.

It developed that all of the algorithms in the one-parameter family generate the same sequence of steps when "exact" one-dimensional searching is employed and that $H + \Delta H$ is positive definite whenever H is, provided only that the scalar $\phi \geq 0$. H tends monotonically toward the inverse Hessian in a certain sense, for $0 \leq \phi \leq 1$. Fletcher's effort at employing the generalized algorithm without one-dimensional searches, and with an attempt to optimize the ϕ-choice, produced mediocre results [16]. These facts have tended to draw attention away from improved variable metrics. Computational experience, however, has shown that BFGS in combination with "exact" searches is significantly more economical of function samples, essentially because the first step taken is a better guess than with DFP [17]. The tendency is for DFP to overestimate the step, the reasons being poorly understood.

Penalty-Function Approximation

The problem is to determine the values of the variables x which minimize $f(x)$ while satisfying constraints $g(x) = 0$, where x is an

n-vector,* f is a known scalar function of x, and g is an m-vector, m < n, of known functions of x.

An approximation technique for treating constraints is due to Courant [10], and consists of forming the function**

$$\bar{f} = f + \frac{1}{2} \sum_{j=1}^{m} k_j g_j^2 \qquad (A.5)$$

and, for "large" $k_j > 0$, seeking its unconstrained minimum. Should solutions of both the approximation problem and the original exist, the former approaches the latter as each $k_j \to \infty$.

The choice of numerical values for the penalty coefficient k_j is subject to requirements which tend to conflict. If very large values are chosen to diminish the constraint violations at the minimum, the numerical errors in the products $k_j g_j^2$ and their partial derivatives become significant. These errors, occurring in each step of a successive improvement procedure, have an adverse effect on convergence. Because of this effect, one may accept appreciable constraint violations in minimizing f in penalty approximation.

For notational simplicity, it is sometimes advantageous to re-write $\bar{f}$ as

$$\bar{f} = f + \frac{1}{2} g^T Kg \qquad (A.6)$$

where K is an m × m diagonal matrix with the k_j values along the diagonal, and $(\ )^T$ is the transpose of ( ). For treatment of

---

*All vectors are column vectors.

**$(\ )_j$ is the jth component of ( ).

inequality constraints, $g_j \geq 0$, each term in the sum (A.6) corresponding to an inequality is multiplied by $h(g_j)$, the Heaviside unit step function with argument g_j.

Variable-Metric Projection

The Kelley-Speyer algorithm minimizes a scalar-valued function $f(x)$ (x an n-vector) subject to m equality and p inequality constraints.

$$g_j = 0 \quad , \quad j = 1,..,m \tag{A.7}$$

and

$$g_j \geq 0 \quad , \quad j = m+1,..,m+p . \tag{A.8}$$

The process employs the formulae

$$\Delta x = -\alpha \, H(f_x + g_x \lambda) \tag{A.9}$$

and,

$$\lambda = - (g_x^T H g_x)^{-1} g_x^T H f_x , \tag{A.10}$$

where a one-dimensional search is carried out to minimize the function $f + g\lambda$, along the search direction, Δx. The dimension of g and λ in eqs. (A.9) and (A.10) is determined by choice of the active-constraint set, to be reviewed subsequently. The one-dimensional search is terminated short of a minimum if the violations g_j build up beyond prescribed tolerances.

Optimization cycles employ an H-matrix [4] updated according to

$$H + \Delta H = H + \frac{\Delta x \, \Delta x^T}{\Delta x^T (\Delta f_x + \Delta g_x \lambda)} - \frac{H(\Delta f_x + \Delta g_x \lambda)(\Delta f_x + \Delta g_x \lambda)^T H}{(\Delta f_x + \Delta g_x \lambda)^T H (\Delta f_x + \Delta g_x \lambda)} \tag{A.11}$$

in the case of DFP. An analogous formula employing changes in the projected gradient $f_x + g_x\lambda$ is used for BFGS updating. The update is performed only if

$$\Delta x^T(\Delta f_x + \Delta g_x\lambda) > 0 \qquad (A.12)$$

which assures positive definiteness of the updated H. The screening feature represents a departure from the original [4] version of the algorithm, this seemingly slight modification having been found to effect a considerable convergence improvement [5]. The update formula (A.11), for a given cycle, is the DFP update for minimization of $f + g\lambda$ [4]; it guarantees definiteness of the updated H if the one-dimensional search terminates on a minimum. The test (A.12) offers a guarantee of definiteness without this restriction. Failure to satisfy (A.12) is associated with nonconvexity of $f + g\lambda$ as a function of α. When failure occurs, the update is merely skipped; it is not necessary to restart H from a diagonal first guess.

Projection optimization processes require that constraints be restored between optimization cycles, ordinarily via one or more correction cycles, which may be of various types. In the H-update formula (A.11), the change in the x-vector, Δx, and the change in the projected gradient vector, $(\Delta f_x + \Delta g_x\lambda)$, are between the beginning and end of the optimization cycle only.

Implementation of the Variable-Metric Algorithms

The material of this and the next section is mainly from [5,12] and is included to make the present report relatively self-contained.

Constraint Restoration

The initial nulling out of constraint functions often proves more challenging than subsequent restorations in that the constraint violations to be dealt with are ordinarily larger in magnitude. For clarity, consider first the case of minimizing a scalar-valued function $f(x)$ (x an n-vector) subject to m equalities of the form (A.7). In this case, the initial constraint nulling is done by minimization of a function $\hat{f}$:

$$\hat{f} = \frac{1}{2} \sum_{j=1}^{m} k_j g_j^2 + \frac{k_0}{2} (f_0 - f)^2 h (f - f_0) \qquad (A.13)$$

This is a weighted sum of squares of the constraint functions plus a term to counter gross increases in f. The term corresponds to penalty-function treatment of an inequality $f_0 - f \geq 0$. Here, again, h is the Heaviside unit step function. The k_j are determined from

$$k_j = \frac{\bar{k}}{m} \frac{\sum_{i=1}^{m} |g_{i_x}|^2}{|g_{j_x}|^2} \qquad j = 1,2,\ldots,m \qquad (A.14)$$

where $\bar{k}$ is input. This choice would make equal the contribution of each equality constraint to the second directional derivative of eq. (A.13) in its own gradient direction at $g_j = 0$, if the constraints were linear. The constraint $f_0 - f \geq 0$ is included quadratic-penaltywise in eq. (A.13) only during the first restoration sequence, with a coefficient k_0 taken as 1/10 the smallest of the k_j calculated from eq. (A.14). The constant f_0 is estimated as the initial value of $f + g\lambda$.

The metric employed in correction sequences may be denoted A (to distinguish it from H of the optimization cycles). It is adjusted approximately for changes in the k_j, one at a time, using

$$A + \Delta A = A - \left[\frac{\Delta k_j}{1 + \Delta k_j \, g_{j_x}^T \, A \, g_{j_x}} \right] A \, g_{j_x} \, g_{j_x}^T \, A \, . \tag{A.15}$$

This correction, from [13], is based on the idea that A approximates $\hat{f}_{xx}^{-1}$. The metric to start the first correction sequence is obtained as $A + \Delta A$ from eq. (A.15), using $A = I$ and $\Delta k_j = k_j - 1$ [k_j from eq. (A.14)]. If n or more updates are completed in this sequence, the emerging DFP metric is carried over to the next; if not, the initial metric is carried over. In either case, adjustments for any changes in the k_j are performed via eq. (A.15) before use. Negative increments Δk_j are limited in magnitude to insure that the denominator of the fraction in brackets does not nearly vanish.

The second and subsequent restoration sequences employ

$$\Delta x = -\alpha \, A \, g_x^T \, (g_x^T \, A \, g_x)^{-1} \, g \tag{A.16}$$

together with a one-dimensional search versus α for a minimum of $\hat{f}$ given by eq. (A.13), but with the last term deleted. This correction scheme, with $\alpha = 1$ and without a search, was originally proposed by Rosen [5]; it effects restoration in a single step for linear g. The existence of the inverse in eq. (A.16) requires that the matrix g_x have rank m. This condition is met at the constrained minimum in the classical "normal" case in which the tangent-plane approximations to

the constraints are well defined and distinct. Note that there is no guarantee that eq. (A.16) provides a direction of descent for $\hat{f}$, with general k_j values; thus the one-dimensional search may fail and reversion to steepest-descent minimization of $\hat{f}$ become necessary.

The magnitude of constraint violation upon which optimization cycles are terminated short of a one-dimensional minimum is $c_j \ \bar{g}_j$, where $\bar{g}_j$ is a preconceived tolerance and c_j, usually $>> 1$, is a factor adjusted with the aim of just permitting restoration with a single cycle of eq. (A.16), to within the tolerance. Since the use of a single c-factor for all constraints met with only limited success, a c-vector is used. The components are adjusted adaptively, if somewhat heuristically, in the following way: c_j is increased 10% if a single restoration proves successful; it is halved if two restoration cycles are required; and it is cut to one-quarter if there are additional cycles.

Treatment of Inequalities

It is of interest to determine a minimum subject to a mix of equality and inequality constraints, the latter expressed by eq. (A.8). During the initial correction sequence, inequalities are handled penalty-function fashion, the function f* to be minimized given by

$$f* = \frac{1}{2} \sum_{j=1}^{m} k_j \ g_j^2 + \frac{1}{2} \sum_{j=m+1}^{m+p} k_j \ g_j^2 \ h(-g_j) + \frac{k_0}{2} (f_0 - f)^2 \ h(f - f_0) \quad (A.17)$$

with the k_j determined as though all constraints were equalities:

$$k_j = \frac{\bar{k}}{(m+p)} \frac{\sum\limits_{i=1}^{m+p} |g_{i_x}|^2}{|g_{j_x}|^2} \quad , \qquad j = 1,2,\ldots,m+p \qquad (A.18)$$

The determination of the active constraint set for optimization and restoration cycles proceeds first by excluding those satisfied with a margin $g_j \geq \bar{g}_j$, where $\bar{g}_j > 0$ is a preset threshold. Those candidate inequality constraints for which $g_j < \bar{g}_j$ are then screened further via the Kuhn-Tucker conditions $\lambda_j \leq 0$ [18,19], using eq. (A.10) first with all the candidates included, then successively with Kuhn-Tucker violators dropped, as many times as necessary, until all $\lambda_j \leq 0$ or all candidates are screened. Inactive constraints are treated in penalty-function approximation.

In the event that there is more than one Kuhn-Tucker violator on a given cycle, dual violators are screened out first, one at a time. (A dual violator is a constraint whose multiplier violates $\lambda_j \leq 0$ both with all other constraint candidates considered and with other inequalities dropped.) This procedure has a sound theoretical basis in the case of two inequality constraints and, in a more general setting, represents an improvement over dropping dual violators in an arbitrary order. The Kuhn-Tucker conditions employed apply to the problem of minimizing a linear approximation to the function f subject to linearized constraints and to a quadratic constraint on step size [5]. They become identical to the Kuhn-Tucker conditions for the original problem when evaluated at the constrained minimum sought. The Kuhn-Tucker screening has generally been found to be worth the computational

expense in reducing tendencies of constraints to switch between active
and inactive status from cycle to cycle. The effort has proceeded on
the assumption that vector-matrix operations are cheap computationally
in relation to the cost of gradient and function samples; this is
realistic for trajectory-optimization applications. A more
sophisticated and somewhat more intricate procedure for Kuhn-Tucker
screening has recently been developed [6] and is incorporated in the
computer program as an option.

References

1. Clohessy, W. H. and Wiltshire, R. S.; "Terminal Guidance System for
    Satellite Rendezvous", Journal of the Aerospace Sciences, September
    1960.

2. Jezewski, D. J. and Donaldson, J. D.; "An Analytic Approach to
    Optimal Rendezvous Using Clohessy-Wiltshire Equations", Journal of
    the Astronautical Sciences, July 1979.

3. Kelley, H. J., Cliff, E. M. and Lutze, F. H.; "Pursuit/Evasion in
    Orbit", Journal of the Astronautical Sciences, July 1981.

4. Kelley, H. J. and Speyer, J. L.; "Accelerated Gradient Projection",
    Lecture Notes in Mathematics 132, Springer, Berlin, 1970.

5. Kelley, H. J., Lefton, L. and Johnson, I. L.; "Curvilinear
    Projection Developments", Journal of Guidance and Control, January
    1978.

6. Das, A., Cliff, E. M. and Kelley, H. J.; "An Active-Constraint Logic
    for Nonlinear Programming", Optimal Control Applications and
    Methods, July 1984.

7. Edelbaum, T. N.; "How Many Impulses?", Astronautics & Aeronautics,
    November 1967.

8. Prussing, J. E. and Chiu, J.-H.; "Optimal Multiple-Impulse
    Time-Fixed Rendezvous Between Circular Orbits", Preprint
    AIAA-84-2036, AIAA/AAS Astrodynamics Conference, Seattle,
    Washington, August 20-22, 1984.

9. Garwin, R. L., Gottfried, K., and Hafner, D. L.; "Antisatellite
    Weapons," Scientific American, June 1984.

10. Courant, R.; "Variational Methods for the Solution of Problems
    of Equilibrium and Vibrations," American Mathematical Society
    Bulletin, January 1943.

11. Kelley, H. J.; "Method of Gradients," Chapter 6 of Optimization
    Techniques, G. Leitmann, Editor, Academic Press, 1962.

12. Lefton, L. and Kelley, H. J.; "Variable-Metric Projection
    Optimization Program Notes," Analytical Mechanics Associates,
    Inc., Report No. 77-12, July 1977; revised April 1978.

13. Kelley, H. J., Denham, W. F., Johnson, I. L. and Wheatley,
    P. O.; "An Accelerated Gradient Method for Parameter Optimiza-
    tion with Non-linear Constraints," Journal of the Astronautical
    Sciences, Vol. 13, July 1966.

14. Fletcher, R. and Powell, M. J. D.; "A Rapidly Convergent Descent Method for Minimization," Computer Journal, July 1963.

15. Johnson, I. L. and Kamm, J. L.; "Accelerating One-Dimensional Searches," AIAA Journal, Vol. 11, No. 5, May, 1973, pp. 757-759.

16. Fletcher, R.; "A New Approach to Variable Metric Algorithms," Computer Journal, August 1970.

17. Gill, P. E. and Murray, W.; "The Design and Implementation of Software for Unconstrained Optimization," in Design and Implementation of Optimization Software, Sijthoff and Noordhoff, Alphen aan den Rijn, Netherlands, 1978.

18. Aoki, M.; Introduction to Optimization Techniques, McMillian, New York, 1971.

19. Kuhn, H. W. and Tucker, A. W.; "Nonlinear Programming," Proceedings of the Second Berkeley Symposium, University of California Press, 1951.

20. Lutze, F. H., Cliff, E. M. and Kelley, H. J.; "Optimal Rendezvous with Cooperative Vehicles," VPI&SU Report, March 1984.

21. Lutze, F. H., Cliff, E. M. and Kelley, H. J.; "Optimal Rendezvous with Cooperative Vehicles II," VPI&SU Report, July 1985.

22. Bate, R. R., Mueller, D. D. and White, J. E.; Fundamentals of Astrodynamics, Dover Publications, New York, N.Y., 1971.

23. Geyling, F. T. and Westerman, H. R.; Introduction to Orbital Mechanics, Addison-Wesley, Reading, Mass., 1971.

24. Roy, A. E.; "The Foundations of Astrodynamics," MacMillan, New York, N.Y., 1965.

25. Lutze, F. H.; "Unaided EVA Intercept and Rendezvous Charts," Journal of Spacecraft & Rockets, November 1979.

BIBLIOGRAPHY

1. Finke, R. G.; "Anti-Satellite Systems: Perceived Capabilities
    and Limitations (U)," IDA Paper P-970, October 1973 (S).

2. Potter, J. S., Smith, P. C. and Mullin, C. R.; "Maneuvering and
    Responsive Survival-Aid Strategies (U)," General Research Corp.
    Report SAMSO TR No. 76-199, Vols. 1-4, April 1976 (S).

3. Kalish, J. H.; "An Overview of Current Antisatellite Programs
    (U)," Journal of Defense Research 78-3, March 1979 (S).

4. Travis, J. C.; "The Soviet Threat to U.S. Satellites (U)," Journal
    of Defense Research, Special Issue 78-3, March 1979 (S).

5. Moiseev, N. N., and Evtushenko, Y. G.; "Interactive Optimiza-
    tion System," IFAC Optimization Workshop, Denver, Colorado,
    June 21, 1979.

6. Kelley, H. J.; "SAWS (Satellite Attack Warning System) Review
    and Recommendations (U)," Optimization Incorporated Report,
    September 1979 (S).

7. Potter, J. S.; "Satellite Analysis Program (SAP) Library,"
    General Research Corp. Report CR-1-1071, Vols. 1-3, March 1982.

8. Anon.; "Attack Geometry for Phase I of Satellite Defense System
    Concept Development (U)," Appendix C to Annex C to Attachment 1
    to RFP F04701-82-R-0009, Satellite Defense System Program,
    1 September 1982 (S).

9. Shanazar, J. H.; "Lateral Target Escape Distances from ASAT
    Attack (U)," USAF Foreign Technology Bulletin FTD-2660P-127/15-84,
    22 February 1984 (S).

10. Anderson, D., Hayes, E., Campbell, C. and Peterson, D.; "Optimal
    Threat Evasion Maneuvering Techniques," Proceedings of the Tenth
    DARPA Strategic Space Symposium, U.S. Naval Post-graduate
    School, Monterey, CA, 16-19 October 1984.